

# **Development of Acoustic Wave Devices to Characterize Viscosity and its Nonlinearity**

by

Peixuan Wu

A dissertation submitted to the Graduate Faculty of  
Auburn University  
in partial fulfillment of the  
requirements for the Degree of  
Doctor of Philosophy

Auburn, Alabama  
August 6, 2011

Key words: acoustic wave device, viscosity, non-linearity, magnetostrictive strip, cantilever

Copyright 2011 by Peixuan Wu

Approved by

Zhongyang Cheng, Chair, Professor of Materials Engineering  
Jeffrey W. Fergus, Professor of Materials Engineering  
Xiaoying Han, Assistant Professor of Mathematics and Statistics  
Dong-Joo Kim, Associate Professor of Materials Engineering

## Abstract

Fluid has many physical properties, such as conductivity, density, heat capacity, surface tension, thermal conductivity and viscosity. Viscosity is one of the most important physical properties of fluid, and it needs to be studied while choosing proper fluids for specific applications. Viscosity measurements are essentially connected with product quality and consistency. When concerned with fluids characterization in design, development, quality control or just liquid transportation, viscosity measurements are always involved. For example, the quality of engine oil is critical to its lubricating property and also plays an important role in engine performance. Therefore, it is important to monitor the oil quality in an engine by measuring its viscosity over time.

Some microacoustic devices have been developed to measure viscosity. It should be mentioned that all these devices have been developed to measure the viscosity only. As it is well known that some small change in viscosity may not affect the engine very much, therefore, it is reasonable to assume that the non-linearity of viscosity may be the real key of determining engine oil conditions. Among these acoustic technologies, magnetostrictive strip and cantilever have some unique advantages over others, such as wireless and good performances in liquids by choosing magnetostrictive strip, and large vibration displacement by selecting cantilever.

In this research, the resonance behaviors of magnetostrictive strip are systemically studied to improve the sensor applications. Different factors which could have influences on resonance behaviors of magnetostrictive strip are examined intensively, such as DC bias field

influence and locations effect. And the view that the AC-driving field could influence resonance frequencies of sensor is proposed. Proofs from three independent methods (lock-in amplifier, impedance analyzer and network analyzer) are given to support the view that resonance frequencies decrease with an increase in the AC-driving field. This discovery shows that AC driving field should be strong enough to avoid the influence on the resonance frequencies. The measurement results of the lock-in amplifier and impedance analyzer are compared to study the principle difference between these two methods. And also by using different coils in impedance analyzer method, the view that the impedance analyzer measures the signal from sensor and equivalent circuits is proved. Combined with the former results from the AC-driving field, it is found that coils with a small diameter and the same length as the sensor are good for resonance behaviors measurement. The location effects study shows the center of the pick-up coil is the best position of measuring the vibration signals of the magnetostrictive strip sensor.

A new method by using properly chosen function of characteristic frequencies versus one of three frequencies is developed to identify the non-linearity of viscosity and also differentiate Newtonian oils and non-Newtonian oils. The resonance behaviors of magnetostrictive strips with different lengths in different oils are studied, and the performances of same length magnetostrictive strips with different length-width ratios are also investigated. All studies show that geometry of magnetostrictive strip is important in identifying non-linearity of viscosity. In order to apply magnetostrictive strips in a real circumstance, the performances of strip sensor are studied under different temperatures, and it is found that a magnetostrictive strip of this size can determine the non-linearity of viscosity well within broad temperature ranges.

The resonance behaviors of cantilever sensors with different lengths in different oils are studied, and the performances of same length cantilever sensors with different length-width

ratios are also investigated. The results show that a longer cantilever with the same width and thickness has better performance in identifying non-linearity of viscosity, and a cantilever sensor of the same length and thickness with a smaller width has better performance in differentiating Newtonian oils and non-Newtonian oils.

And numerical simulation of the vibration of the strip sensor shows non-Newtonian liquids behave like Newtonian liquids at a rather low shear rates and high shear rates in which the range's viscosity does not change with the shear rate and acts totally different with Newtonian liquids at an intermediate shear rate. So based on this conclusion, similar results can be achieved by the method I proposed which can distinguish these two types of liquids. And this also approves the validity of the method proposed in this study.

## Acknowledgments

Pursuing a PhD degree is really a tough journey as a marathon event, and I would not have been able to complete it without the help of countless people over the past years. Firstly, I would like to express my sincere thanks to my advisor, Dr. Z. -Y. Cheng for his invaluable assistance, guidance and encouragement throughout my PhD studies in Auburn University. His intelligence, hard work and attention to details have placed an example I hope to match some day. Then I would like to give my sincere appreciation to Dr. Jeffrey W. Fergus, Dr. Xiaoying Han, Dr. DongJoo Kim, as my committee members and for their generous guidance, recommendations and suggestions, and to Dr. Minseo Park for his helpful discussions. Thanks are also due to Dr. Jung-Hyun Park for his help in engine oil sample preparations; Mr. L.C. Mathison, Mr. Roy Howard and Mr. Steven Moore for the general technical support.

Special thanks also go to all my graduate friends, especially group members; Dr. Suiqiong Li, Dr. Xiaobing Shan, Dr. Liling Fu, Dr. Kewei Zhang, Lin Zhang, Wei Wang, Koichi Yamaguchi, Zhizhi Sheng. I also would like to thank some of my friends: Dr. Wen Shen, Dr. Dan Liu, Yu Zhao, Zijie Cai, Yating Chai, Xiaoyun Yang, and Jing Dai. My time in the PhD program has been more fun and interesting with them together.

Most importantly, I wish to express my love and gratitude to my father Guoqiang Wu and my mother Hanyun Chen for their great love, emotional support, and encouragement which inspire me all the time during my studies and also throughout my life.

## Table of Contents

Abstract.....	ii
Acknowledgments.....	v
List of Figures.....	x
List of Tables .....	xvii
Chapter 1 Introduction & Literature Review.....	1
1.1 Background & identification of the problem .....	1
1.2 Viscosity, Newtonian & non-Newtonian liquids .....	2
1.2.1 General introduction of viscosity .....	3
1.2.2 Newtonian & non-Newtonian liquids .....	6
1.2.3 Different models of typical non-Newtonian liquids .....	9
1.2.4 Temperature dependence of liquid viscosity .....	11
1.2.5 Engine oils and non-linear behaviors of viscosity in engine oils .....	12
1.3 Conventional methods .....	14
1.3.1 U-tube Viscometer .....	14
1.3.2 Falling Ball Viscometers .....	18
1.3.3 Rotational Viscometers .....	21
1.4 Active acoustic wave (AW) resonators as viscometer and current research .....	23
1.4.1 Vibrating Viscometers .....	24

1.4.2	Current research on AW viscometer (advantage over traditional one, and challenges)	27
1.5	Research objectives	31
<b>Chapter 2 Fundamental Study of Magnetostrictive Strip Resonance Behaviors and Location</b>		
	Effects in Pick-up Coils	39
2.1	Introductions	39
2.2	Configuration of a magnetostrictive strip sensor	41
2.3	Current characterizations of resonance behaviors of magnetostrictive strips	44
2.4	Experimental and measurement setup	45
2.4.1	Lock-in amplifier method	45
2.4.2	Impedance analyzer method	48
2.4.3	Network analyzer method	49
2.5	Characterization and experiment results discussion	49
2.5.1	Resonance frequency of magnetostrictive sensor	49
2.5.2	Effect of external DC bias magnetic field on resonance behaviors of strip sensor...	50
2.5.3	Effect of AC-driving magnetic field on resonance behaviors of strip sensor	56
2.5.3.1	Lock-in amplifier method	57
2.5.3.2	Impedance analyzer method	58
2.5.3.3	Network analyzer method	61
2.5.3.4	Conclusion	63
2.5.4	Comparison of impedance analyzer method and lock-in amplifier method	63

2.5.5	Comparison of the influence of different coils on resonance behaviors of magnetostrictive strip by impedance analyzer method .....	64
2.5.6	Location effect of magnetostrictive strip sensor in pick-up coils .....	67
2.6	Conclusions .....	71
Chapter 3	Magnetostrictive Strip Sensors to Identify the Nonlinearity of Viscosity .....	75
3.1	Introduction .....	75
3.2	Experimental and measurement setup .....	76
3.3	Determination of three characteristic frequencies .....	78
3.4	Comparison of the performances of different length magnetostrictive strip sensors in oils .....	80
3.5	Comparison of the performances of different length-ratio magnetostrictive strip sensors in oils .....	85
3.6	The performances of 40 mm × 3 mm × 30 μm magnetostrictive strip sensor in oils at different temperatures .....	86
3.7	Conclusions .....	90
Chapter 4	Piezoelectric Cantilever Sensors to Identify the Nonlinearity of Viscosity .....	92
4.1	Introduction .....	92
4.2	Configuration of piezoelectric cantilever sensor .....	93
4.3	Theory .....	96
4.4	Experimental and measurement setup .....	99
4.5	The performance comparison of PZT cantilevers with same length and thickness but different width and performance comparison of PZT cantilevers with different length but same width and thickness .....	102



4.6	Conclusions .....	107
Chapter 5	Numerical Simulations to Identify the Nonlinearity of Viscosity.....	109
5.1	Introduction .....	109
5.2	Theoretical model (in Newtonian & non-Newtonian liquids) and numerical simulation .....	111
5.3	Model in Newtonian liquids and numerical simulation .....	111
5.3.1	The study of relationship of three characteristic frequencies with B value ..	121
5.4	Model in non-Newtonian liquids and numerical simulation .....	125
Chapter 6	Conclusions and Perspectives .....	129

## List of Figures

Figure 1.1. Simple shear .....	3
Figure 1.2. (a) Shear stress vs. shear rate for different fluids; (b) Viscosity vs. shear rate for different fluids .....	7
Figure 1.3. Illustration of structural viscosity behavior of non-Newtonian liquids .....	8
Figure 1.4. Structural viscosity behavior of some non-Newtonian liquid [13] .....	8
Figure 1.5. Schematic of U-tube viscometer .....	15
Figure 1.6. Schematic of falling sphere viscometer (from Brookfield Engineering Laboratories, Inc. [31]) .....	19
Figure 1.7. (a) Schematic of “Cup and bob” viscometers; (b) Schematic of “Cone and Plate” viscometers .....	21
Figure 1.8. Several different methods to measure the damping factor: (a) Measuring the power input; (b) Measuring the decay time; (c) Measuring the frequency shift .....	25
Figure 1.9. Illustration of small vibration displacement inside liquid contains polymer .....	29
Figure 1.10. Effective region of different AW devices in structural viscosity non-Newtonian liquid based on Table 1.8 .....	31
Figure 1.11. Illustration of different range covered by $f_r$ , $f_r'$ and $f_0$ three experimental characteristic frequencies in structural viscosity non-Newtonian liquid .....	32
Figure 2.1. The magnetostrictive strip configuration .....	42
Figure 2.2. Lock-in amplifier method measurement set-up .....	46

Figure 2.3. The frequency dependence of the phase and amplitude signals from the lock-in amplifier for a magnetostrictive strip in size of 25 mm ( $L$ ) $\times$ 3.0 mm ( $W$ ) $\times$ 30 $\mu$ m ( $t$ ) in R-100 reference oil .....	47
Figure 2.4. Impedance analyzer method measurement set-up .....	48
Figure 2.5. Network analyzer method measurement set-up .....	49
Figure 2.6. Resonance behaviors of 25mm (25mm $\times$ 3mm $\times$ 30 $\mu$ m) magnetostrictive strip sensor (from Metglas alloy 2826MB ribbon) in air under different DC magnetic fields: (a) amplitude vs. frequency; (b) phase vs. frequency; (c) resonance frequencies as a function of external DC bias magnetic field; (d) amplitude and Q value of magnetostrictive strip sensor as a function of external DC bias magnetic field .....	54
Figure 2.7. Typical magnetization versus magnetic field curve for magnetostrictive strip .....	55
Figure 2.8. Comparison of experimental result and theoretical model of resonance behaviors of 25mm (25mm $\times$ 3mm $\times$ 30 $\mu$ m) magnetostrictive strip sensor (from Metglas alloy 2826MB ribbon) in air under different DC magnetic fields .....	55
Figure 2.9. Resonance behaviors of 25mm (25mm $\times$ 3mm $\times$ 30 $\mu$ m) magnetostrictive strip sensor (from Metglas alloy 2826MB ribbon) in air under different DC magnetic fields: $Q \cdot Amplitude^{\frac{5}{3}}$ of the magnetostrictive strip sensor as a function of the external DC bias magnetic field .....	56
Figure 2.10. Lock-in amplifier method: Resonance behaviors of 25mm (25mm $\times$ 3mm $\times$ 30 $\mu$ m) magnetostrictive strip sensor (from Metglas alloy 2826MB ribbon) in air under different AC driving magnetic fields with an optimized DC bias field .....	57
Figure 2.11. Lock-in amplifier method: Influence of AC driving magnetic fields on resonance behaviors of a 25mm (25mm $\times$ 3mm $\times$ 30 $\mu$ m) magnetostrictive strip sensor (from Metglas alloy 2826MB ribbon) in air with an optimized DC bias field .....	58

Figure 2.12. Impedance analyzer method: Resonance behaviors of 25mm (25mm×3mm×30μm) magnetostrictive strip sensor (from Metglas alloy 2826MB ribbon) in air under different AC driving magnetic fields with an optimized DC bias field .....	59
Figure 2.13. Impedance analyzer method: Influence of AC driving magnetic fields on resonance behaviors of 25mm (25mm×3mm×30μm) magnetostrictive strip sensor (from Metglas alloy 2826MB ribbon) in air with an optimized DC bias field .....	60
Figure. 2.14. Impedance analyzer method: Resonance behaviors of 35mm (35mm×3mm×30μm) magnetostrictive strip sensor (from Metglas alloy 2826MB ribbon) in air under different AC driving magnetic fields with an optimized DC bias field .....	60
Figure 2.15. Impedance analyzer method: Influence of AC driving magnetic fields on resonance behaviors of 35mm (35mm×3mm×30μm) magnetostrictive strip sensor (from Metglas alloy 2826MB ribbon) in air with optimized DC bias field .....	61
Figure. 2.16. Network analyzer method: Resonance behaviors of 2mm (2mm×0.4mm×30μm) magnetostrictive strip sensor (from Metglas alloy 2826MB ribbon) in air under different AC driving magnetic fields with an optimized DC bias field .....	62
Figure 2.17. Network analyzer method: Influence of AC driving magnetic fields on resonance behaviors of 2mm (2mm×0.4mm×30μm) magnetostrictive strip sensor (from Metglas alloy 2826MB ribbon) in air with an optimized DC bias field .....	62
Figure 2.18. Comparison of three characteristic resonance frequencies of 25mm × 3mm magnetostrictive strip in 25mm coils (with different AC) by lock-in amplifier method and impedance analyzer method: Influence of different methods on resonance behaviors of magnetostrictive strip .....	64

Figure 2.19. Impedance analyzer method: Resonance behaviors of 25mm (25mm×3mm×30μm) magnetostrictive strip sensor in 40mm coils (with coil diameter = 4.7mm) in air under different AC driving magnetic fields with optimized DC bias field .....	65
Figure 2.20. Impedance analyzer method: Resonance behaviors of 25mm (25mm×3mm×30μm) magnetostrictive strip sensor in 40mm coils (with coil diameter = 6.35mm) in air under different AC driving magnetic fields with an optimized DC bias field .....	66
Figure 2.21. Comparison of resonance frequencies of 25mm × 3mm × 30μm strip from different coils by impedance analyzer method: (a) same coil diameter but different coil length; (b) same coil length but different coil diameter .....	67
Figure 2.22. Two different sizes of self-made pick-up coils: a pair of coil and reverse coil with symmetry .....	68
Figure 2.23. Illustration of the x-coordinate (location of the strip) .....	69
Figure 2.24. The different locations effects on (a) signal amplitudes, (b) phase range and (c) Q value of magnetostrictive strip sensor.....	70
Figure 3.1. The frequency dependence of the phase and amplitude signals from the lock-in amplifier for a magnetostrictive strip in size of 25 mm ( $L$ ) × 3.0 mm ( $W$ ) × 30 μm ( $t$ ) in R-100 reference oil .....	77
Figure 3.2. Schematic diagram of the visco-liquid sensor system .....	78
Figure 3.3. The three characteristic frequencies of 25mm (25mm × 3mm × 30μm) magnetostrictive strip in different oils vs. viscosity of oils .....	80
Figure 3.4. The properly chosen function of characteristic frequencies vs. anti-resonance frequency ( $f_r'$ ) of 25 mm ( $L$ ) × 3 mm ( $W$ ) × 30 μm ( $t$ ) magnetostrictive strip in different oils at room temperature .....	80

Figure 3.5. Resonance behaviors of 30mm (30mm×3mm×30μm) magnetostrictive strip sensor in oils at room temperature ..... 81

Figure 3.6. The properly chosen function of characteristic frequencies *vs.* anti-resonance frequency ( $f_r'$ ) of 30 mm ( $L$ ) × 3 mm ( $W$ ) × 30 μm ( $t$ ) magnetostrictive strip in different oils at room temperature ..... 82

Figure 3.7. The three characteristic frequencies of 40mm (40mm×3mm×30μm) magnetostrictive strip in different oils *vs.* viscosity of BP oils (fresh and artificially degraded) at room temperature ..... 83

Figure 3.8. The three characteristic frequencies of 40mm (40mm×3mm×30μm) magnetostrictive strip in different oils *vs.* viscosity of reference oils ..... 84

Figure 3.9. The properly chosen function of characteristic frequencies *vs.* anti-resonance frequency ( $f_r'$ ) of 40 mm ( $L$ ) × 3 mm ( $W$ ) × 30 μm ( $t$ ) magnetostrictive strip in different oils ..85

Figure 3.10. The comparison of function of characteristic frequencies ( $\frac{f_r}{f_r' - 0.8f_r}$ ) *vs.* anti-resonance frequency ( $f_r'$ ) of magnetostrictive strip in different length-width ratios ..... 86

Figure 3.11. The function of characteristic frequencies ( $\frac{f_r}{f_r' - 0.8f_r}$ ) *vs.* anti-resonance frequency ( $f_r'$ ) of 40 mm ( $L$ ) × 3 mm ( $W$ ) × 30 μm ( $t$ ) magnetostrictive strip in different oils at 50 °C ..... 87

Figure 3.12. The function of characteristic frequencies ( $\frac{f_r}{f_r' - 0.8f_r}$ ) *vs.* anti-resonance frequency ( $f_r'$ ) of 40 mm ( $L$ ) × 3 mm ( $W$ ) × 30 μm ( $t$ ) magnetostrictive strip in different oils at 80 °C ..... 88

Figure 3.13. The function of characteristic frequencies ( $\frac{f_r}{f_r' - 0.8f_r}$ ) *vs.* anti-resonance frequency ( $f_r'$ ) of 40 mm ( $L$ ) × 3 mm ( $W$ ) × 30 μm ( $t$ ) magnetostrictive strip in different oils at 100 °C ... 89

Figure 4.1. Three different operation modes of cantilever sensor: (a) static mode, where unbalance mechanic loads on upper and lower surfaces lead to the bending of cantilever; (b) heat mode sensing temperature changes by static bending caused by different thermal expansion coefficient of two layers (coat and substrate), and (c) dynamic mode sensing the visco-drag force added on the cantilever by resonance frequency change .....	93
Figure 4.2. The schematic of piezoelectric cantilever sensor for visco-liquids .....	95
Figure 4.3. The schematic of principle of piezoelectric cantilever unimorph as visco-sensor platform .....	96
Figure 4.4. The schematic of rectangular cantilever, rigidly clamped at one end and free at the other .....	97
Figure 4.5. The process of prepare the piezoelectric cantilever sensor for visco-liquids .....	99
Figure 4.6. Set-up of impedance analyzer measurement of piezoelectric cantilever .....	100
Figure 4.7. The capacitance and phase vs. frequency of 9 mm × 0.7 mm × 0.5 mm piezoelectric cantilever sensor in different oils .....	100
Figure 4.8. Properly chosen function of characteristic frequencies vs. one of the three characteristic frequencies of 9 mm × 0.7 mm × 0.5 mm PZT cantilever in oils .....	101
Figure 4.9. The schematic of piezoelectric cantilever sensor oscillation in visco-liquids .....	102
Figure 4.10. Resonance behaviors of 6.8 mm × 0.3 mm × 0.5 mm PZT cantilever sensor in oils.. .....	103
Figure 4.11. Properly chosen function of characteristic frequencies vs. one of the three characteristic frequencies of 6.8 mm × 0.3 mm × 0.5 mm PZT cantilever in oils .....	104
Figure 4.12. Properly chosen function of characteristic frequencies vs. one of the three characteristic frequencies of 6.8 mm × 0.7 mm × 0.5 mm PZT cantilever in oils .....	105

Figure 4.13. Properly chosen function of characteristic frequencies vs. one of the three characteristic frequencies of 6.8 mm × 1.0 mm × 0.5 mm PZT cantilever in oils .....	106
Figure 5.1. (a) Forced damped vibration. Normalized amplitude $\frac{A}{B/k}$ as a function of $\omega_{ext}/\omega_0$ for various degrees of damping D; (b) Phase shift $\phi$ as function of $\omega_{ext}/\omega_0$ for various degrees of damping D [5] .....	112
Figure 5.2. Three characteristic resonance frequencies obtained by numerical simulations of the differential Equation (5-3) (before and after modification) .....	116
Figure 5.3. Numerical simulation solutions of the differential Equation (5-3) .....	121
Figure 5.4. The relationship of typical Carreau model viscosity and shear rate with different driving force amplitude .....	126
Figure 5.5. Different $h$ (non-Newtonian liquids with different viscosity) compared with different Newtonian liquids at same range of resonance frequency .....	127



## List of Tables

Table 1.1. Different types of U-Tube viscometers from Cannon instrument .....	16
Table 1.2. Different types of U-Tube viscometers from RHEOTEK™ .....	17
Table 1.3. Different types of U-Tube reverse-flow viscometers from RHEOTEK™ .....	18
Table 1.4. Technical Specifications of falling ball viscometers from Brookfield .....	20
Table 1.5. Technical Specifications of falling ball viscometers from Rheology Solutions .....	20
Table 1.6. Technical Specifications of falling ball viscometers from Thermo Scientific HAAKE .....	21
Table 1.7. Technical Specifications of rotational viscometers VT550 from Thermo Scientific HAAKE .....	23
Table 1.8. Technical Specifications of vibrational viscometers SV-10/100 from A&D Company Ltd .....	26
Table 1.9. Review of AW devices .....	30
Table 1.10. Comparison of AW devices .....	30
Table 2.1. Lock-in amplifier method: Resonance frequencies of 25mm (25mm×3mm×30μm) magnetostrictive strip sensor in air under different AC driving magnetic fields with an optimized DC bias field .....	58
Table 2.2. Impedance analyzer method: Resonance frequencies of 25mm (25mm×3mm×30μm) magnetostrictive strip sensor in air under different AC driving magnetic fields with an optimized DC bias field .....	59

Table 2.3. Impedance analyzer method: Resonance frequencies of 35mm (35mm×3mm×30μm) magnetostrictive strip sensor in air under different AC driving magnetic fields with an optimized DC bias field .....	60
Table 2.4. Network analyzer method: Resonance frequencies of 2mm (2mm×0.4mm×30μm) magnetostrictive strip sensor in air under different AC driving magnetic fields with an optimized DC bias field .....	62
Table 2.5. Impedance analyzer method: Resonance frequencies of 25mm (25mm×3mm×30μm) magnetostrictive strip sensor in 40mm coils (with coil diameter = 4.7mm) in air under different AC driving magnetic fields with an optimized DC bias field .....	65
Table 2.6. Impedance analyzer method: Resonance frequencies of 25mm (25mm × 3mm × 30μm) magnetostrictive strip sensor in 40mm coils (with coil diameter = 6.35mm) in air under different AC driving magnetic fields with an optimized DC bias field .....	66
Table 3.1. Dynamic viscosity and kinematic viscosity of reference oils .....	78
Table 3.2. Viscosity of artificial degraded oil BP 2380 aged at 240 °C .....	79
Table 3.3. Resonance frequencies of 30mm (30mm×3mm×30μm) magnetostrictive strip sensor in oils .....	82
Table 3.4. Resonance frequencies of 40mm (40mm×3mm×30μm) magnetostrictive strip sensor in oils .....	83
Table 3.5. Resonance frequencies of 40mm (40mm×3mm×30μm) magnetostrictive strip sensor in oils at 50 °C .....	87
Table 3.6. Resonance frequencies of 40mm (40mm×3mm×30μm) magnetostrictive strip sensor in oils at 80 °C .....	88

Table 3.7. Resonance frequencies of 40mm (40mm×3mm×30μm) magnetostrictive strip sensor in oils at 100 °C .....	89
Table 4.1. The effective material properties of PZT piezoelectric ceramics layer, brass layer and cantilever beam .....	95
Table 4.2. Resonance frequencies of 9 mm × 0.7 mm × 0.5 mm PZT cantilever sensor in oils.... .....	101
Table 4.3. Resonance frequencies of 6.8 mm × 0.3 mm × 0.5 mm PZT cantilever sensor in oils .....	103
Table 4.4. Resonance frequencies of 6.8 mm × 0.7 mm × 0.5 mm PZT cantilever sensor in oils .....	104
Table 4.5. Resonance frequencies of 6.8 mm × 1.0 mm × 0.5 mm PZT cantilever sensor in oils .....	105
Table 5.1. Maximum shear rate with different $h$ value .....	126

## CHAPTER 1

### INTRODUCTION & LITERATURE REVIEW

#### **1.1 Background & identification of the problem**

Fluid, in physics, is a substance that yields constantly under an applied shear stress or external pressure. Fluids are actually a group of the phases of materials which include gases, liquids, plasmas and somewhat even include plastic solids. However in regular daily use, fluid is often used to refer to “liquid” without the implication which includes the phase “gas” [1]. For example, brake fluid in automobiles is actually hydraulic oil and could not perform its normal function well if there is some gas inside. And the difference between solids and fluids is not quite clear. The difference is made by measuring the viscosity of the substance.

Fluid has many physical properties, such as conductivity, density, heat capacity, surface tension and thermal conductivity. Viscosity is one of the most important physical properties of fluid and it needs to be studied while choosing proper fluid for specific applications [1, 2]. Viscosity measurements are connected essentially with product quality and consistency. When concerned with fluids characterization, in design, development, quality control or just liquid transportation, viscosity measurements are always involved. For example, in the production process of paints and ointments, viscosity quality control testing is required and generally includes an analysis method monitoring viscosity value. Sometimes additional viscosity measurements are needed with the purpose of fully characterizing rheological properties which are very important to end users or consumers [3]. Most pharmaceutical ointments are proposed to be thick enough to avoid flowing away from the applied area, and

at the same time they need to be thin for easy rubbing application. Also, in chemical process design, viscosity, which is one of the most important transport properties, has a straight effect on heat transfer coefficients [4]. There are many aspects which could show the importance of viscosity, such as in quality control areas, where liquid products should be consistent from batch to batch. For this principle, the fluid's viscosity measurement is an indirect evaluation of product quality [3]. Another reason for studying the viscosity and fluid flow behavior is that a direct evaluation of processability can be acquired. For example, it will cost more power to pump up a liquid with high viscosity than a low viscosity one. Thus it is very useful to know fluid viscosity and its rheological performance when designing engine and pumping systems [4, 5].

Good engine performance in vehicles can increase the mileage per gallon, generate better engine efficiency and reduce less exhaust gas. To minimize direct contact of moving parts in engines, engine oil is used for lubricating moving parts by generating a lubricating film on the surface that decreases heat caused by friction and reducing wear, thus protecting the engine. The quality of the engine oil is critical to its lubricating property and also plays an important role in engine performance. Therefore it is important to monitor the oil quality in an engine by measuring viscosity [5]. One of the key properties of engine oil is its viscosity.

## **1.2 Viscosity, Newtonian & non-Newtonian liquids**

Viscosity represents the resistance of a fluid to deformation under shear stress or extensional stress. It's commonly regarded as "thickness" or resistance to flow. Viscosity describes a fluid's internal resistance to flow and sometimes can be treated as a measure of fluid friction [6]. All real fluids have some resistance to stress, but a fluid which has no

resistance to shear stress is known as an ideal fluid or inviscid fluid. The study of viscosity is known as rheology [7].

### 1.2.1 General introduction of Viscosity

Generally there are many layers which move at unlike velocities in any fluid, and the fluid's viscosity arises from the shear stress between layers that are subjected to any applied force.

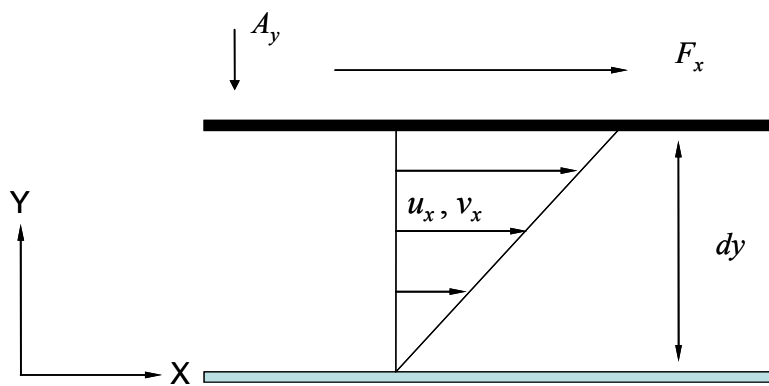


Figure 1.1. Simple shear.

Figure 1.1 shows a thin layer of fluid that is contained between two parallel plates, assuming that the plates are very large (with surface area  $A_y$ ) such that edge effects could be ignored. Under steady state conditions (i.e. the velocity  $v_x$  is constant), the fluid is subjected to a simple shear by the application of a force  $F_x$  on the top plate as shown while the lower plate is stationary. The force  $F_x$  is balanced by an equal and opposite internal frictional force in the fluid. From the total force  $F_x$  and the displacement  $u_x$ , the shear stress  $\tau_{yx}$  and shear strain  $\gamma_{yx}$  can be defined as follows:

$$\tau_{yx} = \frac{F_x}{A_y} \quad (1-1)$$

$$\gamma_{yx} = \frac{du_x}{dy} \quad (1-2)$$

If the interaction among the molecules of the fluid is insignificant, the plate can be moved by a very small force and this fluid can be expressed by the equation  $\tau_{yx} = 0$  and is named an *inviscid fluid*. On the other hand, if the interaction among the molecules is considerable, such that the relative rate of movement (the velocity gradient) is proportional to the applied force (e.g. shear force), the material is known as a *Newtonian fluid* and is defined by

$$\tau_{yx} = \eta \dot{\gamma}_{yx} \quad (1-3)$$

where  $\eta$  is a constant,  $\dot{\gamma}_{yx}$  is the shear rate or rate of shear strain as:

$$\dot{\gamma}_{yx} = \frac{d\gamma_{yx}}{dt} = \frac{dv_x}{dy} \quad (1-4)$$

where  $v_x$  is the velocity and  $v_x = \frac{du_x}{dt}$ .

The  $\eta$  is named as the viscosity of the fluid and its SI units is Pa·s [8].

If the shear stress is not proportional to shear rate and relates to some other factors, the fluid is called *non-Newtonian fluid*. The  $\eta$  (viscosity of fluid) is still defined as  $\frac{\tau_{yx}}{\dot{\gamma}_{yx}}$ , but it is not a constant anymore. In this case, the  $\eta$  is a function of either the shear rate or shear stress and is designated by:

$$\eta = \frac{\tau_{yx}}{\dot{\gamma}_{yx}} = \mathcal{F}(\tau \text{ or } \dot{\gamma}) \quad (1-5)$$

Viscosity coefficient (SI unit: Pa·s, P and cP) is widely used to describe viscous behaviors of a fluid. Different coefficients are used to describe fluids, such as kinematic viscosity  $\nu$ , which is the ratio of dynamic viscosity  $\eta$  to the density  $\rho$ , and they are applied in the measurement of resistance to flow of a liquid under gravity (typical units: m<sup>2</sup>/s, Stokes and cSt).

$$\nu = \frac{\eta}{\rho} \quad (1-6)$$

It indicates the ease of diffusion of shear force which acts on the surface of a fluid into its interior. Due to this reason, sometimes it is also called the *viscous diffusivity* [8].

Viscosity can be defined into several independent components in different ways. The following viscosity coefficients classification is yielded by one of the most usual decompositions.

1. Shear viscosity, the most common one, is often named viscosity, illustrating the response to applied shear stress; simply put, it is the ratio of the shear stress added on the fluid surface to the change in velocity of the fluid as it moves down into the fluid (this velocity change is known as shear rate or velocity gradient).
2. Volume viscosity or bulk viscosity describes the reaction to compression, essential for acoustics in fluids, such as shock waves and sound propagation [7]. In these cases, this viscosity coefficient is supplementary to the normal dynamic viscosity  $\eta$ . Volume viscosity is applied in the Navier-Stokes equation when compressible fluid is studied, as illustrated in common hydrodynamics books [9, 10].

$$\rho \left( \frac{\partial \mathbf{v}}{\partial t} + \mathbf{v} \cdot \nabla \mathbf{v} \right) = -\nabla p + \eta \nabla^2 \mathbf{v} + f + (\eta/3 + \eta^V) \nabla (\nabla \cdot \mathbf{v}) \quad (1-7)$$

where  $\mathbf{v}$  is the flow velocity,  $\rho$  is the fluid density,  $p$  is the pressure, and  $f$  represents forces per unit volume exerting on the fluid and  $\nabla$  is the del operator.

3. Extensional viscosity, a linear combination of shear and volume viscosity, expresses the reaction to elongation, usually used for characterizing polymer solutions. Extensional viscosity can be measured by viscometers when applying extensional stress and is defined as:



$$\eta_e = \frac{\sigma_n}{\dot{\epsilon}} \quad (1-8)$$

where  $\eta_e$  is the extensional viscosity,  $\sigma_n$  is the normal stress, and  $\dot{\epsilon}$  is the strain rate:

$\dot{\epsilon} = \frac{1}{L} \frac{dL}{dt}$ . For a Newtonian fluid, the extensional viscosity is three times its shear

viscosity for incompressible fluids:  $\eta_e = 3\eta$  [11, 12].

### 1.2.2 Newtonian & non-Newtonian Liquids

Most common liquids with simple structures are Newtonian (water, glycerin, oil, etc). However, fluids with complicated structures (polymer melts or solutions, suspensions, etc) are generally non-Newtonian [8-13].

As shown in Figures 1.2(a) and 1.2(b), different types of behaviors and fluid properties can be found when the measured values of shear stress or viscosity are plotted versus shear rate [13]. Most non-Newtonian fluids are shear thinning (or *pseudoplastic*), while shear thickening (or *dilatant*) behavior is rather rare and only can be found in some concentrated suspensions of very small particles and some unusual polymeric fluids. A Bingham plastic is a fluid that acts as a stiff body at low stress, however behaves as Newtonian fluid in a high stress situation. It exhibits a linear behavior of shear stress with shear-rate only after a certain initial shear stress has been achieved [14]. A general case is toothpaste, which can not be pushed out until some certain pressure is added on the tube. Then it is extruded out as a solid strip. And many concentrated slurries and suspensions, such as muds, paints, and ketchup, show Bingham behaviors.

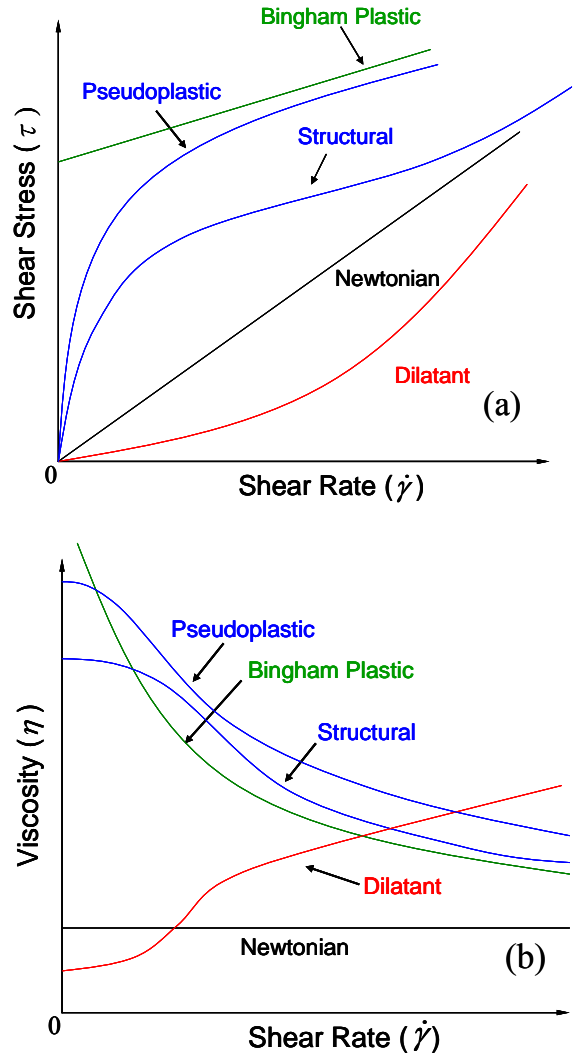


Figure 1.2. (a) Shear stress vs. shear rate for different fluids; (b) Viscosity vs. shear rate for different fluids.

A typical viscosity feature of many non-Newtonian fluids is shown by the *structural viscosity* curve in Figures 1.2 (a) and (b). These fluids show Newtonian behavior at very low and very high shear rates; however they exhibit shear thinning (or *pseudoplastic*) behavior at intermediate shear rates. Normally these fluids are polymeric fluids or with some polymers added in. When the shear force is added on, the polymer coils in the solution are disentangled and the orientations of polymer coils turn into the direction of shear. Newtonian behavior can be attributed to the formation of a reversible structure or network in the “rest” or equilibrium

state. This structure breaks down with increasing shear rate and then shows a shear-dependent behavior [15, 16]. However, with the shear rate increasing, the new structure forms as shown in Figure 1.3, and the viscosity can not decrease further and then becomes rather stable as Newtonian behaviors. Some actual examples of structural viscosity behaviors are shown in Figure 1.4.

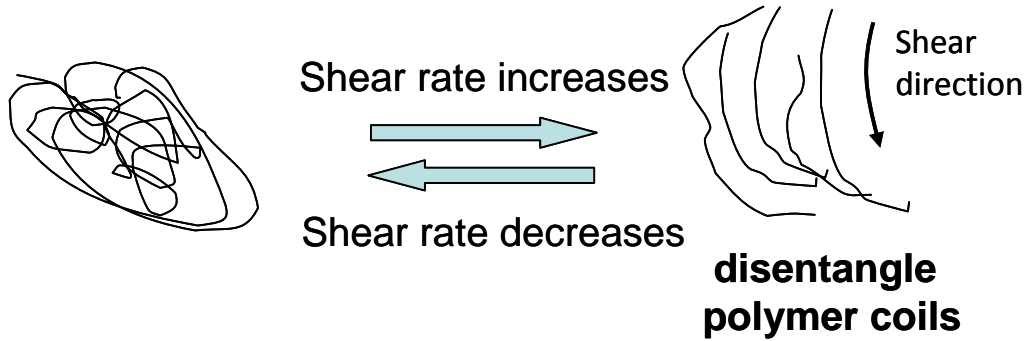


Figure 1.3. Illustration of structural viscosity behavior of non-Newtonian liquids.

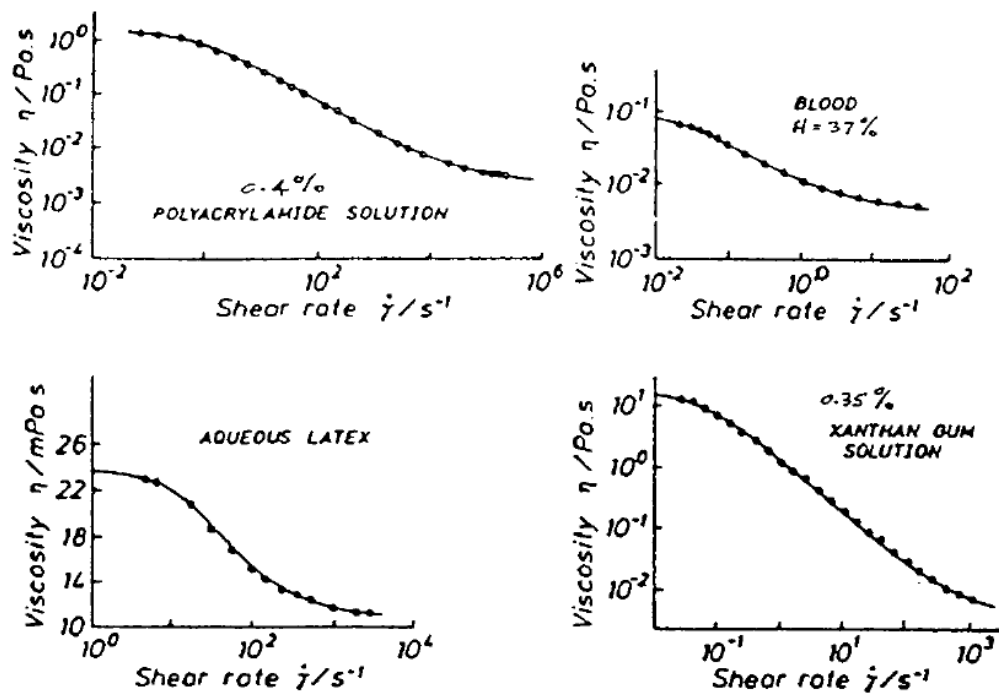


Figure 1.4. Structural viscosity behavior of some non-Newtonian liquid [13].

### 1.2.3 Different models of typical non-Newtonian liquids

Structural viscosity model can be expressed by different equations, including the Carreau model [13]:

$$\eta(\dot{\gamma}) = \eta_{\infty} + \frac{\eta_0 - \eta_{\infty}}{[1 + (\lambda\dot{\gamma})^2]^p} \quad (1-9)$$

This model contains four rheological parameters: the low shear limiting viscosity,  $\eta_0$ ; the high shear limiting viscosity,  $\eta_{\infty}$ ; time constant  $\lambda$ ; and the shear thinning index,  $p$  ( $0 < p < 0.5$ ). It is a very common viscosity model and can express the viscosity properties for many materials. However, in order to figure out all four parameters and draw the curve, a broad range (six to eight decades of shear rate) of data is needed. And by various relationships among  $\eta$ ,  $\eta_0$  &  $\eta_{\infty}$ , the Carreau model can be simplified into different simple models [13, 17].

a. Low to Intermediate Shear Rate Range, Ellis model;

If  $\eta_{\infty} \ll (\eta, \eta_0)$ , the Carreau model reduces to a three-parameter model ( $\eta_0, \lambda$  and  $p$ ) that is equivalent to a power law model with a low shear limiting viscosity:

$$\eta(\dot{\gamma}) = \frac{\eta_0}{[1 + (\lambda\dot{\gamma})^2]^p} \quad (1-10)$$

b. Intermediate to High Shear Rate Range, Sisko model;

If  $\eta_0 \gg (\eta, \eta_{\infty})$  and  $(\lambda\dot{\gamma})^2 \gg 1$ , the Carreau model reduces to the equivalent of a power law model with a high shear limiting viscosity:

$$\eta(\dot{\gamma}) = \eta_{\infty} + \frac{\eta_0}{(\lambda\dot{\gamma})^{2p}} \quad (1-11)$$

Although this appears to have four parameters, it is really a three-parameter model, because the combination of  $\eta_0 / (\lambda)^{2p}$  can be considered as a single parameter, along with two other

parameters  $p$  and  $\eta_\infty$ .

c. Intermediate Shear Rate Behavior, Power law model;

For  $\eta_\infty \ll \eta \ll \eta_0$  and  $(\lambda\dot{\gamma})^2 \gg 1$ , the Carreau model reduces to the power law model:

$$\eta(\dot{\gamma}) = \frac{\eta_0}{(\lambda\dot{\gamma})^{2p}} = m\dot{\gamma}^{n-1} \quad (1-12)$$

where the power law parameters  $m$  and  $n$  are equivalent to the following combinations of Carreau parameters:

$$m = \frac{\eta_0}{\lambda^{2p}}, \quad n = 1 - 2p \quad (1-13)$$

More complex models have been proposed to fit a wider range and group of viscosity data. Some are presented below [13].

The Yasuda model (or Carreau-Yasuda model) is a modification of the Carreau model with one more parameter  $a$  (total five parameters) [18]:

$$\text{Yasuda: } \eta(\dot{\gamma}) = \eta_\infty + \frac{\eta_0 - \eta_\infty}{[1 + (\lambda^2 \dot{\gamma}^2)^a]^{p/a}} \quad (1-14)$$

which reduces to the Carreau model for  $a=1$  ( $a$  is transition constant which describes the breadth of the transition range from zero-shear viscosity  $\eta_0$  to the power-law region). It is especially suitable for viscosity data for melting polymers with a broad molecular weight distribution, for which the zero-shear viscosity is approached very gradually. All these models reduce to Newtonian behavior at very low and very high shear rates and to power law behavior at intermediate shear rates.

The Meter model is a stress-dependent viscosity model, which has several same general parameters as the Carreau model.

$$\text{Meter: } \eta(\tau) = \eta_\infty + \frac{\eta_0 - \eta_\infty}{1 + (\tau/\sigma)^{2p}} \quad (1-15)$$

where  $\sigma$  is a characteristic stress parameter, and  $p$  is the shear thinning index.

#### 1.2.4 Temperature dependence of liquid viscosity

It is common sense that when the temperature of the liquid increases, it gets thinner (or its viscosity decreases). Rather than in gases, the molecular momentum transfer mechanism is dominated by the cohesive forces between the molecules in the liquids because of the closely-packed molecules. When the temperature of the liquid increases, the average energy of the molecules increases and the cohesive connection between the molecules becomes less; therefore the viscosity of the liquids decreases.

It is usually expressed by one of the following models [19]:

- a. Exponential model;

$$\eta(T) = \eta_0 \exp(-bT) \quad (1-16)$$

where  $T$  is the absolute temperature and  $\eta_0$  and  $b$  are coefficients. It is an empirical model and generally only works for a narrow range of temperatures

- b. Arrhenius model;

$$\eta(T) = \eta_0 \exp\left(\frac{E}{RT}\right) \quad (1-17)$$

where  $T$  is the absolute temperature,  $\eta_0$  is an Arrhenius constant,  $E$  is the activation energy and  $R$  is the universal gas constant. This equation is derived from the kinetic theory of thermodynamics based on the assumption that the fluid behaves as the Arrhenius equation for molecular kinetics.

- c. Williams-Landel-Ferry model;

$$\eta(T) = \eta_0 \exp\left(\frac{-C_1(T - T_r)}{C_2 + T - T_r}\right) \quad (1-18)$$

where  $T$  is the absolute temperature,  $C_1$ ,  $C_2$ ,  $T_r$  and  $\eta_0$  are empiric coefficients (only three of

them are independent from each other). This model is generally applied to fluids which have a glass transition temperature [19].

For non-Newtonian liquids, any parameter which is concerned with the dimensions or has viscosity physical significance (such as the Carreau parameters  $\eta_0$  and  $\eta_\infty$ , the power law parameters  $m$  &  $n$ ) has a temperature dependence similar to that of a Newtonian liquid [13, 20].

### **1.2.5 Engine oils and non-linear behaviors of viscosity in engine oils**

In order to improve the performance of engine oils, some viscosity modifiers are added during the production process. Viscosity modifiers can improve the viscosity/temperature properties of oils. After the modification, engine oils will not be too thin at high temperatures and not too thick at low temperatures. However, with viscosity modifiers added in, multigrade engine oils exhibit nonlinear behaviors of viscosity in engine. With long periods of high temperatures and pressure inside the engine, degradations such as chemical changes of the oil itself and pH value changes due to water condensation as well as contaminants and sludge accumulation in the oil are inevitable. All these will change the viscosity and nonlinearity of the oil. If these changes can be monitored by mounting real-time oil quality sensors, the oil condition can be checked instantly, reducing disposal frequency of engine oils, which will greatly benefit our environments and save cost and energy. Using proper engine oil or good quality oil will enhance the performance of engine and increase the lifetime of the automobile [5].

To increase automobile engines lifetime, engine oil manufacturers keep on developing new engine oils with enhanced additives to enhance the engine performance. The service life

of engine oil can fluctuate significantly and is dependent on many factors, such as oil category, engine type, engine condition and ambient circumstances [21, 22]. A device which can examine oil condition in a real time manner by on-line measuring of some important physical and chemical parameters is therefore highly desirable. Nowadays automobile manufacturers build in oil sensors by some algorithms or software which evaluates the actual oil condition indirectly. Normally the condition is attained by means of recording and processing vehicle information such as elapsed mileage since the last oil change and the cold starts times. And some of the algorithms are assisted by sensors which only measure the permittivity or conductivity of the oil due to its easiness [23, 24]. These physical and chemical parameters are usually associated with water content or acidity, which is also vital oil property. However, these are not direct measurements of the oil related to lubricant performance. In order to prolong oil drain intervals and meanwhile avoid engine failure from overly degraded oil, properties like viscosity should be considered. Viscosity is essential since it is one of the major parameters representing oil conditions and it directly relates to the ability to lubricate contacting parts in engine. To monitor the viscosity of the engine oil, some microacoustic devices have been developed and used to measure viscosity as described below [25, 26]. It should be mentioned that all these devices were developed to measure the viscosity only. As it is well known that some small changes in viscosity may not affect the engine very much, and it is also easy to find the viscosity of some fresh engine oil same as that of another type of used engine oil. Therefore, it is reasonable to assume that the non-linearity of viscosity may be the real key of determining engine oil conditions.



### **1.3 Conventional methods**

In order to measure viscosity, many methods have been developed. In traditional ways, viscosity is measured by different types of viscometers, such as the U-tube viscometer, the falling ball viscometer, and rotational viscometer [19]. A viscometer is a device applied to determine the viscosity of a fluid. In current research, sensor platforms such as acoustic wave (AW) devices are used to measure viscosity.

#### **1.3.1 U-tube Viscometer**

U-tube viscometers are known as glass capillary viscometers or Ostwald viscometers which are named after Wilhelm Ostwald. Another type is the Ubbelohde viscometer, which has a U-shaped glass tube fixed vertically in a controlled temperature bath. A vertical section of precise narrow bore (the capillary) is in one arm of the U-shape tube. A bulb is above this U tube, and there is another bulb lower down in the other arm. During use, liquid is extracted into the upper bulb by suction, and then run down into the lower bulb through the capillary. There are two marks (one above and one below the upper bulb) to show the volume of the liquid going through the capillary as shown in Figure 1.5. The time taken for this certain amount of the liquid to go between these two marks is proportional to the kinematic viscosity. Generally most commercial products provide a conversion factor, and with this factor the viscosity can be easily calculated by just measuring the time. And a fluid of known properties can be used in the calibration of this kind of viscometer. These viscometers are used to measure the kinematic viscosity of a liquid at very low shear rate.

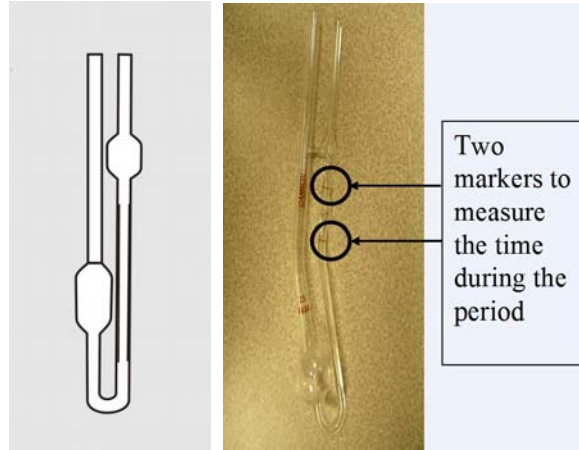


Figure 1.5. Schematic of U-tube viscometer

The physics principle of this type of viscometer is that the volume ( $V$ ) of liquid passing through a pipe per second is shown as [27]:

$$V = \frac{\pi r^4 P}{8l\eta} \quad (1-19)$$

where  $\eta$  is the viscosity of the liquid,  $r$  and  $l$  are the radius and length of the pipe, and  $P$  is the pressure difference between two ends of the pipes. In the U-tube viscometers, the result determined here is the kinematic viscosity of the liquid because the pressure is from the gravity of the liquid itself [27].

By measuring the time for the liquid level to go between two marks labeled on a capillary of a known diameter and multiplying the time by a certain factor of the viscometer, the kinematic viscosity is calculated.

Since the viscosity strongly relies on temperature, the U-tube viscometer usually has a constant temperature water bath to maintain the measuring temperature. This type of viscometer directly measures the viscosity. However, the experimental process is time-consuming and is not appropriate for automatic and engine tests.

U-tube viscometers are also classified as direct flow or reverse flow. Reverse flow

viscometers place the reservoir bulb above the capillary, while the direct flow viscometers have the reservoir bulb below the capillary. With these designs, the level can be easily observed and the time a certain amount of liquids passes by the marks can be determined even when opaque liquids are measured; otherwise the liquid could cover the markings and make it impractical to measure the time the liquid level goes through the markings [12, 27].

There are some commercial products available. For example,

**a) Cannon instrument.** Product: BS/U-Tube Viscometers for transparent liquids; Calibrated BS/U-TUBE (9724-E50) Series [28].

The measurement of kinematic viscosity of transparent Newtonian liquids follows the ASTM D445 and ISO 3104 standards. Specifications conform to ASTM D446 and ISO 3105.

The minimum sample volume is 7 mL for the viscometers in sizes from A to C, 12 mL in sizes D to F, and 23 mL in sizes G and H. This instrument requires a liquid bath depth of 280 mm (11 inches).

Size	Approx. constant, $\text{mm}^2/\text{s}^2(\text{cSt}/\text{s})$	Kinematic Viscosity Range $\text{mm}^2/\text{s}(\text{cSt})$
A	0.003	0.9 - 3
B	0.01	2.0 - 10
C	0.03	6 - 30
D	0.1	20 - 100
E	0.3	60 - 300
F	1	200 - 1000
G	3	600 - 3000
H	10	2000 - 10000




Table 1.1. Different types of U-Tube viscometers from Cannon instrument.

**b) RHEOTEK™.**

*1. Product: U-Tube Viscometers for transparent liquids.*

The measurement of kinematic viscosity of transparent Newtonian liquids follows ISO

3104, ISO 3105, ASTM D445, ASTM D446, IP 71, BS 188 standards.

All these viscometers are designed for measurement of transparent liquids. The nominal overall length is 300 mm. Approximate sample sizes are from 13 to 40 mL. The following table gives the sizes of the U-Tube viscometers [29].

PSL Ref	Size	Nominal Constant	Kinematic Viscosity Range mm <sup>2</sup> /s(cSt)
1619/00	O	0.001	0.3 to 1
1619/01	A	0.003	0.9 to 3
1619/02	B	0.01	2 to 10
1619/03	C	0.03	6 to 30
1619/04	D	0.1	20 to 100
1619/05	E	0.3	60 to 300
1619/06	F	1.0	200 to 1000
1619/07	G	3.0	600 to 3000
1619/08	H	10.0	2000 to 10000

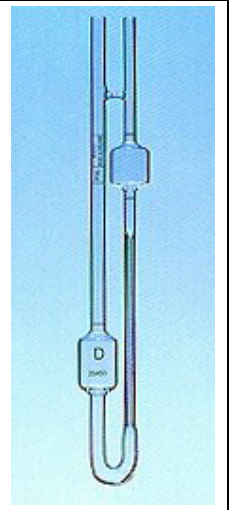


Table 1.2. Different types of U-Tube viscometers from RHEOTEK™.

*2. Product: U-Tube reverse-flow viscometers for transparent & opaque liquids.*

The measurement of kinematic viscosity of transparent & opaque Newtonian liquids follows ISO 3104, ISO 3105, ASTM D445, ASTM D446, IP 71, BS 188 standards.

All these viscometers are designed for the measurement of transparent and opaque liquids. The nominal overall length is 275 mm. The approximate sample size is from 12 to 25 mL. The following table gives the sizes of the U-Tube reverse-flow viscometers [30].

PSL Ref	Size	Nominal Constant	Kinematic Viscosity Range mm <sup>2</sup> /s(cSt)
1637/01	1	0.003	0.6 to 3
1637/02	2	0.01	2 to 10
1637/03	3	0.03	6 to 30
1637/04	4	0.1	20 to 100
1637/05	5	0.3	60 to 300
1637/06	6	1.0	200 to 1000
1637/07	7	3.0	600 to 3000
1637/08	8	10.0	2000 to 10000
1637/09	9	30.0	6000 to 30000
1637/10	10	100.0	20000 to 100000
1637/11	11	300.0	60000 to 300000

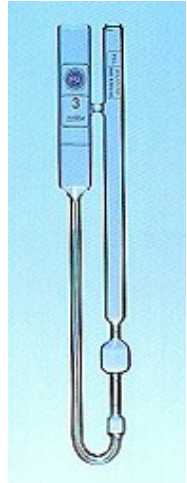


Table 1.3. Different types of U-Tube reverse-flow viscometers from RHEOTEK™.

### 1.3.2 Falling Ball Viscometers

The principle of falling sphere viscometer is based on the Stokes' law [7]:

$$\text{Stokes' law: } F_d = 6\pi\eta Rv \quad (1-20)$$

where  $F_d$  is the drag force of the fluid on a sphere with a velocity  $v$  relative to the fluid,  $\eta$  is the fluid viscosity, and  $R$  is the radius of the sphere. This type of viscometer consists of a circular cylinder containing the stationary fluid and several reference spheres. A reference sphere of known size and density is allowed to fall down through the liquid. The sphere falls down under two forces: visco-drag force and gravity force. The gravity force acting on the sphere is constant during the measurement, but the drag force of the fluid on a sphere depends on the velocity by the Stokes' law. Properly selected sphere reaches terminal velocity, which means the visco-drag force of liquid and gravity force reach equilibrium. And the time that the sphere takes to go by two markings on the cylinder is recorded. Electronic sensing can be applied in the measurement of opaque fluids. The viscosity of the fluid can be calculated using Stokes' law with the terminal velocity, the size and density of the sphere. To

get higher calculation accuracy, a group of steel balls of different diameters is usually applied in the measurement. And this viscometer is used widely in industries to get the viscosity of fluids, including many different oils and polymer liquids. The falling ball viscometer is a conventional and precise device for the viscosity measurement of a Newtonian material [12, 27].



Figure 1.6. Schematic of falling sphere viscometer (from Brookfield Engineering Laboratories, Inc. [31])

Falling ball viscometers are widely commercialized in many companies, such as

**a) Brookfield Engineering Laboratories, Inc.**

The Brookfield Falling Ball Viscometer can determine the viscosity of a Newtonian liquid by counting the time taken for a ball to fall down by its gravity through a tube with liquid inside. The tube is set on a hinge bearing which allows the tube to rotate 180 degrees easily, and in that way a repeat test can be done immediately. The result is the average of three measurements of how long it takes for the ball to fall. A final viscosity value is gotten from the time reading by a conversion formula. This falling ball viscometer is applied in processing control and quality control in different industries and also in academic

institutions to demonstrate basic scientific principles [31].

Technical Specifications	
<b>Viscosity Range</b>	0.5 mPa·s (cP) to 70,000 mPa·s (cP)
<b>Temperature Range</b>	-60 deg C up to 150 deg C
<b>Accuracy</b>	0.5% - 2.0% depending on choice of ball
<b>Material</b>	Balls 1 and 2, Born silica glass; Balls 3 and 4, Nickel iron alloy; Balls 5 and 6, Steel
<b>Ball Diameter</b>	11.0 mm to 15.81 mm
<b>Sample Tube Volume</b>	40mL
<b>Viscometer Dimensions</b>	180 x 220 x 330 mm
<b>Fall Time of Ball in Measurement</b>	30 to 300 seconds**

\*\*Falling times greater than 300 seconds allow measurement of liquids above 70,000 mPa·s (cP)

Table 1.4. Technical Specifications of falling ball viscometers from Brookfield.

#### b) Rheology Solutions, Inc.

The Falling Ball Viscometer type C is used to measure the viscosity of transparent Newtonian liquids. The sample viscosity is associated with the time a ball takes to go through a certain distance. Dynamic viscosity is given in the test results. This falling ball viscometer is mainly used for Newtonian liquids with low viscosities such as polymer solutions, solvents, inks, glycerine, gelatine, sugar solutions, oils, and liquid hydrocarbons [32].

Technical Specifications	
<b>Viscosity Range</b>	0.5 mPa·s (cP) to 10 <sup>5</sup> mPa·s (cP)
<b>Temperature Range</b>	-20 deg C up to 120 deg C
<b>Accuracy</b>	Better than 0.5%
<b>Material</b>	Balls 1, 2 and G, Born silica glass; Balls 3 and 4, Nickel iron alloy; Balls 5 and 6, stainless steel

Table 1.5. Technical Specifications of falling ball viscometers from Rheology Solutions.

#### c) Thermo Scientific HAAKE Falling Ball Viscometer.

The Thermo Scientific HAAKE falling ball viscometer is used to measure the viscosity of transparent Newtonian liquids such as polymers, inks, solvents and oils. This viscometer includes a thermometer with a range of -1°C to 26°C with 0.1°C divisions. Results are given

as dynamic viscosity in the units of milli-Pascal seconds (mPa·s) [33].

Technical Specifications	
Viscosity range	0.5 to 10 <sup>5</sup> mPa·s (cP)
Accuracy	Better than 0.5%
Range	Ball 1: 0.6 to 10 mPa·s; Ball 2: 9 to 140 mPa·s; Ball 3: 40 to 700 mPa·s; Ball 4: 150 to 5000 mPa·s; Ball 5: 5000 to 50,000 mPa·s; Ball 6: >7500 mPa·s
Wetted parts	Falling tube: boron silica glass; Balls 1 and 2: boron silica glass; Balls 3 and 4: nickel iron alloy; Balls 5 and 6: stainless steel
Temp range	-20 to 120°C (-4 to 248°F)

Table 1.6. Technical Specifications of falling ball viscometers from Thermo Scientific HAAKE.

### 1.3.3 Rotational Viscometers

Rotational viscometers are designed from the principle that the torque needed to rotate an object in a fluid is related to the shear stress and is a function of the viscosity of that fluid. The torque needed to turn a bob or disk in a fluid at a certain speed is measured, and the viscosity can be determined by calculations of shear stress, shear rate and torque [27, 34-35].

There are two types of rotational viscometers: “Cup and bob” viscometers and “Cone and Plate” viscometers as shown in Figure 1.7.

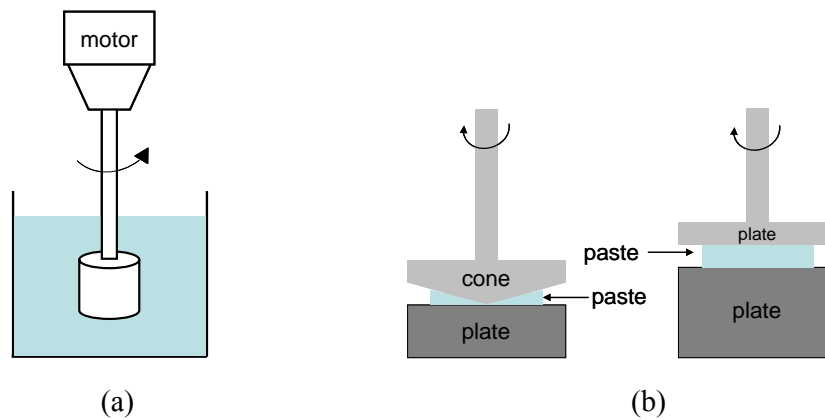


Figure 1.7. (a) Schematic of “Cup and bob” viscometers; (b) Schematic of “Cone and Plate” viscometers.



“Cup and bob” viscometers use a certain volume of liquid sample to be tested. The liquid is sheared within a test container (the cup). The torque required for the bob to reach a preset rotational speed is measured and plotted to get the liquid viscosity value. “Cup and bob” rotational viscometers can be divided into two types, the Couette and the Searle systems, by whether the cup or the bob rotates. The rotating cup is preferred in some cases because it could reduce the beginning of Taylor vortices; however, this type of rotation will cause measurement inaccuracy due to nonuniform temperature distribution [36, 37].

“Cone and Plate” viscometers use a cone of very low angle with little contact to a flat plate. A small amount of fluid is between the cone and the plate, and the cone rotates at a certain angular rate. The shear rate under the plate in this system is constant in a certain precision degree, and the required torque is measured to determine the viscosity value in a direct way [36].

Following are some commercial products from various companies.

**a) Brookfield Engineering Laboratories, Inc.**

The CAP 1000+ Viscometer is a compact, heavy-duty instrument which can measure viscosity of small sample sizes. It also has integrated rapid temperature control with a built-in Peltier element in sample plate. It has standard speeds including 750 and 900 rpm to provide shear rate at  $10,000 \text{ sec}^{-1}$ . The measurement follows ISO 2884, ASTM D4287, and BS 3900 standards [38]. The position of the cone can be automatically changed. The sample size can be as small as 1 mL. Additionally, there are other types of rotational viscometers from Brookfield. For example, CAP 2000+ Viscometer can measure viscosity from 0.2 poise to 10k poise at temperatures from  $5^{\circ}\text{C}$  to  $235^{\circ}\text{C}$  [39].

**b) Thermo Scientific HAAKE Rotational Viscometer.**

The HAAKE Viscotester VT550 is suitable for the comprehensive characterization of Newtonian and non-Newtonian fluids. It is a rotational viscometer with an immersed rotor applied to a fluid. And in order to get high accuracy, the speed of a stepper motor is changed by a micro step controller. The resistance of the fluid against this applied speed is measured by the deflection of a torsion bar with a non-contact transducer to avoid wear. The preset speed, which is maintained by the torque, is proportional to the viscosity. All details about the viscosity, shear stress and the shear rate is gotten from the torque required, the set speed and the geometry factors of the applied sensor [40].

Technical Specifications	
Sample volume	50 - 500 cm <sup>3</sup>
application:	construction materials
viscosity range	50 – 1,000,000 mPa·s
number of speeds	continuous
speeds:	0.5 - 800 rpm / 0.1 steps
temperature range	0 - 100°C
typical measurement time	2 - 3 minutes
repeatability	+/- 3%
voltage	100 - 230 V

Table 1.7. Technical Specifications of rotational viscometers VT550 from Thermo Scientific HAAKE.

**1.4 Active acoustic wave (AW) resonators as viscometer and current research**

In current research, sensor platforms such as acoustic wave (AW) devices are used to measure viscosity. AW devices works as AW resonators using resonance frequency as sensor platform signals, and some of them have already been applied in the industry, such as vibrational viscometers [2, 27].

### **1.4.1 Vibrating Viscometers**

Vibrational viscometers can determine viscosity by measuring the signal damping of a resonator immersed in a fluid. The resonator could be an oscillating sphere or a tuning fork which oscillates in torsion or transversely in the liquid. As known, AW devices have a damping effect when operated in medium, such as engine oil. The higher the viscosity, the larger the damping force added on the resonator. The damping factor can be determined by one of the following methods [2]:

- a. Measuring the power input needed to maintain the oscillator vibrating at constant amplitude. The higher the viscosity, the more power is required to keep the same vibration amplitude.
- b. Measuring the decay time of the vibration when the excitation pulse is turned off. The higher the viscosity, the more rapidly the signal damps.
- c. Measuring the frequency of the resonator as a function of the phase angle between excitation and response signals. The higher the viscosity, the larger the frequency shifts for a certain phase change.

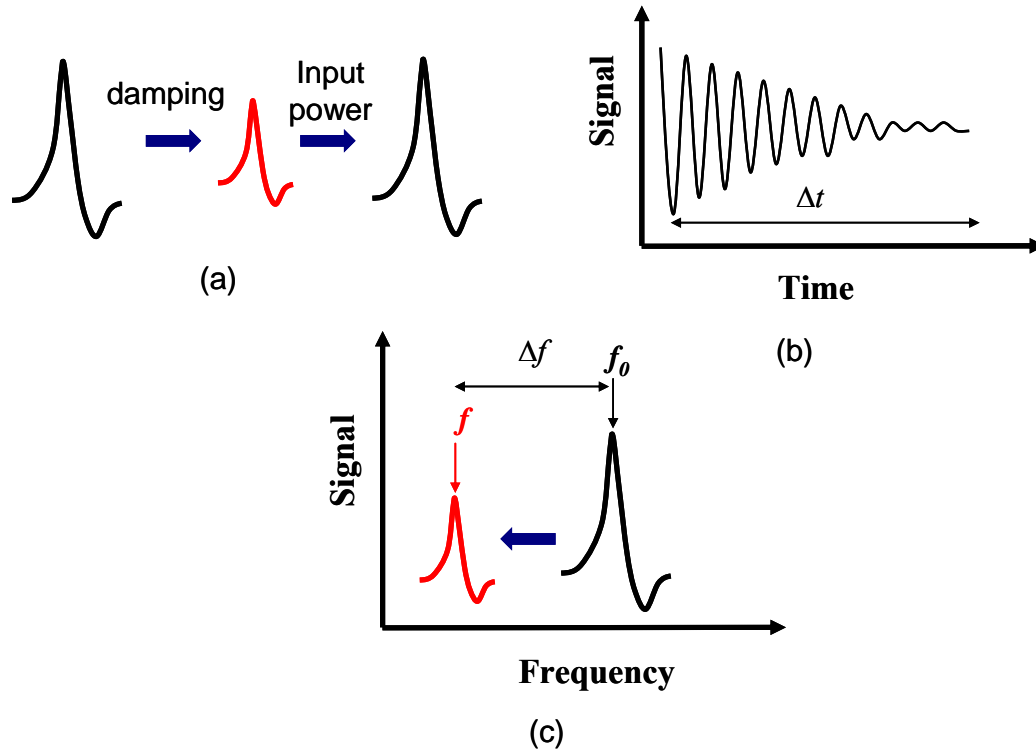


Figure 1.8. Several different methods to measure the damping factor: (a) Measuring the power input; (b) Measuring the decay time; (c) Measuring the frequency shift.

However based on these methods, it is not practical to measure the viscosity of a fluid if we have no idea of this fluid flow behavior before, because vibrational viscometers cannot generate a certain shear rate field.

Vibrating viscometers acting as an industrial system can measure viscosity in tough process conditions. The active sensing part of the viscometer is a vibrating rod or sphere. The vibration amplitude changes with the viscosity of the fluid in which the sensing part is put. These viscometers can measure clogging fluid and high-viscosity fluids, even with fibers inside (up to 1,000 Pa·s). Presently, vibrational viscometers are regarded as the most efficient system by many industries around the world because of their capability of measuring viscosities in quite a broad range, compared to rotational viscometers, which require more maintenance, lack the ability to deal with clogging fluid, and need regular calibration after

extensive use. The sensing part of vibrating viscometers is quite small. And even very basic or acidic fluids can be measured by coating a protective layer or by changing the material of the sensor to a material such as Hastelloy or enamel [2, 27, 36].

There are some commercial vibrational viscometers available. For example,

**a) A&D Company Ltd.** Product: Viscometer SV-10 / SV-100 Series Sine-wave Vibro Viscometer [41];

These series of Vibro Viscometer choose the tuning fork vibration method and provide 1% repeatability for viscosity measurement. A wide range of viscosity can be measured without changing the sensor plates (SV-10: 0.3 mPa·s-10,000 mPa·s; SV-100: 1,000 mPa·s-100,000 mPa·s). The standard sample cup requires 35ml of sample fluid (Optional 10ml/13ml sample cups are also available). The SV series can detect accurate temperature immediately because the sensor plate is very thin and small, so it can reach thermal equilibrium in a few seconds. As a result, viscosity can be monitored in real-time.

Measurement Method	Tuning Fork Vibration Method
Vibration Frequency	30Hz
Viscosity Measurement Unit	SV-10: mPa·s , Pa·s , cP , P SV-100: Pa·s, P
Viscosity Measurement Range	SV-10: 0.3 - 10,000 mPa·s (cP); SV-100: 1-100 Pa·s
Accuracy (Repeatability)	1% of Reading (Full Range)
Operating Temperature	10 – 40 °C ( 50 – 104 °F)
Minimum Sample Amount	Standard Sample Cup 35 ml, Optinal Small Sample Cup 10ml, Optinal Glass Sample Cup 13ml
Temperature Measurement	0 – 160 °C / 0.1 °C(32 – 212 °F)
Interface	RS-232C
Physical Dimensions	Main Unit: 332 ( <i>W</i> ) x 314 ( <i>D</i> ) x 536 ( <i>H</i> ) mm / Approx. 5.0 kg

Table 1.8. Technical Specifications of vibrational viscometers SV-10/100 from A&D Company Ltd.

**b) BiODE Inc.** Product: ViSmart™ Solid State Viscosity Sensor.

The BiODE ViSmart sensor system can measure viscosity from 0 to 100,000 cP ranges with  $\pm 1\%$  repeatability over a temperature range from  $-20^{\circ}\text{C}$  to  $135^{\circ}\text{C}$ . The ViSmart sensor has no moving parts, uses semiconductor technology and is hermetically packaged. It can provide in-line, real-time viscosity and temperature measurements [42].

#### **1.4.2 Current research on AW viscometer (advantage over traditional one, and challenges)**

Compared to traditional types of viscometers which have rather large size and are not easy to carry, AW devices can do better job in visco-liquid because they are small solid-state devices that have no macroscopically moving parts and also can be applied to advanced packaging techniques. They can do instant and in-line measurement. New technologies based on AW principles have been developed and many patents about AW-based viscometers have been issued [43-47].

The damping effect of AW vibration takes place when the viscosity and density of the medium change, and it will have two main results: one is the reduction in the resonance frequency; the other is the reduction in the Q value. The Q value describes the sharpness of the resonance peak, and a high Q value gives more accuracy in determining resonance frequency. Currently, most AW devices of measuring viscosity are based on the resonance frequency [2, 26, 36].

The AW devices that are most generally used for sensing application in visco-liquid include the thickness shear mode (TSM) resonator [48], microcantilever (MC) [49], and magnetostrictive strips [50].

The thickness shear mode (TSM) resonator, also known as the quartz crystal

microbalance (QCM), is the simplest and most used acoustic wave device [48]. TSM typically consists of a thin AT-cut quartz disk with circular electrodes deposited on the center of both sides. Due to piezoelectric effect, a shear deformation across the crystal is generated by applying electric potential between the electrodes. TSM sensors are easy to manufacture, stable over a broad temperature range, sensitive to external forces added on the crystal surface and also can withstand cruel environments [51]. Because of its shear wave propagation component, the TSM resonator is also theoretically applicable for detecting and measuring liquids [52]. However quartz crystals, oscillating in the thickness shear mode, produce lateral displacement amplitudes around 1-2 nm, with around 0.25 $\mu\text{m}$  of solution penetration depth of a 5MHz lateral shear wave in water before being attenuated [53]. At this high frequency range, the shear wave is not properly formed due to the short transient time between the maxima and minima of the driving force or velocity. Also, these high frequency shear waves greatly weak and dissipate quickly in a very short distance, especially in the liquids such as used engine oils that contain particles. All these factors hinder efficient measurement of shear wave velocity and determination of viscosity.

If the fluid contains polymers or higher molecular weight surfactants, then it is likely that the measured viscosity will depend on the measurement method which means different results are obtained at different shear rates. Due to very small lateral displacement amplitudes ( $\sim 1\text{nm}$ , much smaller than 100nm, which is the normal chain length of polymers [54, 55]) on the QCM surface, non-Newtonian behavior related to nonlinear effects may not be presented in QCM measurement. Compared to polymer chain length, a small lateral vibration amplitude cannot really characterize the structure (with polymer contained) and flow behaviors inside

the liquids as shown in Figure 1.9. Furthermore, viscous drags in oils result in significantly high values of resistance, which would cause a small lateral displacement to decrease further.

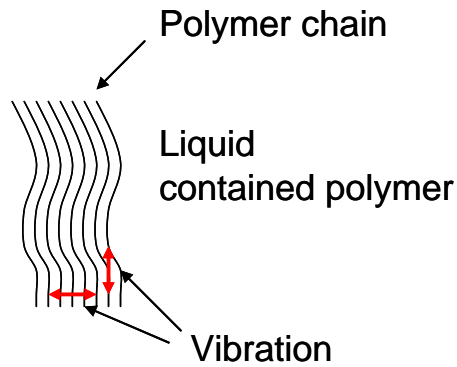


Figure 1.9. Illustration of small vibration displacement inside liquid contains polymer.

Because of a small vibration amplitude not suitable for presenting non-Newtonian behavior, AW devices with a lower resonance frequency and higher vibration displacement are applied to visco-liquid measurement. Bending modes normally have lower resonance frequencies than the thickness mode. It makes bending-mode devices more suitable for sensing the nonlinearity of viscosity [27]. PZT-based piezoelectric unimorph cantilever can act as a liquid viscosity-and-density sensor. It can deduce the viscosity by sensing resonance frequency change and/or resonance peak width change in the liquid from some models, such as the oscillating-sphere model [56, 57] and beads model [58]. And it is found that in some viscosity ranges (1~600cP) the experiment results are in close agreement with the prediction of the model [56]; however, in higher viscosity environments the cantilever has rather poor performance, such as low amplitude and low quality factor value ( $<10$ ) [59].

Magnetostrictive strip is an excellent candidate for liquid sensing because of relatively small damping in liquid compared to the cantilever [50, 60], while the strong damping effect of the cantilever in liquid produces a very low quality factor (Q) of 2-10, about two orders of



magnitude lower than in air [59]. A longitudinal elastic standing wave is excited in the magnetostrictive strip sensors by a small AC magnetic field superimposing on a relatively larger DC magnetic field (bias). The phase velocity of elastic wave and its resonant frequency is dependent on the characteristics (such as viscosity, density) of the ambient medium which touches the sensor surface [50, 61]. And magnetostrictive strip sensor shows a linear shift in resonant frequency and quality factor with the properties of the liquid (square root of the product of density and viscosity) [61].

Below are the review of AW devices and a comparison of vibration displacement and maximum shear rate of different AW devices.

Techniques	Advantages	Disadvantages
<b>TSM Resonator</b> Thickness Shear Mode	Withstand cruel environments; Easy to manufacture; Stable over broad temperature range.	Very high frequency (~5MHz) and small lateral displacement (~nm).
<b>Cantilevers</b>	Low resonance frequency and big displacement at tip of cantilever.	Rather poor performance in a viscous environment.
<b>Magnetostrictive Strip</b>	Compact size; Wireless (stimulated by magnetic field); High Q value in visco-liquid.	Medium high resonance frequency (~100kHz)

Table 1.9. Review of AW devices.

Techniques	Vibration Displacement (in R-100 reference oil)	Maximum Shear rate ( $\dot{\gamma}$ ) (in R-100 reference oil)
<b>QCM Resonator</b>	2 nm (for 5MHz QCM)	$3 \times 10^4$ (s <sup>-1</sup> )
<b>Cantilevers</b>	2 $\mu$ m (tip-displacement for 9mm*0.8mm*0.5mm PZT cantilever)	92 (s <sup>-1</sup> ) for $f_r=1000$ Hz 322 (s <sup>-1</sup> ) for $f_r=2300$ Hz
<b>Magnetostrictive Strip</b>	0.15 $\mu$ m (for 25mm*3mm*30 $\mu$ m Magnetostrictive Strip)	$5 \times 10^3$ (s <sup>-1</sup> ) for $f_r=80$ kHz

Table 1.10. Comparison of AW devices.

The effective regions of different AW devices in structural viscosity non-Newtonian liquid

are shown in Figure 1.10 based on Table 1.10.

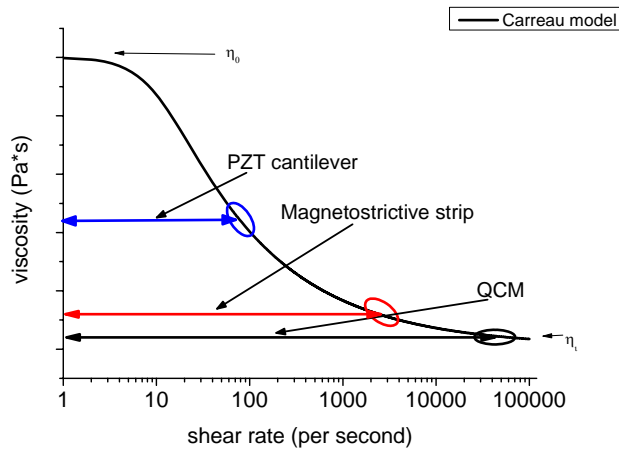


Figure 1.10. Effective region of different AW devices in structural viscosity non-Newtonian liquid based on Table 1.8.

Although there are many advantages of current AW devices mentioned above, still two issues remain behind: Firstly, due to the working principle of AW devices, the shear rate is not constant during the vibration. This will cause problems when applied in a non-Newtonian liquid because its apparent viscosity depends on the shear rate, which means different results could be gotten at different shear rates. The typical method to characterize viscosity, which is based on only one parameter  $f_r$  (resonance frequency), is no longer effective. Secondly, the displacement of AW devices is not infinite during the vibration, which is not in accordance with simple shear case.

### 1.5 Research objectives

Most AW sensors in visco-liquid only use a single characteristic frequency as the experimental parameter to represent the liquid properties, which is enough for Newtonian oil because of its linearity of viscosity. However for non-Newtonian oil, nonlinearity behavior cannot be presented by just one characteristic resonance frequency of the liquid.

In this research, multiple experimental characteristic frequencies which can be gotten simultaneously for each liquid are used to set up the model. For Newtonian oil, due to the independence of viscosity with shear rate, one experimental parameter, such as  $f_r$  (resonance frequency), is enough to describe the liquid viscosity, while in non-Newtonian oil viscosity changes with shear rate and velocity. Additional parameters are needed to present this nonlinearity, such as  $f_r$ ,  $f_r'$  and  $f_0$ . Normally  $f_r$  (resonance frequency) is selected at the maximum signal point,  $f_r'$  (anti-resonance frequency) is selected at the minimum signal point and  $f_0$  (experimental-resonance frequency) is picked up somewhere between these two points. These three experimental characteristic frequencies distribute within a rather broad range in which displacement, velocity and shear rate change greatly as shown in Figure 1.11. The nonlinearity of viscosity is also apparent in this range. And based on Figure 1.10, the effective regions of all three types of AW devices cover Newtonian and non-Newtonian behaviors. However due to the small lateral displacement of QCM resonator, only cantilever and magnetostrictive strip are chosen in this study.

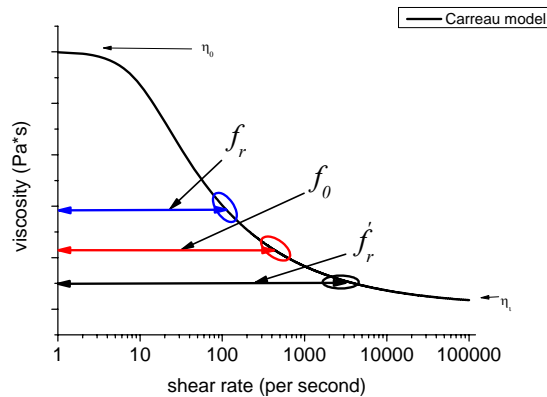


Figure 1.11. Illustration of different range covered by  $f_r$ ,  $f_r'$  and  $f_0$  three experimental characteristic frequencies in structural viscosity non-Newtonian liquid.

The information of the whole resonance behavior curve can be fully used to illustrate the

liquid's properties by using  $f_r$ ,  $f_r'$  and  $f_0$  three experimental characteristic frequencies.

Therefore, to solve the above problems, my research includes four parts:

- (1) Characterize the resonance behaviors of magnetostrictive strip sensors;
- (2) Develop magnetostrictive strip sensors to identify the nonlinearity of liquids;
- (3) Develop piezoelectric cantilever sensors to identify the nonlinearity of liquids;
- (4) Numerical simulations to identify the nonlinearity of viscosity by using AW sensors.

**References:**

- [1] John Harris, Walter Benenson, Horst Stöcker, *Handbook of physics*, Springer, 2002.
- [2] Dabir S. Viswanath, Tushar K. Ghosh, Dasika H. L. Prasad, *Viscosity of Liquids: Theory, Estimation, Experiment, and Data*, Springer, 2006.
- [3] M. A. Rao, *Rheology of Fluid and Semisolid Foods: Principles and Applications*, Springer, 2007.
- [4] George E. Totten, *Handbook of Lubrication and Tribology: Application and Maintenance*, CRC Press, 2006.
- [5] Arthur Caines, Roger Haycock, *Automotive Lubricants Reference Book*, Society of Automotive Engineers, Inc. 1996.
- [6] Symon, Keith, *Mechanics* (Third ed.). Addison-Wesley. 1971.
- [7] L. D. Landau and E. M. Lifshitz, *Fluid Mechanics*, Pergamon, London, 1959,
- [8] James A. Fay, *Introduction to Fluid Mechanics*, MIT press, 1994.
- [9] J. Happel and H. Brenner, *Low Reynolds number hydrodynamics*, Prentice-Hall, 1965.
- [10] Joseph A. Schetz, Allen E. Fuhs, *Fundamentals of fluid mechanics*, John Wiley, 1999.
- [11] Raymond A. Serway, *Physics for Scientists & Engineers* (4th ed.). Saunders College Publishing, 1996.

- [12] H. A. Barnes, *A handbook of elementary rheology*, Institute of non-Newtonian Fluid Mechanics, 2000.
- [13] Ron Darby, *Chemical Engineering Fluid Mechanics*, Marcel Dekker, Inc., 2001.
- [14] E.C. Bingham, "An Investigation of the Laws of Plastic Flow", U.S. Bureau of Standards Bulletin, 1916, 13, 309-353.
- [15] Fixman, M. Polymer Dynamics: Non-Newtonian Intrinsic Viscosity, J. Chem. Phys. 1966, 45, 793-803.
- [16] R. Pamies, M. C. Lopez Martinez, J. G. Hernandez Cifre, and J. Garcia de la Torre, Non-Newtonian Viscosity of Dilute Polymer Solutions, *Macromolecules*, 2005, 38, 1371-1377.
- [17] Hsuan-Wei Hu, George A. Carson, and Steve Granick, Relaxation time of confined liquids under shear, *Phys. Rev. Lett.* 66, 2758-2761 (1991).
- [18] K. Yasuda, R. C. Armstrong and R. E. Cohen, Shear flow properties of concentrated solutions of linear and star branched polystyrenes, *Rheologica Acta*, Volume 20, 2, 163-178, 1981.
- [19] Christopher J. Seeton, Viscosity–temperature correlation for liquids, *Tribology Letters*, 22, 1, 67-78, 2006.
- [20] S. Girardo, R. Cingolani and D. Pisignano, *Investigating the temperature dependence of the viscosity of a non-Newtonian fluid within lithographically defined microchannels*, J. Chem. Phys., 127, 164701-5, 2007.
- [21] S.E. Schwartz, D.J. Smolenski, Development of an Automatic Engine Oil-Change Indicator System, SAE Technical Paper 870403, 1987.
- [22] R. Thom, K. Kollmann, W. Warnecke, M. Frend, Extended Oil Drain Intervals: Conservation of Resources or Reduction of Engine Life, SAE Technical Paper 951035, 1995.
- [23] F. García-Goldinga, M. Giallorenzoa, N. Morenoa and V. Changa, Sensor for determining the water

content of oil-in-water emulsion by specific admittance measurement, *Sensors and Actuators A*, 47, Issues 1-3, (1995) pp. 337-341.

[24] S. S. Wang, Road tests of oil condition sensor and sensing technique, *Sens. Actuators B* 73 (2–3) (2001) 106–111.

[25] J. M. Hammond, R. M. Lec, X. J. Zhang, D. G. Libby, L. A. Prager, An acoustic automotive engine oil quality sensor, Frequency Control Symposium, 1997., Proceedings of the 1997 IEEE International, May 1997, pp. 72-80.

[26] B. Jakoby, M. Scherer, M. Buskies, H. Eisenschmid, Microacoustic viscosity sensor for automotive applications, *Ind. Sensor Syst.*, Vienna Univ. of Technol., Austria; *Sensors*, 2002. Proceedings of IEEE, vol.2, pp.1587-1590.

[27] A. A. Collyer, D. W. Clegg, *Rheological measurement* (2nd edition), Springer, 1998.

[28] “<http://www.cannoninstrument.com/bsutube.htm>”

[29] “<http://www.rheotek.com/scat.asp?id=72>”

[30] “<http://www.rheotek.com/scat.asp?id=82>”

[31] “<http://www.brookfieldengineering.com/products/viscometers/laboratory-falling-ball.asp>”

[32] “[http://www.rheologysolutions.com/fallingball\\_techs.html](http://www.rheologysolutions.com/fallingball_techs.html)”

[33] “[http://www.thermo.com.cn/Resources/200802/productPDF\\_2604.pdf](http://www.thermo.com.cn/Resources/200802/productPDF_2604.pdf)”

[34] T. Seckin and S. M. Kormaly, An Easy-to-Build Rotational Viscometer with Digital Readout, *J. Chem. Educ.*, 1996, 73 (2), p 193-194.

[35] J. F. Hills, A rotational viscometer employing a reference liquid, *Journal of Scientific Instruments*, 35, (1958), pp 415-418.

[36] Thomas G. Mezger, *The rheology handbook: for users of rotational and oscillatory rheometers*,

Vincentz Network GmbH & Co KG, 2006, p 259.

[37] U. A. Al-Mubaiyedh, R. Sureshkumar and AND B. Khomami, The effect of viscous heating on the stability of Taylor-Couette flow, *J. Fluid Mech.* (2002), vol. 462, pp. 111-132.

[38] "<http://www.brookfieldengineering.com/products/viscometers/laboratory-cap-1000.asp>"

[39] "<http://www.brookfieldengineering.com/download/files/CAPBro.pdf>"

[40] "<http://rotationalviscometer.org/haake-vt550/>"

[41] "[http://www.aandd.jp/products/test\\_measuring/pdf/sv.pdf](http://www.aandd.jp/products/test_measuring/pdf/sv.pdf)"

[42] "<http://www.controlglobal.com/vendors/products/2006/079.html>"

[43] J. G. Gallagher, Mechanical resonator system, United States Patent 6813935.

[44] J. C. Andle, Sensor, system, and method for measuring fluid properties using multi-mode quasi-shear-horizontal resonator, United States Patent 7878044.

[45] F. Herrmann, D. Hahn, G. Flik, Sensor array and method for determining the density and viscosity of a liquid, United States Patent 6543274.

[46] S. J. Martin et al, Quartz resonator fluid density and viscosity monitor, United States Patent 5741961.

[47] Miura, Shinsuke, T. Odagiri, Resonant liquid detecting device, United States Patent 5596139.

[48] D. S. Ballantine, White, R.M., Martin, S.J., Ricco, A.J., Frye, G.C., Zellers, E.T., Wohltjen, H., *Acoustic wave sensors: theory, design and physico-chemical applications*: Academic Press, 1997.

[49] A. Agostona, F. Keplingerb and B. Jakobyb, Evaluation of a vibrating micromachined cantilever sensor for measuring the viscosity of complex organic liquids, *Sensors and Actuators A*, Volumes 123-124, (2005) pp. 82-86.

[50] P. G. Stoyanov, C. A. Grimes, A remote query magnetostrictive viscosity sensor, *Sensors and Actuators*, 80 (2000), 8-14.

- [51] M.G. Schweyer, J.A. Hilton, J.E. Munson, J.C. Andle, J.M. Hammond, R.M. Lec, A novel monolithic piezoelectric sensor, pp. 32-40 Proc Ultrasonics Symposium, Vol. 1, 1997 IEEE INTERNATIONAL FREQUENCY CONTROL SYMPOSIUM.
- [52] B. Drafts, Acoustic wave technology sensors, *IEEE Transactions on Microwave Theory and Techniques*, vol. 49, pp. 795-802, 2001.
- [53] C. Steinem, A. Janshoff, *Piezoelectric sensors*, pp374, Springer, 2007.
- [54] Y. Roiter, S. Minko, AFM Single Molecule Experiments at the Solid-Liquid Interface: In Situ Conformation of Adsorbed Flexible Polyelectrolyte Chains, *Journal of the American Chemical Society* 127 (45): 15688-15689, 2005.
- [55] P. C. Painter, M. M. Coleman, *Fundamentals of Polymer Science: an introductory text*, Lancaster, PA, Technomic Pub. Co., 1997.
- [56] W.Y. Shih, X. Li, H. Gu, W. H. Shih, I.A. Aksay, Simultaneous liquid viscosity and density determination with piezoelectric unimorph cantilevers, *Journal of Applied Physics*, 89, 2 (2001).
- [57] P. I. Oden, G. Y. Chen, R. A. Steele, R. J. Warmack, and T. Thundat, Viscous drag measurements utilizing microfabricated cantilevers, *Appl. Phys. Lett.* 68 (26), 24 (1996)
- [58] Y. Hirai, R. Mori, H. Kikuta, N. Kato, K. Inoue, and Y. Tanaka, Resonance characteristics of micro cantilever in liquid, *Jpn. J. Appl. Phys.* Vol. 37 (1998) pp. 7064-7069
- [59] Javier Tamayo, Energy dissipation in tapping-mode scanning force microscopy with low quality factors, *Appl. Phys. Lett.* 75, 3569 (1999)
- [60] C. A. Grimes, C. S. Mungle, K. Zeng, M. K. Jain, W. R. Dreschel, M. Paulose and K. G. Ong, Wireless Magnetoelastic Resonance Sensors: A Critical Review, *Sensors* 2002, 2, pp. 294-313.
- [61] M. K. Jain and C. A. Grimes, Effect of surface roughness on liquid property measurements using



mechanically oscillating sensors, *Sensors and Actuators A* 100 (2002), pp. 63-69.

## CHAPTER 2

### FUNDAMENTAL STUDY OF MAGNETOSTRICTIVE STRIP RESONANCE

#### BEHAVIORS AND LOCATION EFFECTS IN PICK-UP COILS

##### 2.1 Introductions

Development of viscometers based on AW devices has caught much attention because AW devices have no macroscopically moving parts and can do instant measurement [1]. However, current AW devices still have some big challenges in realistic applications. Some AW devices, such as quartz crystal microbalance (QCM), can work well in liquid [2], but have a small lateral displacement and high shear rate, where in this shear rate range non-Newtonian oils start to exhibit Newtonian behaviors [2, 3]; while other AW devices, such as cantilevers, exhibit a big lateral displacement, but with a small Q value [4].

Developing high-performance portable on-line sensors is in urgent need. Magnetostrictive materials have been studied for the development of high-performance sensors of measuring temperature, pressure, liquid density and viscosity for their unique features such as magnetostrictive interactions and remote sensing [5].

Magnetostrictive strip is introduced as a high performance sensor platform. It is a free standing magnetostrictive sensor operating based on magnetostriction. The direction of magnetization inside the magnetostrictive strips will change to the external magnetic field direction when exposed to an external field. A magnetostrictive stress will generate due to the redirection, and in bulk material this stress causes the dimensions to be changed [6]. Typically this ribbon-like strip is made from amorphous ferromagnetic alloys, such as  $\text{Fe}_{40}\text{Ni}_{38}\text{Mo}_4\text{B}_{18}$

(Metglas 2826MB, one of the commercially available magnetostrictive materials). Magnetostrictive films mechanically deform when a magnetic field adds on. Longitudinal vibrations occur and the elastic waves generate within the sensor, while the maximum amplitude is achieved at the mechanical resonance frequency. The magnetic flux emission which is generated by the mechanical deformations can be sensed remotely [6]. And the resonance frequency can be measured by acoustic, magnetic and optical methods. The  $n^{\text{th}}$  resonance frequency of the longitudinal vibrations can be expressed as [7]:

$$f_n = \frac{n}{2l}v \quad (n=1, 2, 3\dots) \quad (2-1)$$

where  $l$  is the length of the sensor and  $v$  is the acoustic velocity in the magnetostrictive material and is normally regarded as a constant in certain materials. The acoustic velocity depends on the Young's modulus ( $E$ ), the density ( $\rho$ ) and the Poisson's ratio ( $\sigma$ ) of the material as below:

$$v = \sqrt{\frac{E}{\rho(1-\sigma^m)}} \quad (m=1 \text{ or } 2) \quad (2-2)$$

The value of  $m$  is either one or two which depends on the geometry of the magnetostrictive strip [7, 8].

When magnetostrictive strip is put into liquids, a damping effect will act on the sensor oscillations due to the viscosity and density changes of the surrounding medium. The resonance frequency shift  $\Delta f$  is shown as [9]:

$$\Delta f = \frac{\sqrt{f_0}}{2\pi\rho d} \sqrt{\eta\rho_l} \quad (2-3)$$

where  $f_0$  is the initial resonance frequency,  $\rho_l$  and  $\eta$  are the density and viscosity of the liquid,  $d$  is strip thickness and  $\rho$  is the density of the strip sensor.

The sensing mechanism is established based on the resonance behaviors' change of

magnetostrictive materials when the surrounding medium changes. Based on this principle, magnetostrictive materials can be used in many applications, such as mechanical stress sensors [10], pressure sensors [11, 12], temperature sensors [13], flow rate sensors [14], and liquid density and viscosity sensors [15, 16]. For driving and sensing strips, no physical connection is needed between the sensor and interrogation system since it can be stimulated through a magnetic field. Therefore, magnetostrictive strips are wireless sensors, which enable remote detection. Furthermore, the feasibility study demonstrates that magnetostrictive strips exhibit a high Q-value and work well in liquid media. And magnetostrictive strips are cost-effective because magnetostrictive alloys are very inexpensive. When magnetostrictive strips are put into a liquid, the resonance frequency will shift downward to lower values due to the damping force related to some function of the liquid density and viscosity added on the sensors [9, 15-17]. The wireless, remote-detection properties of magnetostrictive strip sensors could have many advantages where direct electrical connections are not practicable.

## **2.2 Configuration of magnetostrictive strip sensor**

The magnetostrictive strip sensor platform has a rather simple configuration compared to other systems: it is a free-standing strip made from magnetostrictive alloy. The dimensions of the strip are the length of  $L$ , width of  $w$  and thickness of  $t$ . The length is bigger than the width, and the width is bigger than its thickness ( $L > w > t$ ). Figure 2.1 shows the configuration of the strip.

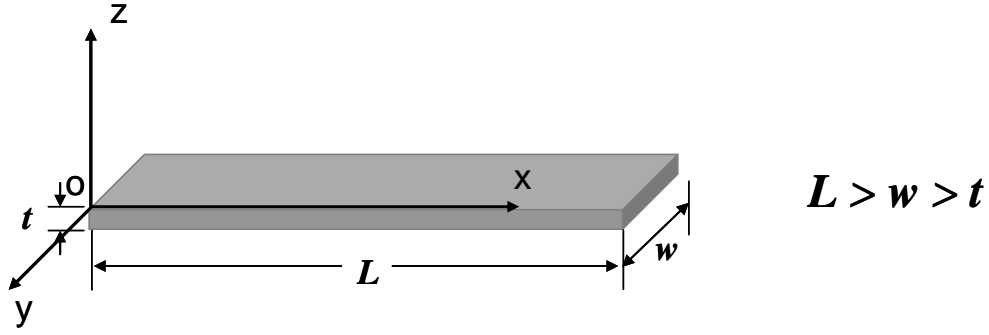


Figure 2.1. The magnetostrictive strip configuration.

Due to the magnetostrictive effect, the magnetostrictive strip will vibrate when exposed to a time-varying external magnetic field. Extensions or compressions along all directions will be generated when an alternating magnetic field is applied. In the sensor design, resonance along the length direction is used due to the longitudinal vibration mode. As shown in Fig. 2.1, the magnetostrictive strip is in its basal XY plane, with the length of the strip along the  $x$ -axis. By the theoretical model which expresses thin elastic plate longitudinal oscillation [18], the vibration of the magnetostrictive strip along its length direction ( $x$ -direction) can be illustrated as following:

$$\frac{\partial^2 u(x,t)}{\partial t^2} - \frac{E}{\rho(1-\sigma^m)} \frac{\partial^2 u(x,t)}{\partial x^2} = 0 \quad (2-4)$$

where  $E$ ,  $\rho$ , and  $\sigma$  are the Young's modulus, density, and Poisson ratio of the material correspondingly,  $m$  is either 1 or 2 which depends on the geometry of the magnetostrictive strip [7, 8], and the  $u(x, t)$  is the displacement vector along  $x$ -axis. For harmonic oscillations, the displacement can be described as [19]:

$$u(x,t) = u(x)e^{j\omega t} \quad (2-5)$$

where  $\omega$  is the resonance frequency. Hence equation (2-4) can be written as [19]:

$$\frac{E}{\rho(1-\sigma^m)} \frac{\partial^2 u(x)}{\partial x^2} + \omega^2 u(x) = 0 \quad (2-6)$$

The general solution of the wave Equation (2-6) is [19]:

$$u(x) = A \sin kx + B \cos kx = u_0 \sin(kx + \varphi) \quad (2-7)$$

where  $k = \omega \sqrt{\frac{\rho(1-\sigma^m)}{E}}$  is the wave number [19], and  $u_0 = \sqrt{A^2 + B^2}$  is the displacement amplitude.

When a free standing strip shown in Fig. 2.1 is applied, two ends of the strip are stress-free because there is no restoring force added on, which indicates that  $\partial u(x)/\partial x = 0$  at both ends of the strip ( $x=0$  and  $x=L$ ). By adding these boundary conditions to Equation (2-7), we can get:

$$u_0 k \cos \varphi = 0 \quad (2-8)$$

$$u_0 k \cos(kL + \varphi) = 0 \quad (2-9)$$

Equation (2-8) and (2-9) yields:

$$\varphi = \frac{\pi}{2} \quad (2-10)$$

$$kL = n\pi \quad (n=1, 2, 3\dots) \quad (2-11)$$

From the condition of Equation (2-11) we get:

$$\omega_n = 2\pi f_n = k \sqrt{\frac{E}{\rho(1-\sigma^m)}} = \frac{n\pi}{L} \sqrt{\frac{E}{\rho(1-\sigma^m)}} \quad (2-12)$$

Consequently, the longitudinal oscillation characteristic frequency of the magnetostrictive strip shown in Fig. 2.1 is given by [18]:

$$f_n = \frac{n}{2L} \sqrt{\frac{E}{\rho(1-\sigma^m)}} \quad (n=1, 2, 3\dots) \quad (2-13)$$

Equation (2-13) shows that the characteristic frequency of the magnetostrictive strip depends

only on its length and material properties.

The displacement amplitude at resonance can be calculated by considering the boundary conditions of the magnetostrictive strip oscillation. The longitudinal resonance displacement along the strip length can be determined via inserting Equation (2-10) and (2-11) into Equation (2-7) as below [20].

$$u(x,t) = u_0 \cos\left(\frac{n\pi}{L}x\right)e^{j\omega t} \quad (2-14)$$

where  $u_0$  is the displacement amplitude and  $\omega$  is the angular excitation frequency ( $\omega=2\pi f$ ). In Equation (2-14),  $e^{j\omega t}$  stands for the oscillation of each point of the strip, and  $u_0 \cos\left(\frac{n\pi}{L}x\right)$  stands for the length direction displacement amplitude of the strip at resonance frequency.

### 2.3 Current characterizations of resonance behaviors of magnetostrictive strips

The resonance behaviors of magnetostrictive strip can be characterized by different methods. In this study, three techniques are used independently, which are lock-in amplifier, impedance analyzer and network analyzer respectively. The resonance frequency of the magnetostrictive strip can be obtained directly or indirectly. Because the vibration reaches its maximum amplitude at the resonance frequency, this characteristic frequency can be directly gotten by measuring the strip's vibration amplitude in a certain frequency region. And also by measuring the electrical properties of magnetostrictive strip, resonance frequency can be indirectly obtained. In this study, all three techniques are indirect methods.

In the lock-in amplifier method, the AC driving signal is provided by a lock-in amplifier and input into the Helmholtz coils to generate a uniform driving magnetic field. The vibration of the magnetostrictive strip causes a magnetic flux change inside the pick-up coils. And by

measuring and comparing the induction voltage of the pick-up coils and AC driving signal from the lock-in amplifier, the resonance frequency can be determined.

In the impedance analyzer method, AC driving signal is provided by an impedance analyzer and generates the AC driving magnetic field inside a coil. The magnetostrictive strip vibrates under this driving field inside the coil, and at the resonance frequency ( $f_r$ ) it has the maximum vibration and causes the maximum magnetic flux change and impedance. By measuring the impedance within a wide frequency range, the resonance frequency can be determined.

In the network analyzer method, the principle is similar to the impedance analyzer method. Instead of the impedance  $Z$ , the network analyzer output  $S_{11}$  signal is applied to find out the resonance frequency. And  $S_{11}$  and the equivalent impedance  $Z$  can be converted to each other by Equation (2-15) [21]:

$$Z = 50 \frac{1 + S_{11}}{1 - S_{11}} \quad (2-15)$$

## **2.4 Experimental and measurement setup**

### **2.4.1 Lock-in amplifier method**

This set-up includes a custom-designed Helmholtz coil and a pair of homemade pick-up coils to characterize the resonance behavior of the magnetostrictive strip, as shown in Figure 2.2. The Helmholtz coil consists of two pairs of coils: one pair can generate an AC magnetic field at a frequency up to 500 kHz and the other pair can create a DC magnetic field. The magnetostrictive strip was put into a chamber that was put in the middle of the Helmholtz coil.



Two pick-up coils were wound in opposite directions and connected in a series so that the output signal is zero if there is no vibration of the magnetostrictive strip. Therefore, the output of the pick-up coils only represents the magnetic signal generated by the vibration of the magnetostrictive strip.

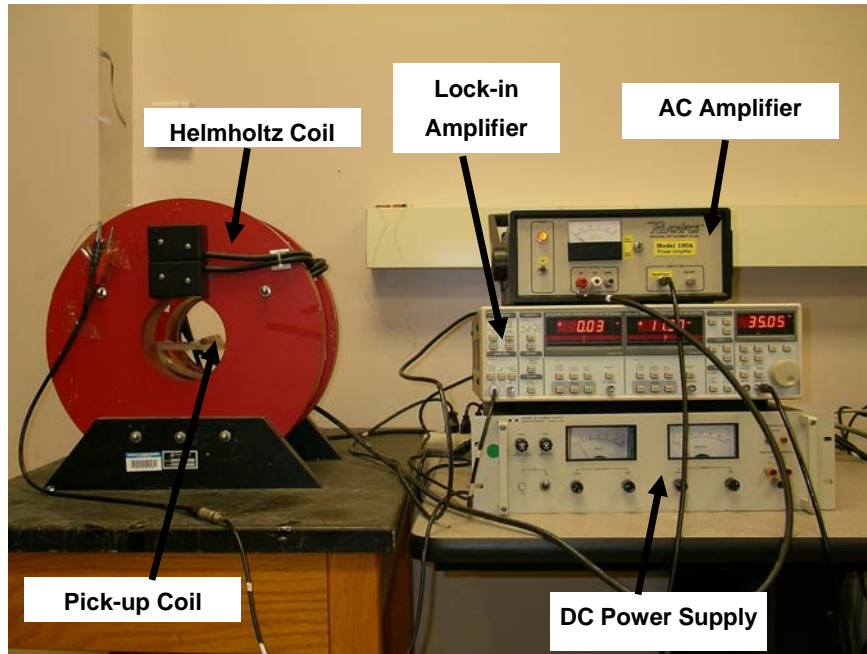


Figure 2.2. Lock-in amplifier method measurement set-up.

In the experiments, the amplitude of the AC magnetic field was 0.1 Oe, while the DC field was adjusted to an optimized value based on different lengths of magnetostrictive strip. The homemade pick-up coil pair, which consists of two coils, was wound outside the sample chamber to measure the magnetic signal generated by the vibration of the magnetostrictive strip. The pick-up coil pair was connected to a lock-in amplifier (SRS830, Stanford Research Systems, Sunnyvale, CA) to measure the electric potential generated in the coils, which has two outputs – the amplitude and phase of the electric potential. The amplitude of the output signal from the lock-in amplifier is proportional to the amplitude of the magnetostrictive strip's vibration, while the phase signal represents the phase difference

between the magnetostrictive strip's vibration and the driving magnetic field. A set of typical results is given in Figure 2.3, where a magnetostrictive strip in size of 25 mm ( $L$ )  $\times$  3.0 mm ( $W$ )  $\times$  30  $\mu$ m ( $t$ ) was operated in R-100 reference oil. In this case, the resonance frequency ( $f_r$ ) and anti-resonance frequency ( $f_r'$ ) of the device are 82610 Hz and 87170 Hz, respectively.

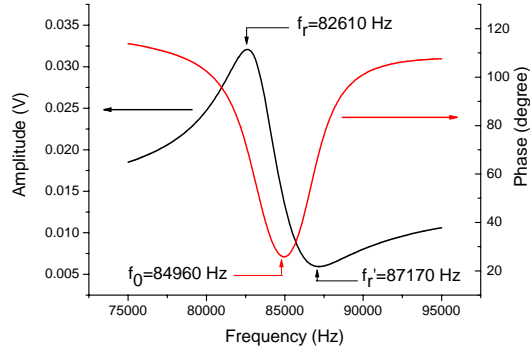


Figure 2.3. The frequency dependence of the phase and amplitude signals from the lock-in amplifier for a magnetostrictive strip in size of 25 mm ( $L$ )  $\times$  3.0 mm ( $W$ )  $\times$  30  $\mu$ m ( $t$ ) in R-100 reference oil.

The magnetostrictive sensors are driven to vibrate by a sine wave signal that is generated by a lock-in amplifier (SRS830, Stanford Research Systems, Sunnyvale, CA). The set-up includes a custom-designed Helmholtz coil and a pair of homemade pick-up coils to characterize the resonance behavior of the magnetostrictive strip. The Helmholtz coil consists of two pairs of coils: one pair can generate an AC magnetic field at frequency up to 500 kHz and the other pair can create a DC magnetic field. The magnetostrictive strip was put into a chamber that was put in the middle of the Helmholtz coil. The DC bias current adds static magnetic field to the magnetostrictive sensor, which can be adjusted to achieve the maximum vibration amplitude of the sensor. At the same time, the lock-in amplifier records the signals in the proper frequency range through a pickup coil and shows the resonant frequency at signal peak. Adjustable DC current controlling the magnitude of the static magnetic field also

decides the signal's strength.

Metglas alloy 2826MB ribbon (iron nickel-based alloy) obtained from Honeywell International (Conway, SC) was used as the sensor platform. Metglas 2826MB thin film was diced into the exact size of sensor by a micro-dicing saw. To remove the grease remnant after dicing, the particles were cleaned in acetone by using an ultrasonic cleaner (Cole Parmer) for 30 minutes and dried by nitrogen gas. Then these magnetostrictive strips are ready for visco-liquid properties study.

#### 2.4.2 Impedance analyzer method

This set-up includes a custom-designed Helmholtz coil and homemade coil to characterize the resonance behavior of the magnetostrictive strip, as shown in Figure 2.4. The DC bias magnetic field is provided by the Helmholtz coil, and an AC magnetic field is provided by impedance analyzer. The coil with a magnetostrictive strip inside is connected to Agilent impedance analyzer (4294A, 40Hz~110MHz) to measure the impedance of the coil during the vibration of strip. DC bias is adjusted in order to get the maximum signal strength.

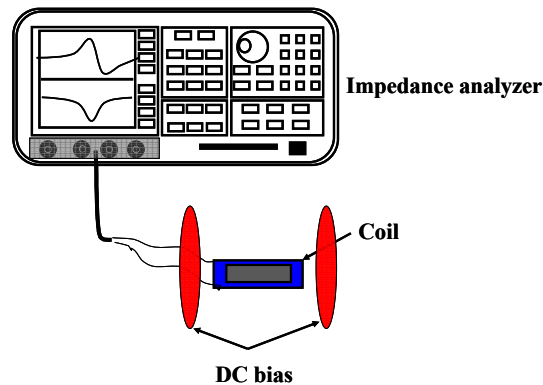


Figure 2.4. Impedance analyzer method measurement set-up.

### 2.4.3 Network analyzer method

The network analyzer output  $S_{11}$  signal of magnetostrictive strip in coil is got by using HP network analyzer (8751A) with HP S-parameter adapter (87511A). The measurement set-up is shown as Figure 2.5, in which the permanent magnet provides DC bias field on strip and the network analyzer generates AC field in the coil to drive the strip vibration. The resonance frequency of magnetostrictive strip is determined at where the  $S_{11}$  signal achieves its minimum [22].

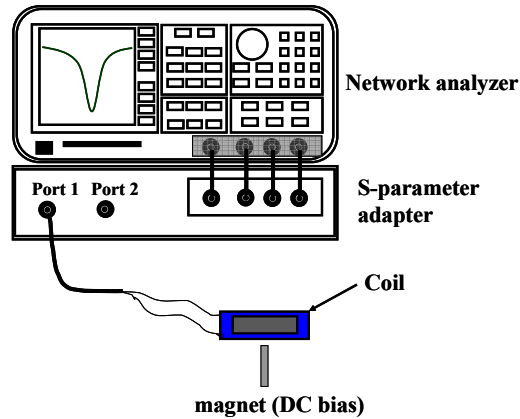


Figure 2.5. Network analyzer method measurement set-up.

## 2.5 Characterization and experiment results discussion

### 2.5.1 Resonance frequency of magnetostrictive sensor

As mentioned in previous sections, the sensor oscillates along the longitudinal direction in an alternating magnetic field because of the magnetostriction effect. The resonance frequency of magnetostrictive sensor in air is considered the intrinsic frequency. The intrinsic frequency of the sensor is dependent of the sensor material properties and geometries and can

be described as Equation (2-1). However when the sensor is in medium, the external DC bias magnetic field and the density/viscosity of the medium could change the characteristic resonance frequency of the sensor.

Previous research indicated that the fundamental resonance frequency  $f$  of a freestanding beam in its longitudinal vibration can be described as Equation (2-16) [23, 24]:

$$f = \frac{1}{2L} v = \frac{1}{2L} \sqrt{\frac{E_{eff}}{\rho}} = \frac{1}{2L} \sqrt{\frac{E}{\rho(1-\sigma^m)}} \quad (2-16)$$

where  $L$ ,  $E_{eff}$ ,  $E$  and  $\rho$  are the length, effective Young's modulus, Young's modulus and density of the beam, correspondingly. The equation is the general case of the longitudinal vibration mode of a beam.  $E_{eff}$  in equation (2-16) is regarded as the isotropic Young's modulus of a rectangular cross-section beam. And it is based the assumption that all the dimensions are of comparable size. In the case which the beam thickness and width are similar, however much smaller than the length, the beam is regarded as being in plane-strain condition. And the Young's modulus of plane-strain can be stated as  $E_{eff} = E_{plane-strain} = E/(1-\sigma^2)$  [18], where  $\sigma$  is the Poisson ratio of the material. Previous work pointed out that the Young's modulus should be adjusted as  $E_{eff} = E_{plane-stress} = E/(1-\sigma)$  when length is much bigger than width [7]. Here  $E$  is a constant at zero applied magnetic field in theory, that is  $H = 0$ . Therefore, the resonance frequency of the magnetostrictive strip sensor at  $H = 0$  is linear dependent on the inverse length.

### 2.5.2 Effect of external DC bias magnetic field on resonance behaviors of strip sensor

It has been reported that the resonance behaviors of amorphous, magnetostrictive sensors could change with different external DC bias magnetic fields [25, 26]. The amplitude

and phase changes with DC bias is generally ascribed to the  $\Delta E$  effect, which is a dependency of the Young's modulus on the coupling of magnetization, fundamentally attributable to a re-orientation of the magnetic domains under external factors (such as magnetic field, external stress) creating a magnetostriction strain [26, 27]. With the applied DC bias magnetic field, the internal magnetization changes from its initial steady state (external magnetic field  $H=0$ ) to a state in external magnetic field ( $H$ ). The Young's modulus of magnetostrictive sensor changes with the magnetization alteration and is shown in Equation (2-17) [28]:

$$\frac{1}{E_H} = \frac{1}{E_M} + \frac{9\lambda_s^2 H^2}{M_s H_{A\sigma}^3} \quad (2-17)$$

where  $E_H$  is the Young's modulus of elasticity in a magnetic field  $H$ ,  $E_M$  is the Young's modulus without an external magnetic field,  $\lambda_s$  is the saturation magnetostriction,  $M_s$  is the saturation magnetization and  $H_{A\sigma}$  is reduced anisotropy field.

The magnetic susceptibility ( $\chi$ ) is defined as [29]:

$$\chi = \frac{M}{H} \quad (2-18)$$

And the dependence of  $M$  on  $H_{A\sigma}$  and  $H$  is depicted by [28]:

$$M = M_s \frac{H}{H_{A\sigma}} \quad (2-19)$$

Thus, from equations (2-17), (2-18) and (2-19),

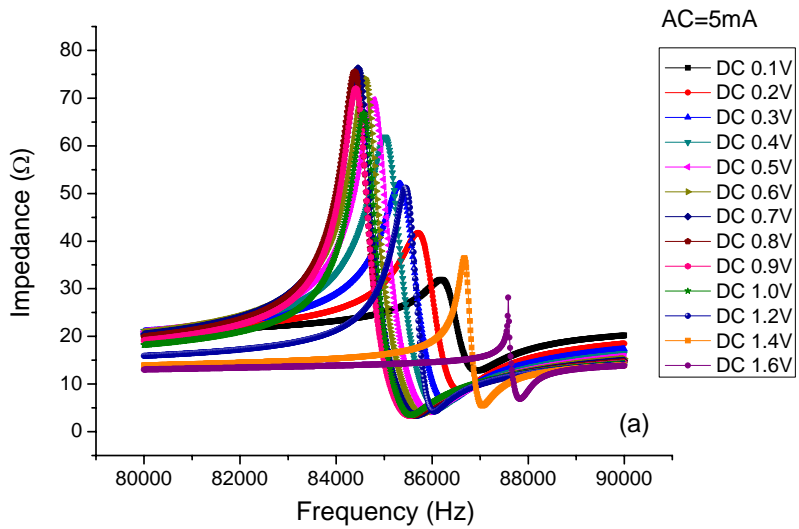
$$\frac{1}{E_H} = \frac{1}{E_M} + \frac{9\lambda_s^2 H^2 \chi^3}{M_s^4} \quad (2-20)$$

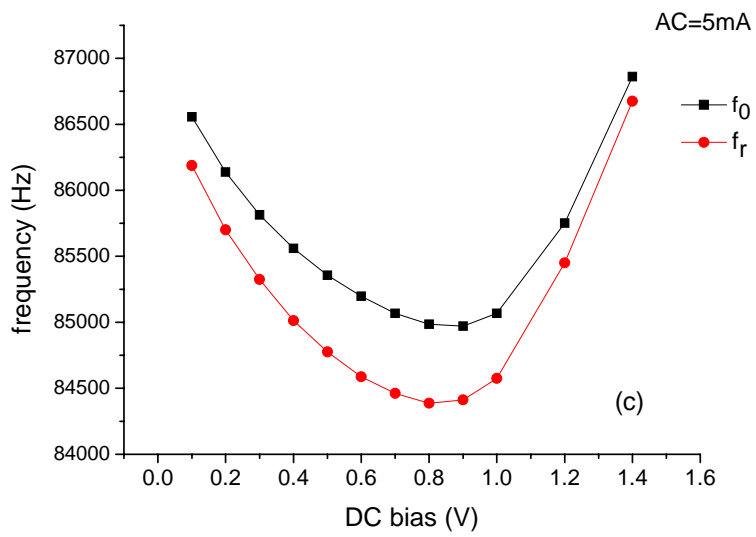
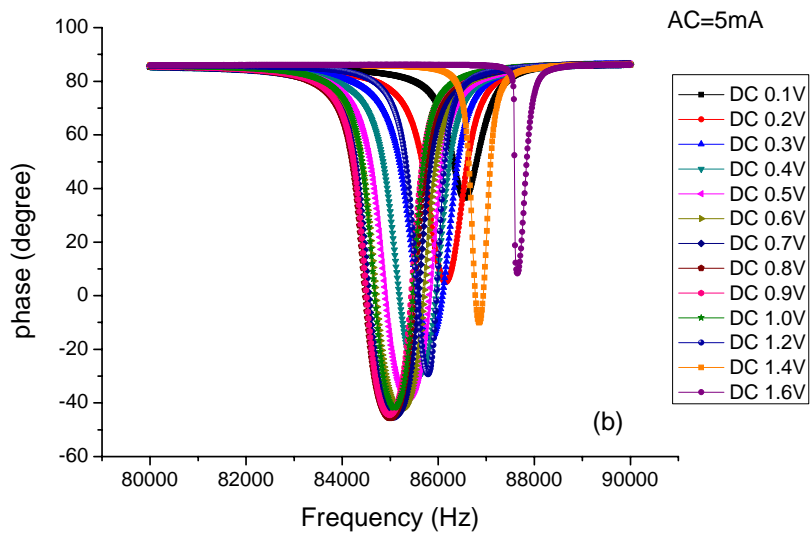
And combining equations (2-16) and (2-20) generates the resonance frequency of a freestanding beam in magnetic field  $H$  [30]:

$$f_H = \left(1 + \frac{9E_M \lambda_s^2 H^2 \chi^3}{M_s^4}\right)^{-1/2} f \quad (2-21)$$

The equation (2-21) describes that the resonance behaviors of a freestanding magnetostrictive beam change with different DC magnetic fields. The  $f_H$  changes with DC magnetic field strength H and magnetic susceptibility  $\chi$  of beam material.

To find out the effect of external DC bias magnetic field on freestanding magnetostrictive beam by experiments, the resonance behaviors of 25mm (25mm×3mm×30μm) magnetostrictive strip sensor (from Metglas alloy 2826MB ribbon) in air was studied in different DC magnetic fields and the results are illustrated in Figure 2.6.







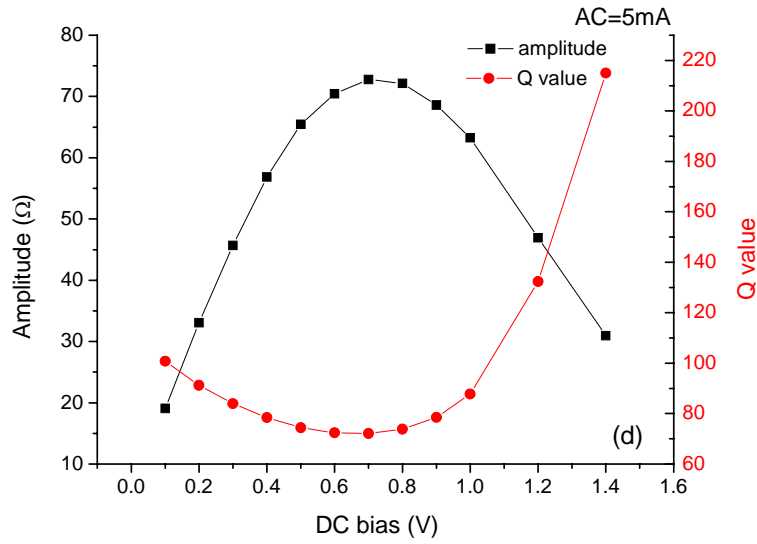


Figure 2.6. Resonance behaviors of 25mm (25mm×3mm×30μm) magnetostrictive strip sensor (from Metglas alloy 2826MB ribbon) in air under different DC magnetic fields: (a) amplitude vs. frequency; (b) phase vs. frequency; (c) resonance frequencies as a function of external DC bias magnetic field; (d) amplitude and Q value of magnetostrictive strip sensor as a function of external DC bias magnetic field.

It is found that sensor amplitude reaches maximum at the optimal DC bias magnetic field where the magnetoelastic coupling coefficient is the maximum. And this happens when the DC bias magnetic field reaches the anisotropy field of the sensor  $H_a$  [26, 30-31]. The theoretical model curve is calculated from Equation (2-16) & (2-21) with density ( $\rho$ ) of 7.9 g/cm<sup>3</sup>, Young's modulus ( $E_M$ ) of 105 GPa, saturation magnetostriction ( $\lambda_s$ ) of 12 ppm [32] and Poisson's ratio of 0.33 [7]. The susceptibility ( $\chi$ ) and saturation magnetization ( $M_S$ ) are got from the  $M-H$  curve in Figure 2.7. The theoretical model of the resonance frequency under magnetic field can be gotten from Equation (2-21), and the trend is the same with the experimental results in Figure 2.6. The comparison results are shown in Figure 2.8. And when an external DC magnetic field added on the strip sensor keeps increasing, the magnetization saturation reaches with the vibration amplitude decreasing. At the same time the Q value

increases.

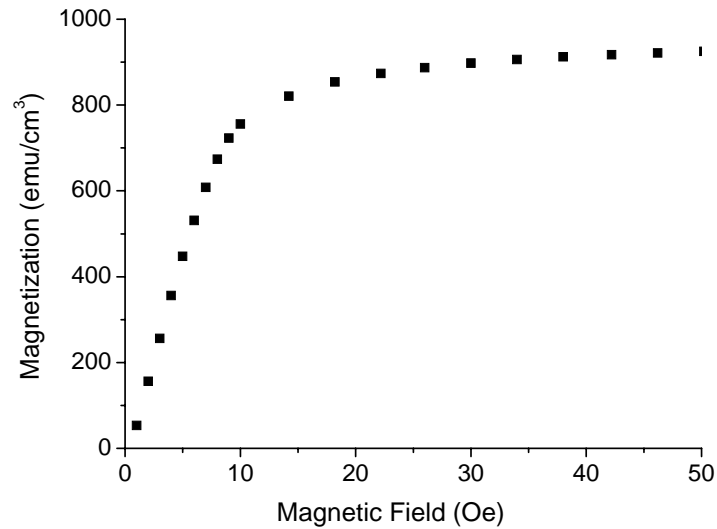


Figure 2.7. Typical magnetization versus magnetic field curve for magnetostrictive strip.

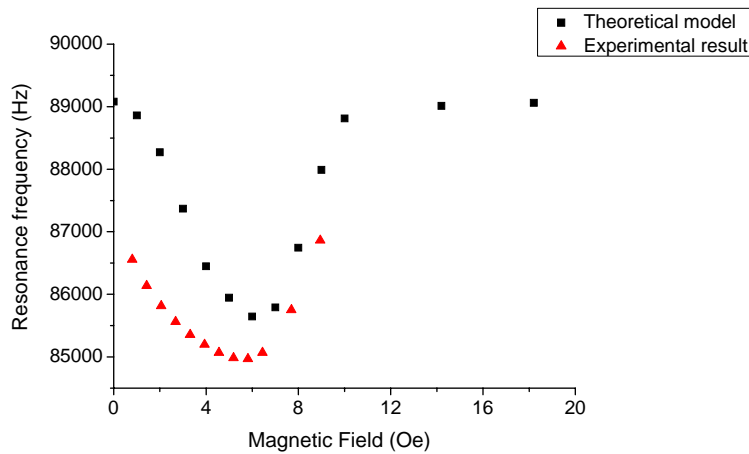


Figure 2.8. Comparison of experimental result and theoretical model of resonance behaviors of 25mm (25mm×3mm×30µm) magnetostrictive strip sensor (from Metglas alloy 2826MB ribbon) in air under different DC magnetic fields.

A high Q value improves the resolution and accuracy of resonance frequency, and a large signal amplitude is also needed in the measurement to select the resonance frequency. Both factors should be considered in the measurement for a good signal-to-noise ratio and sharp resonance peak. However, with the DC external bias magnetic field changing, the

change patterns of Q value and signal amplitude are different. And a factor of  $Q \cdot Amplitude^{\frac{5}{3}}$  is selected to find the pattern with different DC magnetic fields in Figure 2.9. Compared with figure 2.6 (d), it is found that the peak shifts from DC bias 0.7V to DC bias 0.8V. And the optimum DC external bias magnetic field for a 25mm strip sensor is determined to be a DC bias of 0.8V for the best performance.

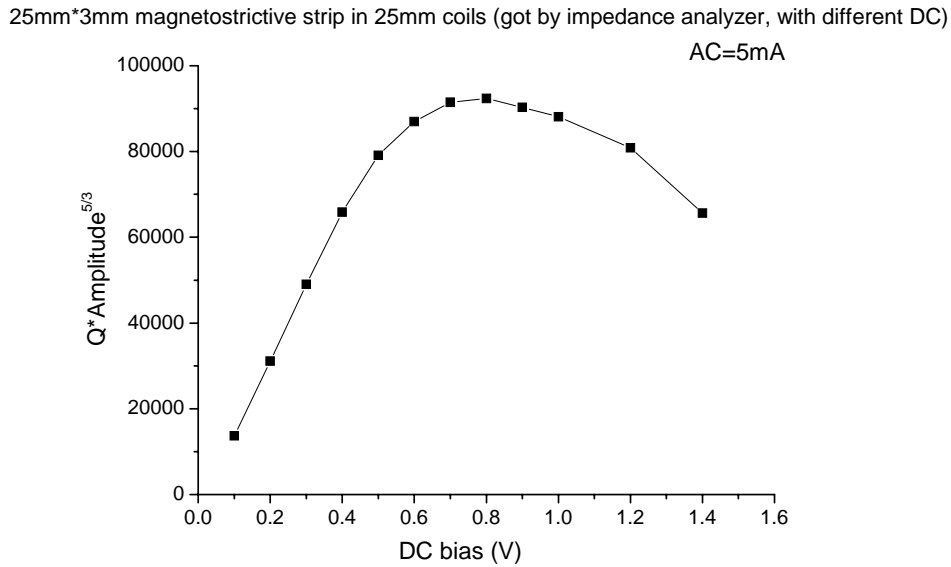


Figure 2.9. Resonance behaviors of 25mm (25mm×3mm×30μm) magnetostrictive strip sensor (from Metglas alloy 2826MB ribbon) in air under different DC magnetic fields:  $Q \cdot Amplitude^{\frac{5}{3}}$  of the magnetostrictive strip sensor as a function of the external DC bias magnetic field.

### 2.5.3 Effect of AC driving magnetic field on resonance behaviors of strip sensor

To stimulate the vibration of magnetostrictive strip sensor, both an AC magnetic field and DC bias field are needed to apply on the sensor. It is difficult to get a uniform AC magnetic field within a large region and also hard to get exactly the same magnetic field

strength for each measurement. The magnetic field added on the strip sensor could be different due to a non-uniform magnetic field or different locations of the strip sensor. Consequently, it is necessary to study the influence of the AC driving field on the resonance behavior of the magnetostrictive strip sensor. To find the effect of AC driving magnetic field, the resonance behaviors of magnetostrictive strip sensor in the size of  $25\text{ mm} \times 3\text{ mm} \times 30\text{ }\mu\text{m}$  was studied in different AC driving magnetic fields with an optimized DC bias field by different methods (lock-in amplifier, impedance analyzer and network analyzer).

### 2.5.3.1 Lock-in amplifier method

In this method, the Helmholtz coil consists of two pairs of coils: one pair can generate an AC magnetic field at frequency up to 500 kHz and the other pair can create a DC magnetic field. Vibration signals of a  $25\text{ mm} \times 3\text{ mm} \times 30\text{ }\mu\text{m}$  magnetostrictive strip are picked up by lock-in amplifier at an optimized DC voltage (0.8V). And AC current range is from 1mA to 10mA. The results are shown in Figure 2.10.

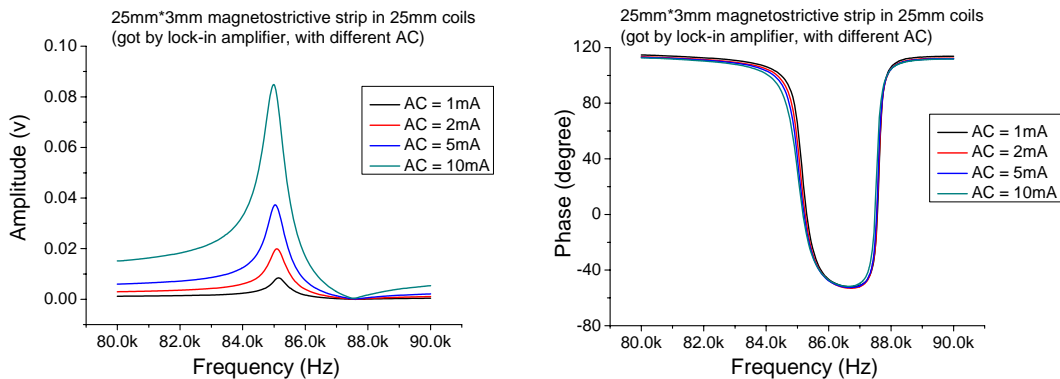


Figure 2.10. Lock-in amplifier method: Resonance behaviors of 25mm ( $25\text{mm} \times 3\text{mm} \times 30\text{ }\mu\text{m}$ ) magnetostrictive strip sensor (from Metglas alloy 2826MB ribbon) in air under different AC driving magnetic fields with an optimized DC bias field.

Oscillation AC level current (mA)	frequency $f_r$ (Hz)	frequency $f_0$ (Hz)	frequency $f_r'$ (Hz)
1	85150	86710	87620
2	85090	86700	87590
5	85040	86700	87570
10	84990	86620	87520

Table 2.1. Lock-in amplifier method: Resonance frequencies of 25mm (25mm×3mm×30μm) magnetostrictive strip sensor in air under different AC driving magnetic fields with an optimized DC bias field.

From Figure 2.10 and Table 2.1, it can be found that vibration amplitude increases with AC magnetic field increases, and all three characteristic resonance frequencies decrease with AC magnetic field increases. The effect of AC driving field on the resonance behaviors of the magnetostrictive strip sensor is shown in Figure 2.11.

25mm\*3mm magnetostrictive strip in 25mm coils (got by lock-in amplifier, with different AC)

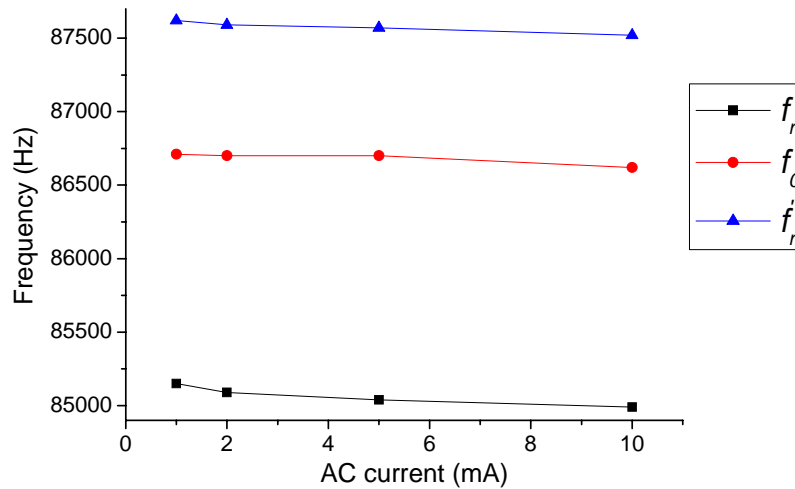


Figure 2.11. Lock-in amplifier method: Influence of AC driving magnetic fields on resonance behaviors of a 25mm (25mm×3mm×30μm) magnetostrictive strip sensor (from Metglas alloy 2826MB ribbon) in air with an optimized DC bias field.

### 2.5.3.2 Impedance analyzer method

In this method, the DC bias magnetic field is provided by the Helmholtz coil, and the

AC magnetic field is provided by Agilent impedance analyzer (4294A, 40Hz~110MHz). Vibration signals of different length magnetostrictive strip ( $25\text{ mm} \times 3\text{ mm} \times 30\text{ }\mu\text{m}$  and  $35\text{ mm} \times 3\text{ mm} \times 30\text{ }\mu\text{m}$ ) are picked up by impedance analyzer at an optimized DC voltage. And the AC current range is from 1mA to 10mA. The results are shown as follows:

(1)  $25\text{ mm} \times 3\text{ mm} \times 30\text{ }\mu\text{m}$  magnetostrictive strip;

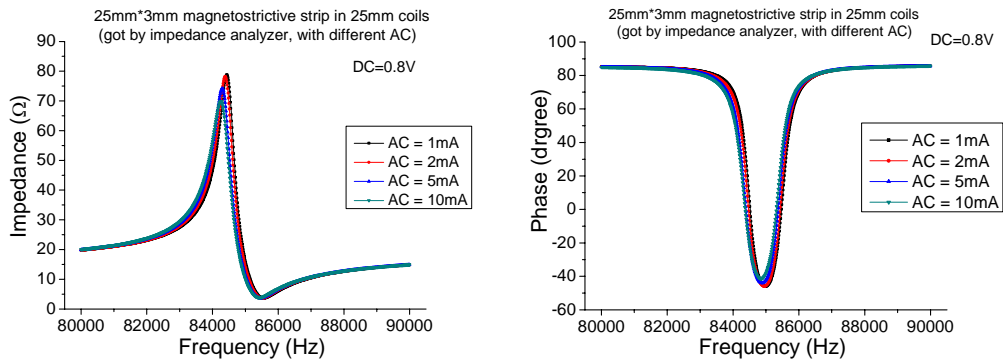


Figure 2.12. Impedance analyzer method: Resonance behaviors of 25mm ( $25\text{mm} \times 3\text{mm} \times 30\text{ }\mu\text{m}$ ) magnetostrictive strip sensor (from Metglas alloy 2826MB ribbon) in air under different AC driving magnetic fields with an optimized DC bias field.

Oscillation AC level current (mA)	frequency $f_r$ (Hz)	frequency $f_0$ (Hz)	frequency $f_r'$ (Hz)
1	84437.5	84987.5	85562.5
2	84387.5	84950	85512.5
5	84300	84887.5	85462.5
10	84250	84850	85425

Table 2.2. Impedance analyzer method: Resonance frequencies of 25mm ( $25\text{mm} \times 3\text{mm} \times 30\text{ }\mu\text{m}$ ) magnetostrictive strip sensor in air under different AC driving magnetic fields with an optimized DC bias field.

25mm\*3mm magnetostrictive strip (got by impedance analyzer, with different AC)

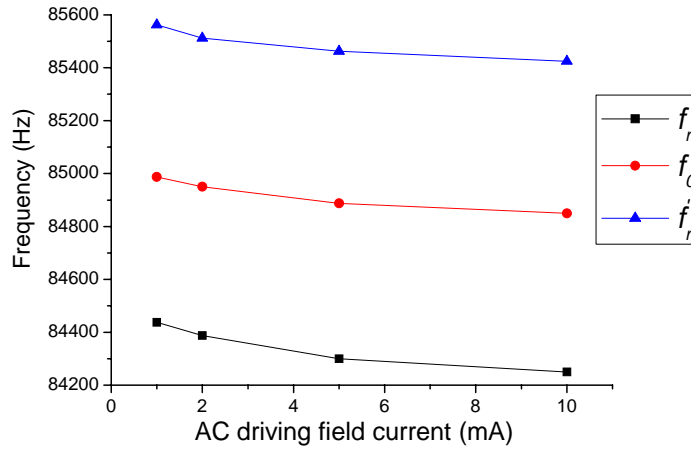


Figure 2.13. Impedance analyzer method: Influence of AC driving magnetic fields on resonance behaviors of 25mm (25mm×3mm×30μm) magnetostrictive strip sensor (from Metglas alloy 2826MB ribbon) in air with an optimized DC bias field.

(2) 35 mm × 3 mm × 30 μm magnetostrictive strip.

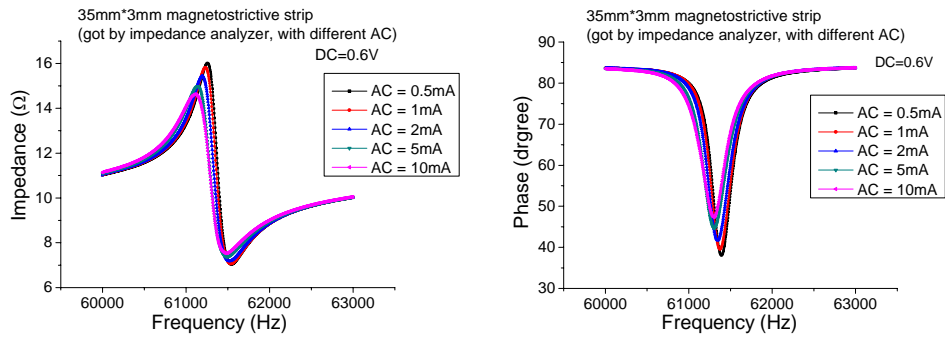


Figure. 2.14. Impedance analyzer method: Resonance behaviors of 35mm (35mm×3mm×30μm) magnetostrictive strip sensor (from Metglas alloy 2826MB ribbon) in air under different AC driving magnetic fields with an optimized DC bias field.

Oscillation AC level current (mA)	frequency $f_r$ (Hz)	frequency $f_0$ (Hz)	frequency $f_r'$ (Hz)
0.5	61256.25	61391.25	61545
1	61233.75	61376.25	61537.5
2	61196.25	61346.25	61518.75
5	61136.25	61305	61492.5
10	61110	61297.5	61473.75

Table 2.3. Impedance analyzer method: Resonance frequencies of 35mm (35mm×3mm×30μm) magnetostrictive strip sensor in air under different AC driving magnetic fields with an optimized DC bias field.

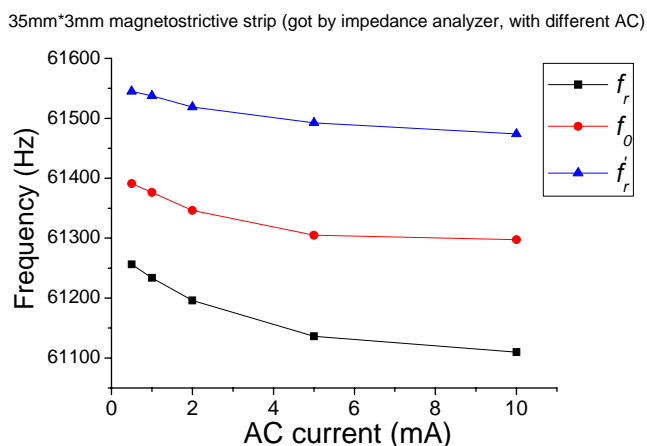


Figure 2.15. Impedance analyzer method: Influence of AC driving magnetic fields on resonance behaviors of 35mm (35mm×3mm×30μm) magnetostrictive strip sensor (from Metglas alloy 2826MB ribbon) in air with optimized DC bias field.

By studying the resonance behaviors of magnetostrictive strips of different lengths, it can be found that all three characteristic resonance frequencies decrease with AC magnetic field increases. The effect of AC driving field on the resonance behaviors of the magnetostrictive strip sensor is shown in Figure 2.13 and Figure 2.15.

### 2.5.3.3 Network analyzer method

In this method, a permanent magnet provides a DC bias field on the strip and the network analyzer generates an AC field in the coil to drive the strip vibration. Vibration signals of a 2 mm magnetostrictive strip (2 mm × 0.4 mm × 30 μm) are picked up by network analyzer at an optimized DC bias field (proper permanent magnet position). The AC current range is from 1 mA to 10 mA. The results are shown as follows:



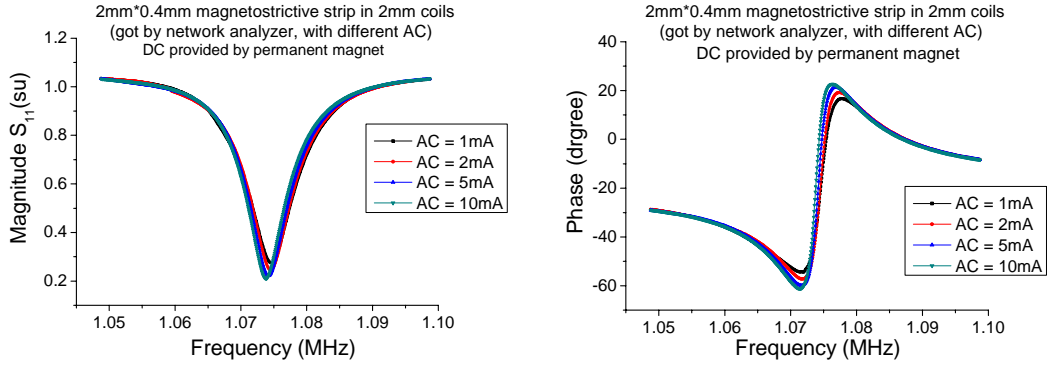


Figure. 2.16. Network analyzer method: Resonance behaviors of 2mm (2mm×0.4mm×30μm) magnetostrictive strip sensor (from Metglas alloy 2826MB ribbon) in air under different AC driving magnetic fields with an optimized DC bias field.

Oscillation AC level current (mA)	frequency $f_r$ (Hz)	frequency $f_0$ (Hz)	frequency $f_r'$ (Hz)
1	1071937.5	1074625	1077625
2	1071687.5	1074562.5	1077437.5
5	1071562.5	1074187.5	1076812.5
10	1071375	1073812.5	1076375

Table 2.4. Network analyzer method: Resonance frequencies of 2mm (2mm×0.4mm×30μm) magnetostrictive strip sensor in air under different AC driving magnetic fields with an optimized DC bias field.

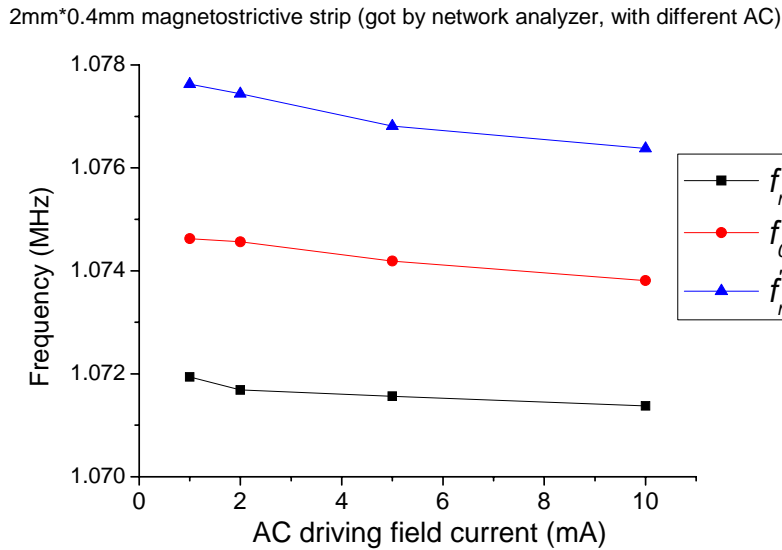


Figure 2.17. Network analyzer method: Influence of AC driving magnetic fields on resonance behaviors of 2mm (2mm×0.4mm×30μm) magnetostrictive strip sensor (from Metglas alloy 2826MB ribbon) in air with an optimized DC bias field.

#### **2.5.3.4 Conclusion**

Although the effect of DC bias field on the resonance behavior of the magnetostrictive strip sensor has been mentioned and studied for a while [22, 26, 28, 30], the influence of AC driving field on the vibration of the magnetostrictive strip sensor hasn't been well discussed yet. And some mentioned resonance frequency is independent of the amplitude of AC field [22]. However in this study, all three characteristic resonance frequencies clearly decrease with AC driving field increasing by three independent methods (lock-in amplifier, impedance analyzer and network analyzer) and the decreasing rate become smaller when AC field goes higher. Different lengths of the strip sensor were also studied with different AC driving fields and the pattern was the same: resonance frequencies decrease with AC driving field increase. This discovery shows that AC driving field should be strong enough to avoid the influence on the resonance frequencies.

#### **2.5.4 Comparison of impedance analyzer method and lock-in amplifier method**

In order to find whether the resonance frequencies ( $f_r$ ,  $f_r'$  and  $f_0$ ) obtained by impedance analyzer are the same with the results acquired by lock-in amplifier, the results from two independent methods are compared by using the same AC driving field, same DC bias field, and same magnetostrictive strip.

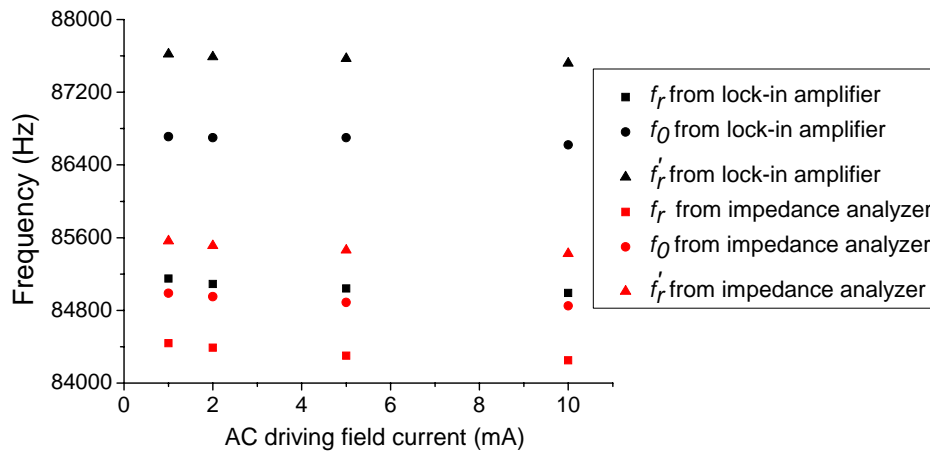


Figure 2.18. Comparison of three characteristic resonance frequencies of 25mm × 3mm magnetostrictive strip in 25mm coils (with different AC) by lock-in amplifier method and impedance analyzer method: Influence of different methods on resonance behaviors of magnetostrictive strip.

From Figure 2.18, we can find the characteristic resonance frequencies ( $f_r$ ,  $f_r'$  and  $f_0$ ) gotten by impedance analyzer method are all different from the corresponding frequencies obtained by lock-in amplifier method at the same conditions, which means the principle of impedance analyzer method is different with that of lock-in amplifier method and also give reason to the following study of different coils influence on the frequencies by impedance analyzer method.

### 2.5.5 Comparison of the influence of different coils on resonance behaviors of magnetostrictive strip by impedance analyzer method

Lock-in amplifier method measures real sensor vibration signals, while impedance analyzer method measures signals from sensor and equivalent circuits. And by changing coils, equivalent circuits could be different. By measuring the signals got from different coils, we

can determine whether the resonance frequencies ( $f_r, f_r'$  and  $f_0$ ) got by impedance analyzer are the same as the results gotten by lock-in amplifier in an indirect way, and also know the influence of coils on resonance behaviors of sensors.

Three different coils are selected to measure resonance signals of 25mm (25mm × 3mm × 30μm) magnetostrictive strip by impedance analyzer method. The result of 25mm coils (with coil diameter = 4.7mm) is shown in Figure 2.12. The results of 40mm coils (with coil diameter = 4.7mm & 6.35mm) are shown below:

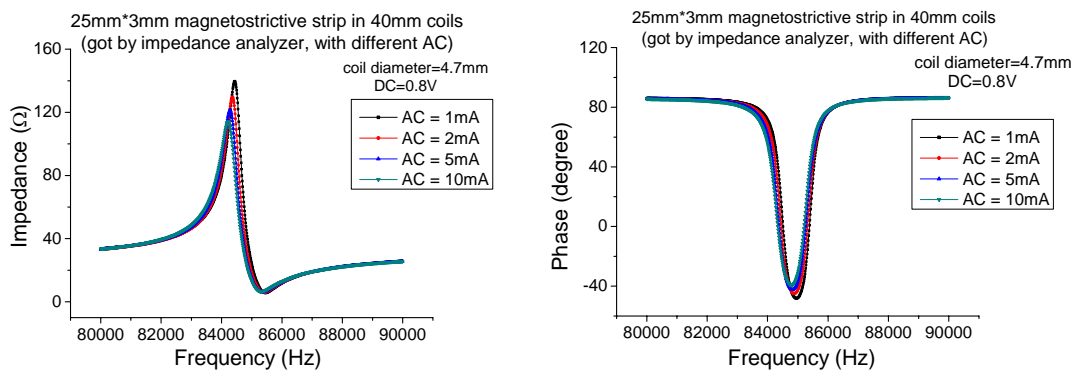


Figure 2.19. Impedance analyzer method: Resonance behaviors of 25mm (25mm×3mm×30μm) magnetostrictive strip sensor in 40mm coils (with coil diameter = 4.7mm) in air under different AC driving magnetic fields with optimized DC bias field.

Oscillation AC level current (mA)	frequency $f_r$ (Hz)	frequency $f_0$ (Hz)	frequency $f_r'$ (Hz)
1	84437.5	84950	85450
2	84362.2	84887.5	85400
5	84287.5	84825	85350
10	84225	84787.5	85312.5

Table 2.5. Impedance analyzer method: Resonance frequencies of 25mm (25mm×3mm×30μm) magnetostrictive strip sensor in 40mm coils (with coil diameter = 4.7mm) in air under different AC driving magnetic fields with an optimized DC bias field.

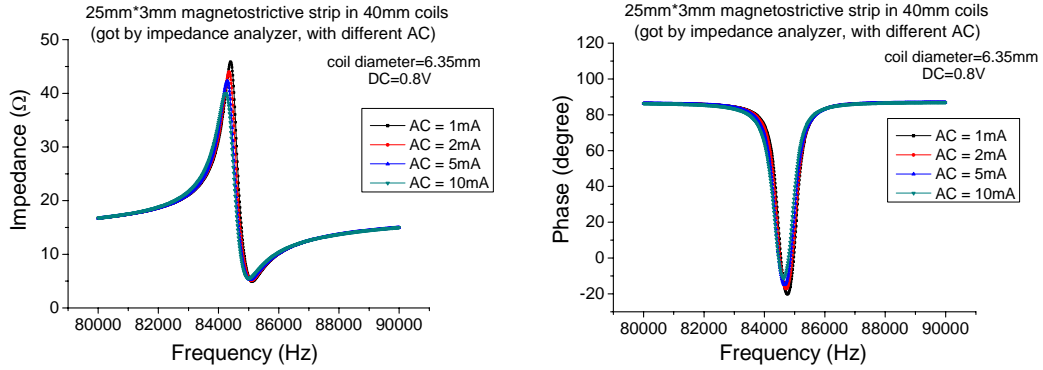


Figure 2.20. Impedance analyzer method: Resonance behaviors of 25mm (25mm×3mm×30μm) magnetostrictive strip sensor in 40mm coils (with coil diameter = 6.35mm) in air under different AC driving magnetic fields with an optimized DC bias field.

Oscillation AC level current (mA)	frequency $f_r$ (Hz)	frequency $f_{\theta}$ (Hz)	frequency $f_r'$ (Hz)
1	84400	84762.5	85112.5
2	84350	84725	85100
5	84287.5	84675	85050
10	84237.5	84637.5	85000

Table 2.6. Impedance analyzer method: Resonance frequencies of 25mm (25mm × 3mm × 30μm) magnetostrictive strip sensor in 40mm coils (with coil diameter = 6.35mm) in air under different AC driving magnetic fields with an optimized DC bias field.

Based on the results of different coils, the comparison of resonance frequencies ( $f_r$ ,  $f_r'$  and  $f_{\theta}$ ) are demonstrated in Figure 2.21. From this figure, we can find that with the coil changing, three characteristic resonance frequencies change. This means what impedance analyzer method measures is not the real sensor vibration signals. The size and geometry of the coils have some effects on resonance frequencies of the sensor. With the same coil diameter, a shorter coil length leads to higher resonance frequencies results. And with the same coil length, smaller coil diameter causes higher resonance frequencies results. It can be found coil with small diameter and same length with the strip sensor is chosen in measurement to get strong signals. These are understandable that although longer length coil could provide more uniform AC driving field, the noise issue and the inductance of coil also

inevitably increase with coil length increasing, so the coil of the same length as strip sensor is the optimization. And also magnetic flux leakage could be reduced by using a coil with small diameter.

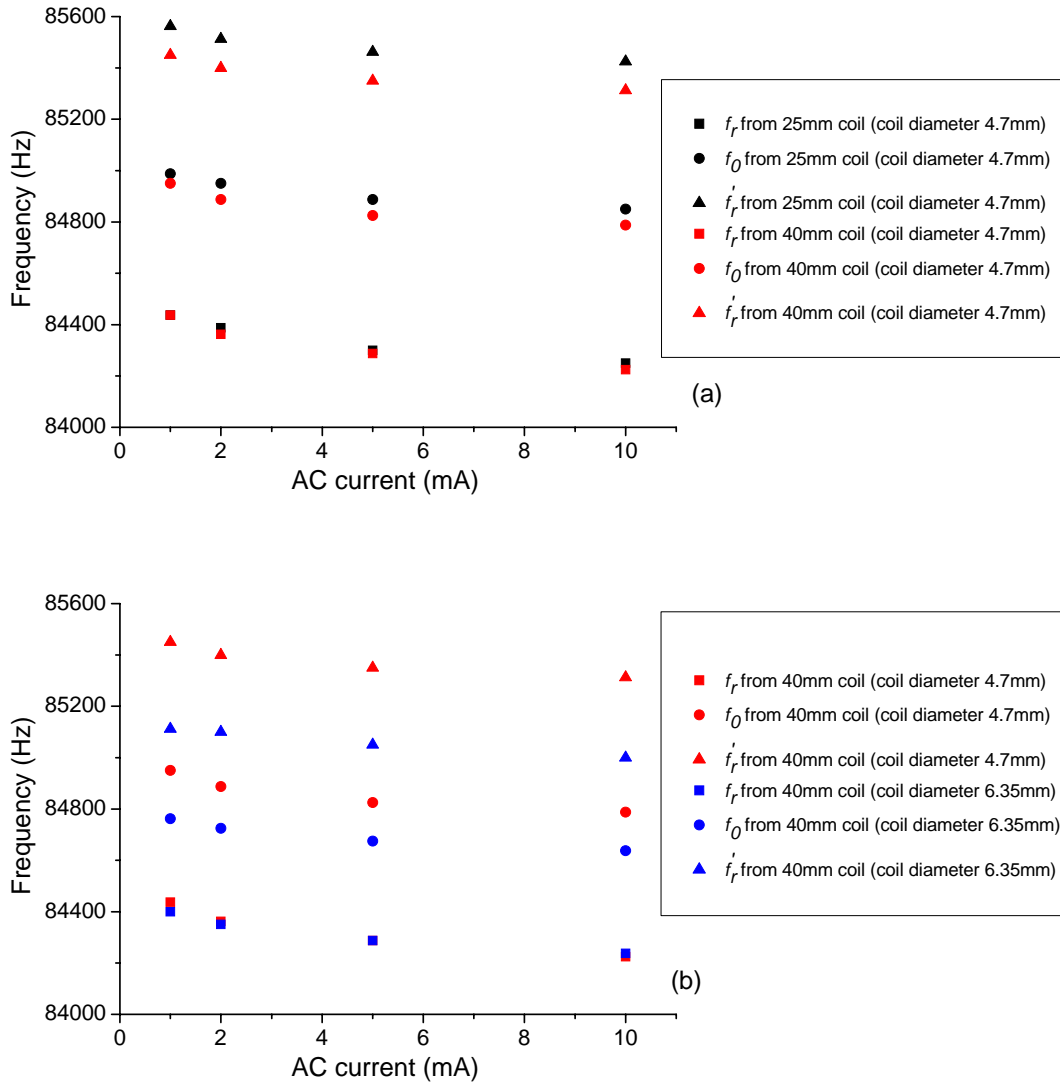


Figure 2.21. Comparison of resonance frequencies of 25mm × 3mm × 30μm strip from different coils by impedance analyzer method: (a) same coil diameter but different coil length; (b) same coil length but different coil diameter.

### 2.5.6 Location effect of magnetostrictive strip sensor in pick-up coils

To drive magnetostrictive strip sensor, AC driving & DC bias magnetic fields are added and the sensor is at some certain location inside pick-up coils as shown in Figure 2.22. And different locations could have some influences on the resonance behaviors of the strip sensor due to the non-uniform magnetic field and the size of the strip sensor compared to the size of the pick-up coils.

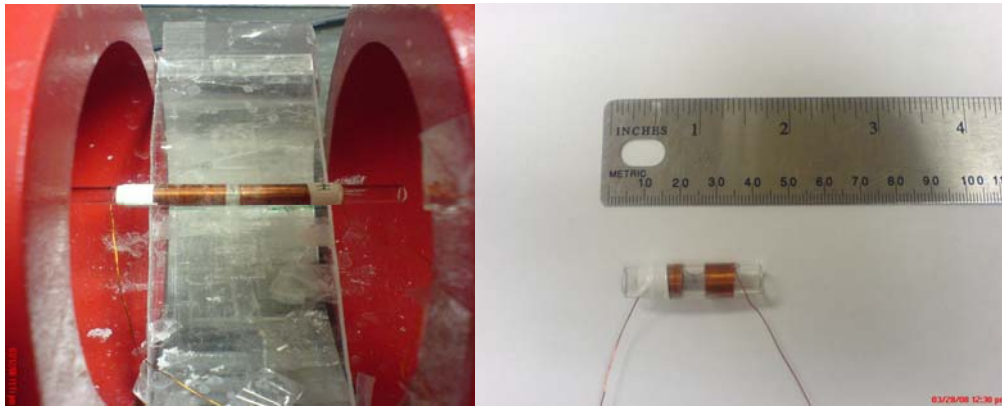


Figure 2.22. Two different sizes of self-made pick-up coils: a pair of coil and reverse coil with symmetry.

To study the effect of different locations of magnetostrictive strip sensor, the resonance behaviors of magnetostrictive strip sensor in the size of  $25 \text{ mm} \times 3 \text{ mm} \times 30 \text{ }\mu\text{m}$  was studied in different locations inside pick-up coils with an optimized DC bias field.

Following is the schematic relationship of amplitude range ( $\Delta A$ ), minimum amplitude with the location of the strip:

Illustration of the x-coordinate (location of the strip):

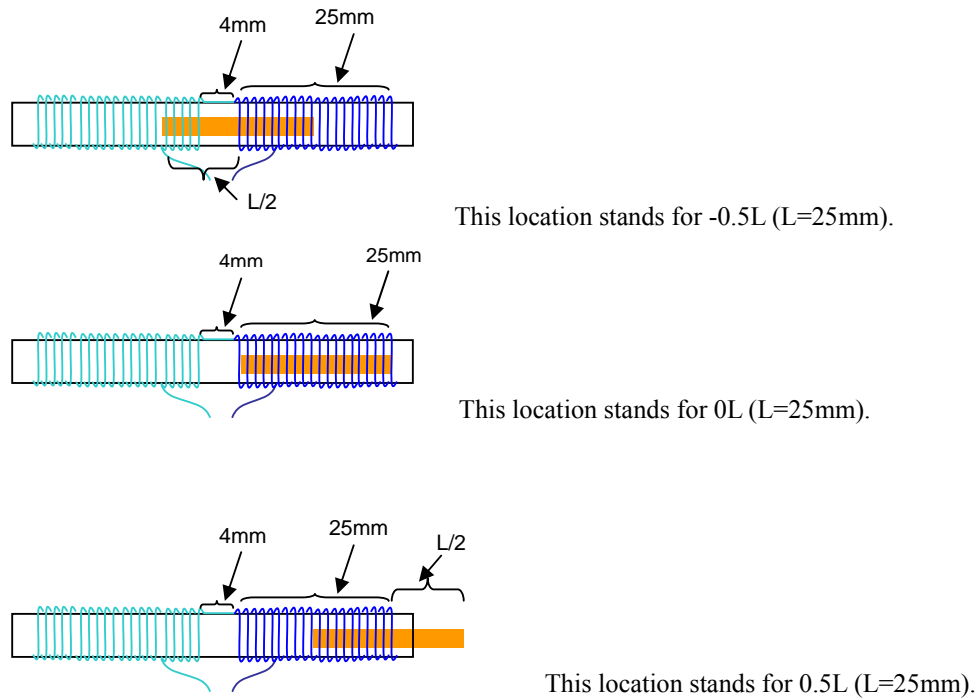


Figure 2.23. Illustration of the x-coordinate (location of the strip).



Following are the effect of different locations on the signal amplitudes, phase range, and Q value of magnetostrictive strip sensor.

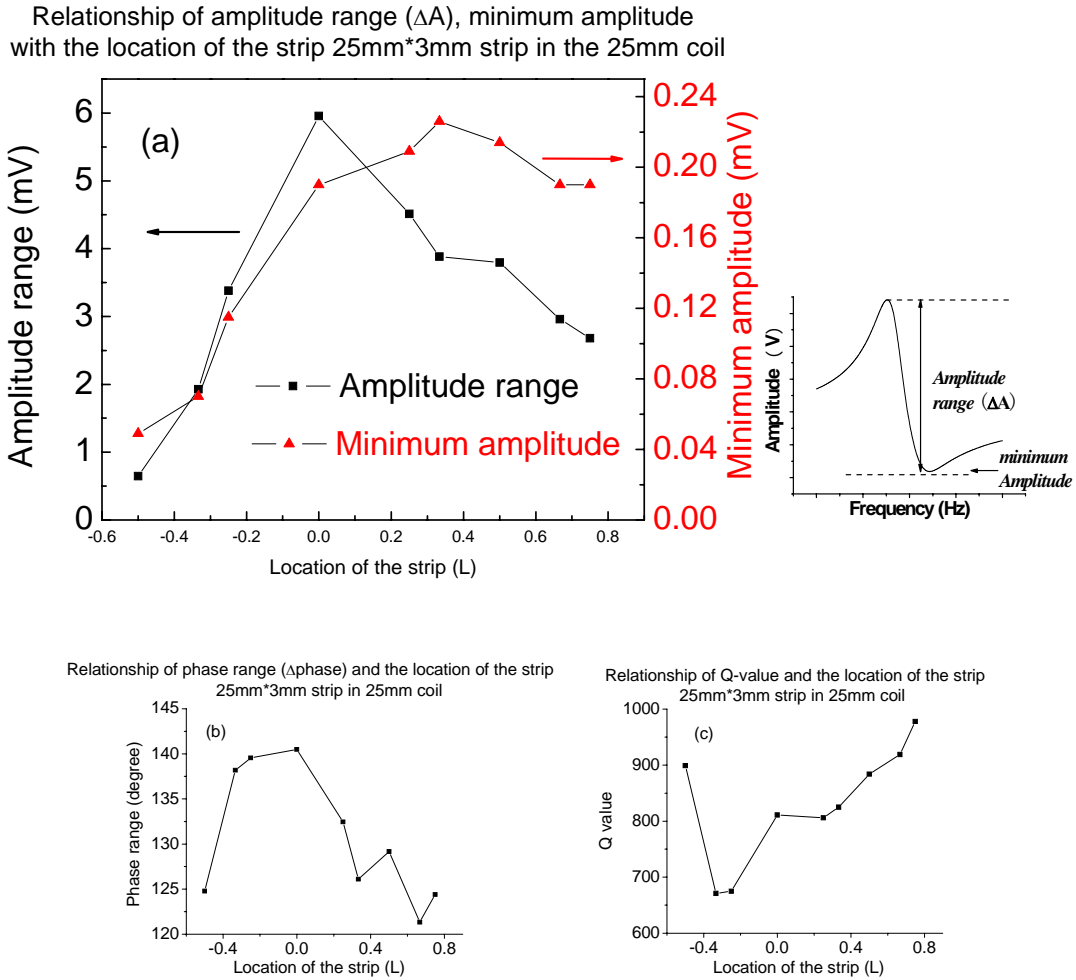


Figure 2.24. The different locations effects on (a) signal amplitudes, (b) phase range and (c) Q value of magnetostrictive strip sensor.

The biggest amplitude range ( $\Delta A$ ) arises at the location of 0L {the strip (25mm\*3mm) is fully inside the coil (25mm), L stands for length of strip (L=25mm)}. The biggest phase range ( $\Delta$ phase) also arises at the location of 0L {the strip (25mm\*3mm) is fully inside the coil (25mm), L stands for length of strip (L=25mm)}. However the Q value is not the best at the 0L position. And different length strip sensors are also studied. The location effects are the

same which means the location of OL (the center of the pick-up coil) is the best position of measuring the vibration signals of magnetostrictive strip sensor.

## 2.6 Conclusions

The resonance behaviors of magnetostrictive strip were systemically studied. Different factors which could have influences on resonance behaviors of magnetostrictive strip are examined intensively, such as DC bias field influence and the locations effect. And the view that AC driving field could influence resonance frequencies of sensor was proposed. Proofs from three independent methods (lock-in amplifier, impedance analyzer and network analyzer) were given to support this view that resonance frequencies decrease with AC driving field increase. This discovery shows that AC driving field should be strong enough to avoid the influence on the resonance frequencies. The measurement results of lock-in amplifier and impedance analyzer are compared to study the principle differences between the two methods. And also by using different coils in impedance analyzer method, the view that impedance analyzer measures the signal from sensor and equivalent circuits is proved. Combined with former results from AC driving field, it is found that coils with a small diameter and same length as the sensor are good for resonance behaviors' measurement. The location effects study shows the center of the pick-up coil is the best position of measuring the vibration signals of the magnetostrictive strip sensor.

### References:

- [1] B. Drafts, Acoustic wave technology sensors, *IEEE Transactions on Microwave Theory and Techniques*, vol. 49, pp. 795-802, 2001.

- [2] K. K. Kanazawa, J. G. Goradan II, *The oscillation frequency of a quartz resonator in contact with a liquid*, *Anal. Chem. Acta* 175 (1985) 99-105.
- [3] C. Steinem, A. Janshoff, *Piezoelectric sensors*, pp374, Springer, 2007.
- [4] Javier Tamayo, *Energy dissipation in tapping-mode scanning force microscopy with low quality factors*, *Appl. Phys. Lett.* 1999, 75, 3569.
- [5] C.A. Grimes, S.C. Roy, S. Rani, Q. Cai, *Theory, Instrumentation and Applications of Magnetoelastic Resonance Sensors: A Review*, *Sensors*, 2011, 11, 2809-2844.
- [6] Etienne Du Tremolet De Lachesserie, *Magnetostriction: Theory and Applications of Magnetoelasticity*: CRC Press, Boca Raton, 1993.
- [7] C. Liang, S. Morshed, B.C. Prorok, *Correction for longitudinal mode vibration in thin slender beams*, *Applied Physics Letters*, 90 (2007) 221912-221914.
- [8] C.A. Grimes, C.S. Mungle, K.F. Zeng, M.K. Jain, W.R. Dreschel, M. Paulose, K.G. Ong, *Wireless Magnetoelastic Resonance Sensors: A Critical Review*, *Sensors* 2 (2002) 294-313.
- [9] P.G. Stoyanov, C.A. Grimes, *A remote query magnetostrictive viscosity sensor*, *Sens. Actuat. B Chem.* 2000, 80, 8-14.
- [10] Hison C, Iannotti V, Ausanio G, Luponio C and Lanotte L. *A magnetoelastic amorphous ribbon in a silicone sheath as stress sensor and self indicator of strain threshold*, *Sensors Actuators A: Phys.* 2003, 106, 164–7.
- [11] Grimes, C.A.; Stoyanov, P.G.; Kouzoudis, D.; Ong, K.G. *Remote query pressure measurement using magnetoelastic sensor*. *Rev. Sci. Instrum.* 1999, 70, 4711-4714.
- [12] Kouzoudis, D.; Grimes, C.A. *The frequency response of magnetoelastic sensors to stress and atmospheric pressure*. *Smart Mater. Struct.* 2000, 9, 885-889.

- [13] Jain, M.K.; Cai, Q.Y.; Grimes, C.A. A wireless micro-sensor for simultaneous measurement of pH, temperature, and pressure. *Smart Mater. Struct.* 2001, 10, 347-353.
- [14] Kouzoudis, D.; Grimes, C.A. Remote query fluid-flow velocity measurement using magneto-elastic thick-film sensors. *J. Appl. Phys.* 2000, 87, 6301-6303.
- [15] Loisel, K.T.; Grimes, C.A. Viscosity measurements of viscous liquids using magnetoelastic thick-film sensors. *Rev. Sci. Instrum.* 2000, 71, 1441-1446.
- [16] C. A. Grimes, D. Kouzoudis, C. Mungle, *Simultaneous measurement of liquid density and viscosity using remote query magnetoelastic sensors*, *Rev. Sci. Instrum.* 2000, 71, 3822-3824.
- [17] M. K. Jain and C. A. Grimes, *Effect of surface roughness on liquid property measurements using mechanically oscillating sensors*, *Sensors and Actuators A*, 2002, 100, pp. 63-69
- [18] L. D. Landau and E. M. Lifshitz, *Theory of elasticity*: Pergamon Press, 1986.
- [19] J. Merhaut, *Theory of electroacoustics*: New York ; London : McGraw-Hill, International Book Co., 1981.
- [20] D. S. Ballantine, White, R.M., Martin, S.J., Ricco, A.J., Frye, G.C., Zellers, E.T., Wohltjen, H., *Acoustic wave sensors: theory, design and physico-chemical applications*: Academic Press, 1997.
- [21] "Agilent 4395A Network/Spectrum/Impedance Analyzer Operation Manual", Agilent Technologies.
- [22] S.Q. Li, Development of Novel Acoustic Wave Biosensor Platforms Based on Magnetostriction and Fabrication of Magnetostrictive Nanowires, Dissertation, Auburn University, 2007.
- [23] S. Timoshenko and D. H. Young, *Vibration Problems in Engineering*, 3<sup>rd</sup> ed., Van Nostrand, New York, 1955, p. 297.
- [24] K. N. Tong, *Theory of Mechanical Vibration*, Wiley, New York, 1960, p. 252.
- [25] Schmidt, S.; Grimes, C.A. Characterization of nano-dimensional thin film elastic moduli using

magnetoelastic sensors. *Sens. Actuat. A Phys.* 2001, 94, 189-196.

[26] Perov N S, Pan'kova E V, Kuznetsov G S, Rodionov V V and Inoue M, Magnetoelastic waves in amorphous ribbons excited by local AC magnetic fields: effect of stresses and DC magnetic field, *J. Magn. Mater.*, 2007, 310, 2633-5.

[27] Hubert, O.; Daniel, L., Measurement and Analytical Modeling of the  $\Delta E$  Effect in a Bulk Iron-Cobalt Alloy, *Magnetics*, *IEEE Transactions on* , vol.46, no.2, pp.401-404, Feb. 2010.

[28] Livingston, J. D. Magnetomechanical properties of amorphous metals, *Phys. Stat. Sol. A* 1982, 70, 591-596.

[29] Chikazumi S and Charap S H, *Physics of Magnetism*, New York: Wiley, 1964.

[30] Wen Shen, Leslie C Mathison, Valery A Petrenko and Bryan A Chin, Design and characterization of a magnetoelastic sensor for the detection of biological agents, *J. Phys. D: Appl. Phys.* 43 (2010) 015004 (9pp).

[31] C. Mungle, C. A. Grimes, W. R. Dreschel, Magnetic field tuning of the frequency-temperature response of a magnetoelastic sensor, *Sensors and Actuators A: Physical*, 101, 1-2, 2002, 143-149.

[32] "<http://www.metglas.com/downloads/2826mb.pdf>", Metglas Inc, 440 Allied Drive, Conway, SC 29526.

## CHAPTER 3

# MAGNETOSTRICTIVE STRIP SENSORS TO IDENTIFY THE NONLINEARITY OF VISCOSITY

### 3.1 Introduction

As discussed in Chapter 2, magnetostrictive strip is introduced to develop high performance portable on-line detection sensors because of the high Q-value and good performance in liquid media. And also for driving and sensing strips through magnetic fields, no physical connection is needed between the sensor and interrogation system. It is convenient to have this kind of sensor system to measure liquid properties [1-3].

When magnetostrictive strip is placed into liquids, the damping force which exerts on the sensor vibrations will change due to the viscosity and density changes of the surrounding medium. The resonance frequency shift  $\Delta f$  is shown as [4]:

$$\Delta f = \frac{\sqrt{\pi f_0}}{2\pi\rho d} \sqrt{\eta\rho_l} \quad (3-1)$$

where  $f_0$  is the initial resonance frequency,  $\rho_l$  and  $\eta$  are the density and viscosity of the liquid,  $d$  is strip thickness and  $\rho$  is the density of the strip sensor. And the sensing mechanism is established based on the resonance behaviors change of magnetostrictive materials with surrounding medium changes.

Because of the working principle of AW devices, the shear rate of magnetostrictive strip always changes during the vibration. Inconsistent results could be obtained at different shear rates when measured in non-Newtonian liquids, whose apparent viscosity depends on shear rate. Regular methods to characterize viscosity that is based on only one resonance frequency

$(f_r)$  is no longer effective. In this study, multiple experimental characteristic frequencies, which can be obtained simultaneously for one measurement are used to set up the model to identify the nonlinearity of liquids. And different factors which have influences on resonance behaviors of magnetostrictive strip have been already discussed in the previous chapter. Based on these results, optimized conditions are chosen during the measurement.

### **3.2 Experimental and measurement setup**

This set-up includes a custom-designed Helmholtz coil and a pair of homemade pick-up coils to characterize the resonance behavior of the magnetostrictive strip. The AC driving magnetic field at a frequency up to 500 kHz and DC bias magnetic field are provided by Helmholtz coil. The magnetostrictive strip was put into a chamber that was put in the middle of the Helmholtz coil. Two pick-up coils were wound in opposite directions and connected in a series so that the output signal is zero if there is no vibration of the magnetostrictive strip. Therefore, the output of the pick-up coils only represents the magnetic signal generated by the vibration of the magnetostrictive strip. The pick-up coil pairs were connected to a lock-in amplifier (SRS830, Stanford Research Systems, Sunnyvale, CA) to measure the electric potential generated in the coils, which has two outputs – the amplitude and phase of the electric potential. The amplitude of the output signal from the lock-in amplifier is proportional to the amplitude of the magnetostrictive strip's vibration, while the phase signal represents the phase difference between the magnetostrictive strip's vibration and the driving magnetic field. A set of typical results is given in Figure 3.1, where a magnetostrictive strip in size of 25 mm ( $L$ )  $\times$  3.0 mm ( $W$ )  $\times$  30  $\mu$ m ( $t$ ) was operated in R-100 reference oil. In this case, the resonance frequency ( $f_r$ ) and anti-resonance frequency ( $f_r'$ ) of the device are 82610 Hz and

87170 Hz, respectively.

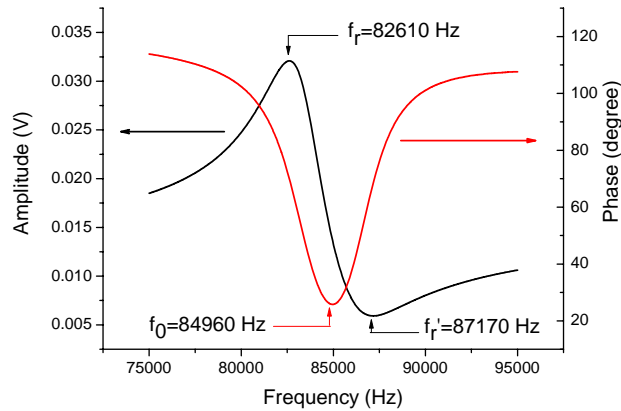


Figure 3.1. The frequency dependence of the phase and amplitude signals from the lock-in amplifier for a magnetostrictive strip in size of 25 mm ( $L$ )  $\times$  3.0 mm ( $W$ )  $\times$  30  $\mu$ m ( $t$ ) in R-100 reference oil.

Metglas alloy 2826MB ribbon (iron nickel-based) obtained from Honeywell International (Conway, SC) was used as the sensor platform. Metglas 2826MB thin film was diced into the exact size of the sensor by a micro-dicing saw. To remove the grease remnant after dicing, the particles were cleaned in acetone by using an ultrasonic cleaner (Cole Parmer) for 30 minutes and dried by nitrogen gas. Then these magnetostrictive strips are ready for visco-liquid properties study.

Eight reference oils were acquired from Tannas Company, including five Newtonian oils (R-100, R-300, R-2350, R2450, LNP-5) and three non-Newtonian oils (NNR-80, NNR-03, NNR-10). Fresh BP Turbo oil 2380 is used for an engine oil sample. The used oil samples are gotten by artificially degrading fresh oil at 240°C for 24, 48, 72, 96 and 120 hours.

The performance of the visco-liquid sensor system, with magnetostrictive strips, was evaluated by completely immersing the sensor in the liquid. The schematic of system was shown in Figure 3.2. At first the temperature was room temperature (23.5~24.1 °C).



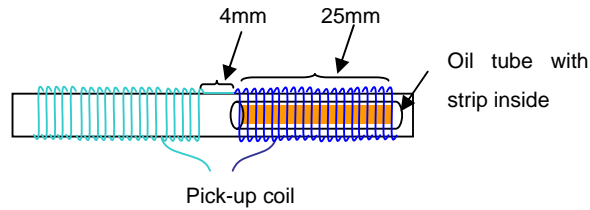


Figure 3.2. Schematic diagram of the visco-liquid sensor system.

### 3.3 Determination of three characteristic frequencies

Three easily determined characteristic frequencies are used to compare the performance of magnetostrictive strip in different liquids, respectively the resonance frequency ( $f_r$ ), the experimental resonance frequency ( $f_0$ ) and anti-resonance frequency ( $f_r'$ ) shown in Figure 3.1. With media changes, these parameters also change. By comparing them, the difference of the liquids can be shown.

A traditional viscometer can also identify these liquids. In order to compare the results, the viscosities were measured by a traditional viscometer and densitometer firstly; the results are listed in Table 3.1 & 3.2. (Viscosity measurement: Viscoliner® 1710 series viscometer; Density measurement: Sigma 702 Tensiometer)

	R-100	R-300	NNR-80	R-2350	NNR-03	NNR-10	LNP-5	R-2450
$\rho$ (g·ml <sup>-1</sup> )	0.8379	0.8675	0.8534	0.8714	0.8579	0.8617	0.8370	0.8815
$\eta\rho$	16.66	53.73	66.813	132.9	148.6	184.7	180.3	328.5
$\eta$ (mPa·s)	19.9	61.9	78.3	152.5	173.2	214.3	215.4	372.7
$\nu$ (cSt)	23.7	71.4	91.7	175.0	201.9	248.7	257.4	422.8
Temp(°C)	22.87	22.77	20.4	22.46	22.03	21.90	22.10	22.14

Table 3.1. Dynamic viscosity and kinematic viscosity of reference oils.

oil	$\rho$ g·ml <sup>-1</sup>	$\eta \cdot \rho$	$\eta$ cP	$\nu$ cSt
0 h	0.9713	50.68	52.2	53.7
24 h	0.9803	65.13	66.4	67.8
48h	0.9880	84.69	85.7	86.8
72 h	0.9973	114.28	114.6	114.9
96 h	1.0102	201.24	199.2	197.2
120 h	1.0162	419.78	413.1	406.5

Table 3.2. Viscosity of artificial degraded oil BP 2380 aged at 240 °C.

Then all the three parameters of each liquid are picked up and put into the Figure 3.3. The three non-Newtonian oils are in the circles, and they didn't fall on the main curve. By this feature, we can identify Newtonian oils and non-Newtonian oils preliminarily. However, the X-axis is viscosity of oils, obtained by a Viscoliner® 1710 series viscometer. It is time and labor consuming because either two devices have to be used or measurements have to be done at least twice to identify these kinds of oils. So a new method to identify Newtonian oils and non-Newtonian oils is put forward which uses multiple characteristic frequencies to get the figure. Because different gaps lies between Newtonian and non-Newtonian on each curve, the difference can be found by choosing the proper Y-axis (some function of  $f_r$ ,  $f_0$  &  $f_r'$ ) if choosing one of three frequencies as X-axis. All the data can be gotten from one device and  $f_r$ ,  $f_0$  &  $f_r'$  can be gotten by one measurement. Compared to the traditional way to identify non-Newtonian oils which needs to contrast viscosity at different shear rate or shear stress, this method is more directly and easy. Figure 3.4 shows the results mentioned above.

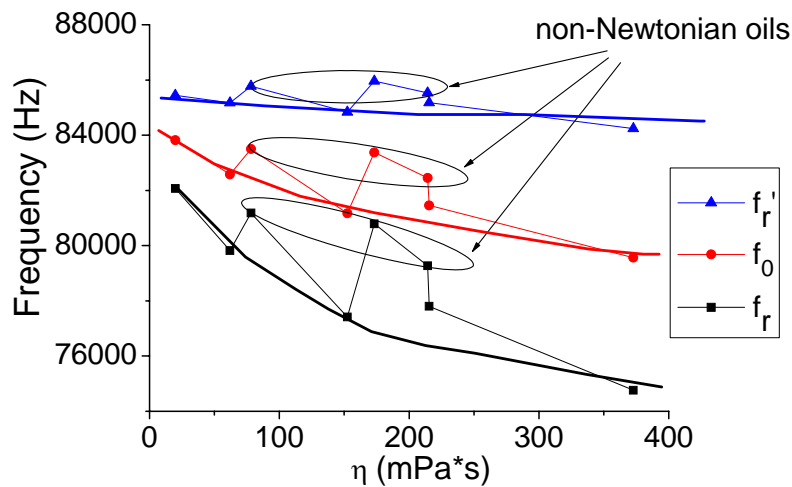


Figure 3.3. The three characteristic frequencies of 25mm (25mm × 3mm × 30μm) magnetostrictive strip in different oils vs. viscosity of oils.

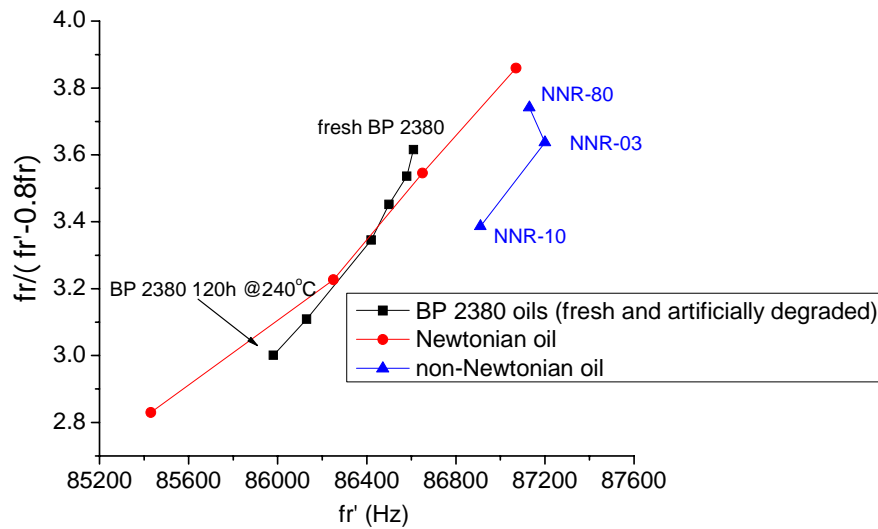


Figure 3.4. The properly chosen function of characteristic frequencies vs. anti-resonance frequency ( $f_r'$ ) of 25 mm ( $L$ ) × 3 mm ( $W$ ) × 30 μm ( $t$ ) magnetostrictive strip in different oils at room temperature.

It is found the black curve, which contains six oil samples from fresh BP 2380 oil to artificially degraded oil 120 hours @ 240 °C, matches mostly to the red curve (Newtonian oils). And the tendency is also the same. The red curve of Newtonian reference oils does not include LNP-5 oil, which is designed for low temperature working circumstances (-40 °C ~ -5

°C) [5]. The blue curve is non-Newtonian reference oils. And magnetostrictive strip can perform well even in high viscosity circumstance (such as in R-600 oil, whose viscosity is 1733 mPa·s).

### 3.4 Comparison of the performances of different length magnetostrictive strip sensors in oils

Magnetostrictive strips with different lengths will generate various vibration signals in oils under a magnetic field. In order to maximize the signal difference between Newtonian oils and non-Newtonian oils, the performances of magnetostrictive strips of different lengths but same width are studied and compared.

Beside 25 mm × 3 mm × 30 μm magnetostrictive strip, two others 30 mm × 3 mm × 30 μm and 40 mm × 3 mm × 30 μm strips, are used to compare resonance behaviors in oils. The results are shown as follows:

(1) 30 mm × 3 mm × 30 μm magnetostrictive strip;

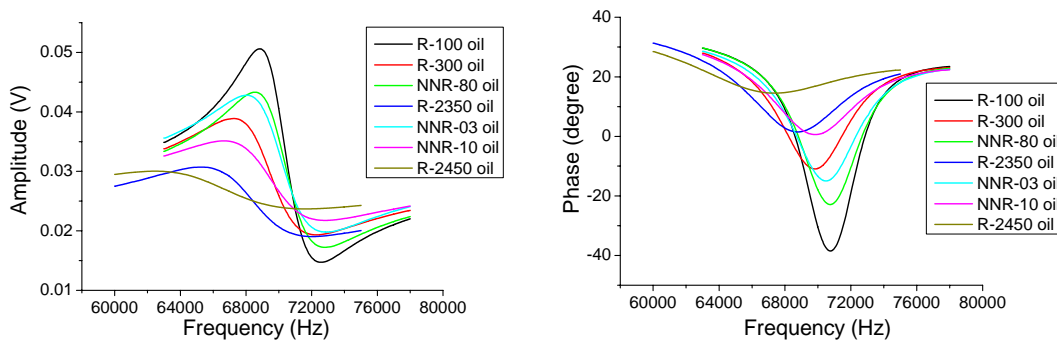


Figure 3.5. Resonance behaviors of 30mm (30mm×3mm×30μm) magnetostrictive strip sensor in oils at room temperature.

And  $f_r$ ,  $f_0$  and  $f_r'$  are picked up from Figure 3.5 and listed below:

30mm×3mm×30μm Metglas 2826mb strip at room temperature			
Media	$f_r$ (Hz)	$f_0$ (Hz)	$f_r'$ (Hz)
R-100	68840	70760	72560
R-300	67270	69820	72280
<b>NNR-80</b>	68550	70750	72790
R-2350	65250	68780	72080
<b>NNR-03</b>	68040	70490	72890
<b>NNR-10</b>	66670	69840	72830
R-2450	62480	67350	71640

Table 3.3. Resonance frequencies of 30mm (30mm×3mm×30μm) magnetostrictive strip sensor in oils.

By selecting the same function of characteristic frequencies as the Y-axis and anti-resonance frequency as X-axis, we find the gap between Newtonian and non-Newtonian oils becomes wider, compared to Figure 3.4.

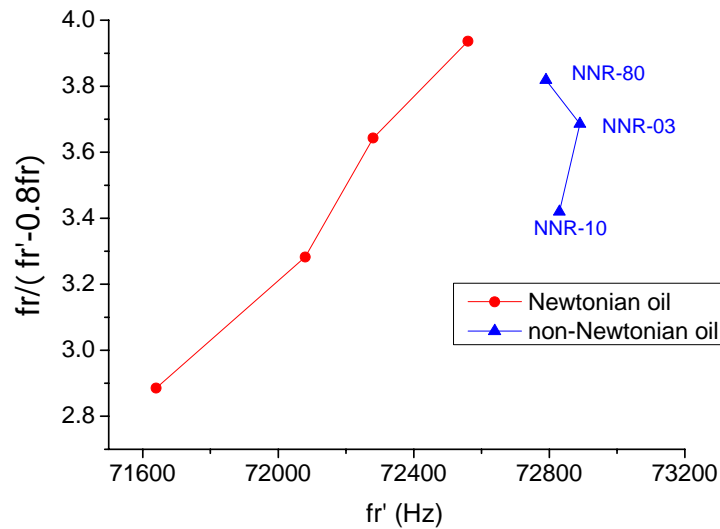


Figure 3.6. The properly chosen function of characteristic frequencies vs. anti-resonance frequency ( $f_r'$ ) of 30 mm ( $L$ ) × 3 mm ( $W$ ) × 30 μm ( $t$ ) magnetostrictive strip in different oils at room temperature.

(2) 40 mm × 3 mm × 30 μm magnetostrictive strip;

Measures of the resonance behaviors in BP 2380 oils and  $f_r$ ,  $f_0$  and  $f_r'$  are picked up to list

below:

40mm×3mm×30μm Metglas 2826mb strip at room temperature				
Media(BP 2380)	$f_r$ (Hz)	$f_0$ (Hz)	$f_r'$ (Hz)	$\eta$ (mPa·s)
fresh (0h)	50110	52270	54350	52.18
24h	49610	52020	54360	66.44
48h	49120	51710	54190	85.72
72h	48510	51360	54050	114.59
96h	47250	50580	53750	199.21
120h	46980	50440	53640	413.09

Table 3.4. Resonance frequencies of 40mm (40mm×3mm×30μm) magnetostrictive strip sensor in oils.

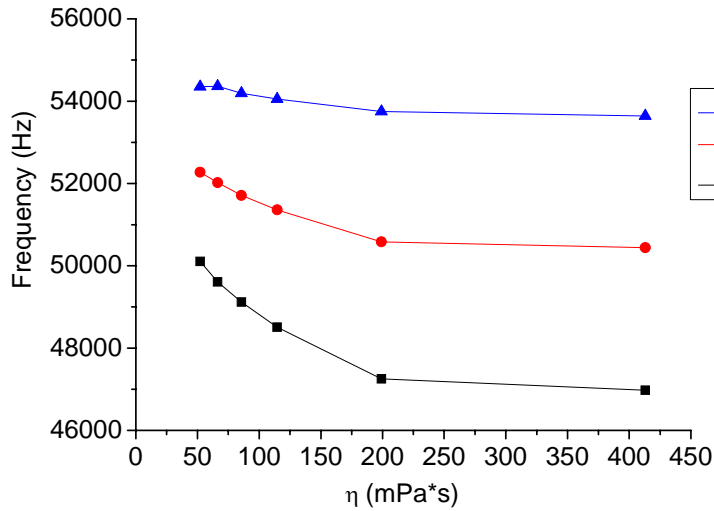


Figure 3.7. The three characteristic frequencies of 40mm (40mm×3mm×30μm) magnetostrictive strip in different oils vs. viscosity of BP oils (fresh and artificially degraded) at room temperature.

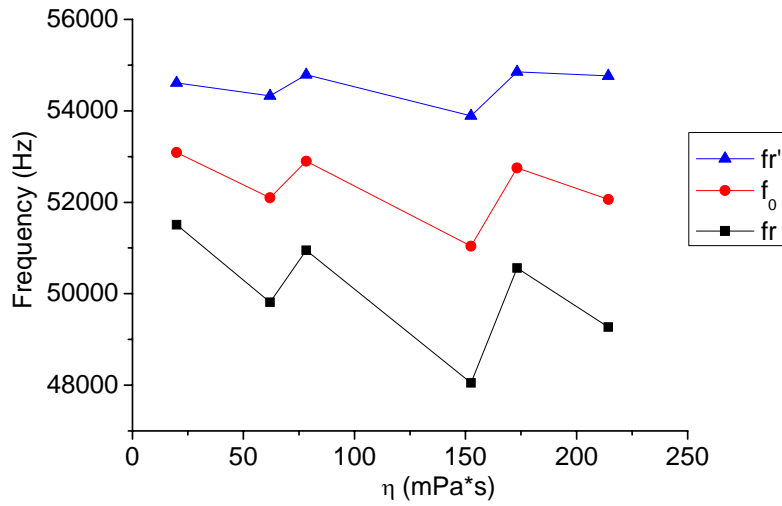


Figure 3.8. The three characteristic frequencies of 40mm (40mm×3mm×30μm) magnetostrictive strip in different oils vs. viscosity of reference oils.

From the Figure 3.7 and 3.8, by selecting the same function of characteristic frequencies

$(\frac{f_r}{f_r - 0.8f_r})$  as the Y-axis and anti-resonance frequency ( $f_r'$ ) as the X-axis, we have Figure

3.9, in which we find the gap between Newtonian and non-Newtonian oils becomes wider, compared to Figure 3.4. The black curve which contains six oil samples from fresh BP 2380 oil to artificially degraded oil 120 hours @ 240 °C, matches together mostly with the red curve (Newtonian oils). And the tendency is also the same.

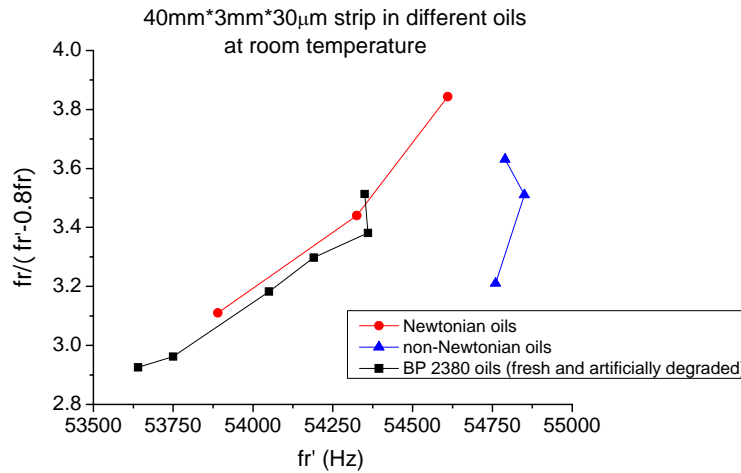


Figure 3.9. The properly chosen function of characteristic frequencies vs. anti-resonance frequency ( $f_r'$ ) of 40 mm ( $L$ )  $\times$  3 mm ( $W$ )  $\times$  30  $\mu$ m ( $t$ ) magnetostrictive strip in different oils.

By comparing performances of magnetostrictive strips with different lengths from Figure 3.4, Figure 3.6 and Figure 3.9, it can be found the difference between Newtonian and non-Newtonian oils becomes more obvious with an increase in strip length. And also by using larger strip, vibration signal could be stronger.

### 3.5 Comparison of the performances of different length-width ratio magnetostrictive strip sensors in oils

The viscous drags which act on the main surface and edge are very different even for the same magnetostrictive strip. And this will affect the performance of magnetostrictive strip. The optimized results can be achieved by studying same length with different length-width ratios magnetostrictive strips in this study.

Based on the former study of different length magnetostrictive strips, 40 mm  $\times$  3 mm  $\times$  30  $\mu$ m magnetostrictive strip which has the best performance is chosen in this study. And the performances of different length-width ratio (ratio = 8, 10 and 13.3) magnetostrictive strips are shown in Figure 3.10. It is found that as the length-width ratio grows larger (up to 13.3),



the gap between the Newtonian curve and non-Newtonian curve becomes wider (using the same range and same increment for the X-axis for the comparison). Because the same length strip sensor with a smaller width has larger sensitivity to the viscous damping force and viscous drags, which act on the sensor edge, is more significant with an increased length-width ratio, it is much easier to show a tiny difference between liquids by using a large length-width ratio strip sensor. And the conclusion is that magnetostrictive strip of same length with a smaller width has better performance in this study.

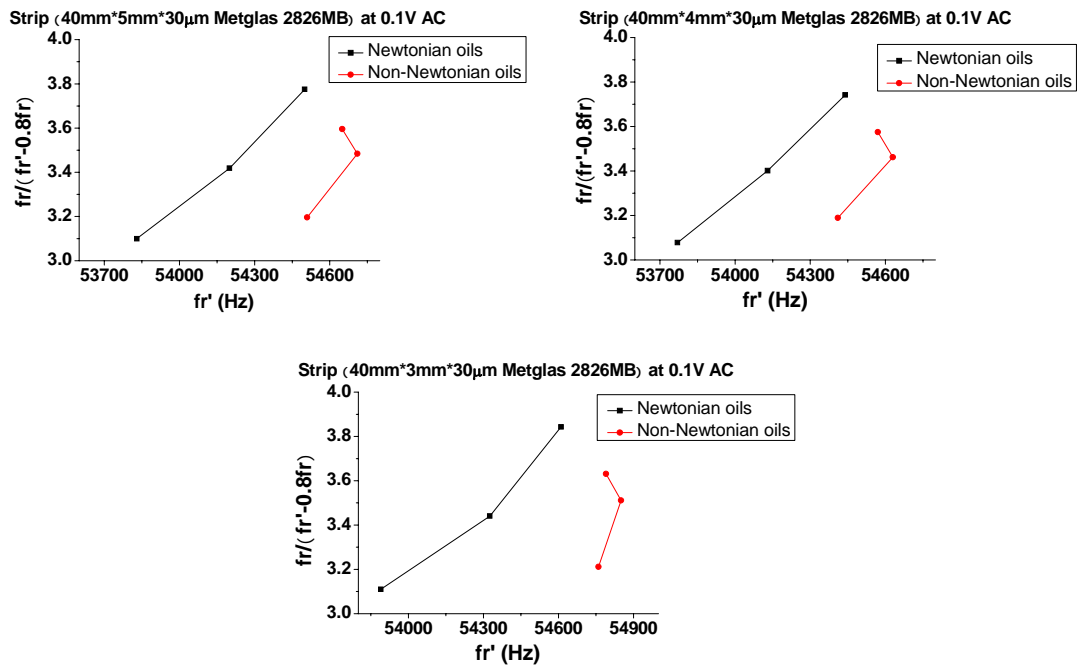


Figure 3.10. The comparison of function of characteristic frequencies  $\left(\frac{f_r}{f_r - 0.8f_r}\right)$  vs. anti-resonance frequency ( $f_r'$ ) of magnetostrictive strip in different length-width ratios.

### 3.6 The performances of 40 mm × 3 mm × 30 µm magnetostrictive strip sensor in oils at different temperatures

In order to apply magnetostrictive sensor to liquids which work in a broad temperature range such as engine oil and vacuum pump oil, it is necessary to study the performances of

the sensor in different temperatures. Based on former studies of different length magnetostrictive strips and different length-width ratio strip sensors, a 40 mm × 3 mm × 30 μm magnetostrictive strip is chosen in this study. And the results are shown below:

(1) At 50°C;

magnetostrictive strips (40mm*3mm*30μm Metglas 2826mb) 50 °C			
Media	$f_r$ (Hz)	$f_0$ (Hz)	$f_r'$ (Hz)
R-100	52230	53200	54150
R-300	51470	52830	54130
<b>NNR-80</b>	51920	53210	54450
R-2350	50680	52380	54000
<b>NNR-03</b>	51740	53190	54580
<b>NNR-10</b>	51280	52960	54530
R-2450	49420	51730	53920

Table 3.5. Resonance frequencies of 40mm (40mm×3mm×30μm) magnetostrictive strip sensor in oils at 50°C.

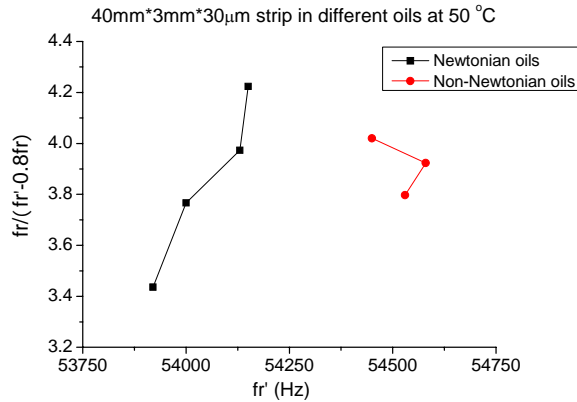


Figure 3.11. The function of characteristic frequencies ( $\frac{f_r}{f_r' - 0.8f_r}$ ) vs. anti-resonance frequency ( $f_r'$ ) of 40 mm ( $L$ ) × 3 mm ( $W$ ) × 30 μm ( $t$ ) magnetostrictive strip in different oils at 50°C.

(2) At 80 °C;

magnetostrictive strips (40mm*3mm*30µm Metglas 2826mb) 80 °C			
Media	$f_r$ (Hz)	$f_0$ (Hz)	$f_r'$ (Hz)
R-100	52790	53480	54140
R-300	52350	53240	54110
<b>NNR-80</b>	52470	53470	54420
R-2350	51960	53050	54130
<b>NNR-03</b>	52350	53460	54540
<b>NNR-10</b>	52050	53320	54570
R-2450	51510	52820	54120

Table 3.6. Resonance frequencies of 40mm (40mm×3mm×30µm) magnetostrictive strip sensor in oils at 80 °C.

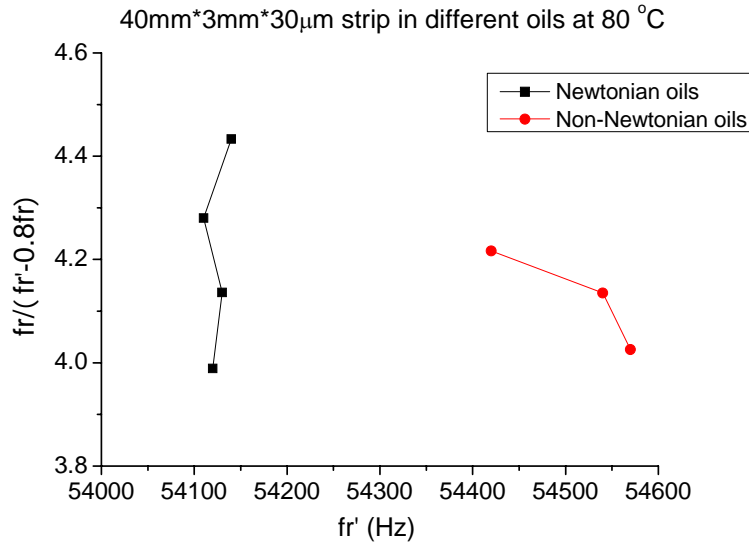


Figure 3.12. The function of characteristic frequencies ( $\frac{f_r}{f_r - 0.8f_r'}$ ) vs. anti-resonance frequency ( $f_r'$ ) of 40 mm ( $L$ ) × 3 mm ( $W$ ) × 30 µm ( $t$ ) magnetostrictive strip in different oils at 80 °C.

(3) At 100°C.

magnetostrictive strips (40mm*3mm*30µm Metglas 2826mb) 100 °C			
Media	$f_r$ (Hz)	$f_0$ (Hz)	$f_r'$ (Hz)
R-100	52920	53520	54110
R-300	52590	53350	54080
<b>NNR-80</b>	52610	53500	54410
R-2350	52430	53300	54110
<b>NNR-03</b>	52510	53500	54470
<b>NNR-10</b>	52280	53400	54500
R-2450	52030	53100	54110

Table 3.7. Resonance frequencies of 40mm (40mm×3mm×30µm) magnetostrictive strip sensor in oils at 100°C.

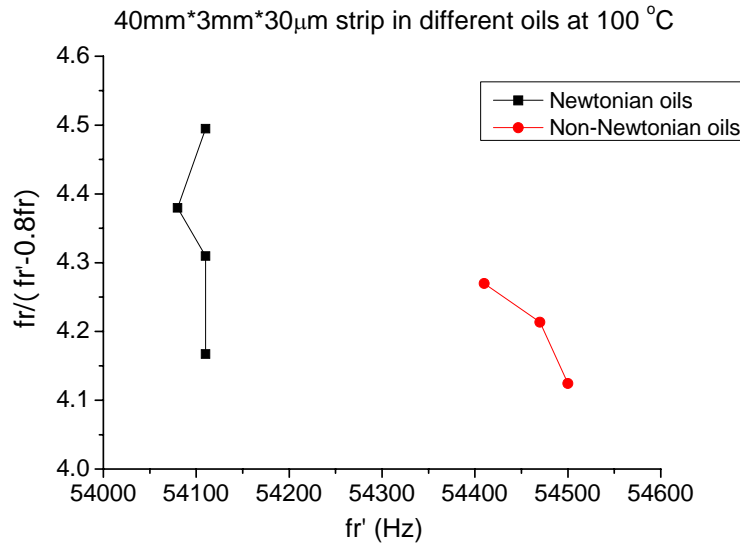


Figure 3.13. The function of characteristic frequencies ( $\frac{f_r}{f_r - 0.8f_r}$ ) vs. anti-resonance frequency ( $f_r'$ ) of 40 mm ( $L$ ) × 3 mm ( $W$ ) × 30 µm ( $t$ ) magnetostrictive strip in different oils at 100°C.

From these results, it is found that the 40mm × 3mm × 30µm Metglas 2826mb strip has good performance at high temperatures (at 50 °C, 80 °C and 100 °C) as well as room temperature. And this aspect ratio is good for magnetostrictive strip to differentiate

Newtonian oils and non-Newtonian oils. As discussed in Chapter One, all microacoustic devices which monitor engine oils are currently developed to measure the viscosity only, and it is also well known that a tiny change in viscosity will not influence engine performance very much. Therefore, it is reasonable to come to the conclusion that the non-linearity of viscosity may be the real key of determining engine oil conditions. And in this study of different temperatures, we found that the  $40\text{mm} \times 3\text{mm} \times 30\mu\text{m}$  Metglas 2826mb strip had a good performance within a broad temperature range when differentiating Newtonian oils & non-Newtonian oils and also identifying the non-linearity of viscosity.

### **3.7 Conclusions**

Combined characteristic frequencies together, AW devices can identify the non-linearity of viscosity and also differentiate Newtonian oils & non-Newtonian oils. The resonance behaviors of magnetostrictive strips with different lengths in different oils are studied, and the performances of same length magnetostrictive strips with different length-width ratios are also investigated. All studies show that geometry of AW sensor is important. Longer length is better and also larger length-width ratio is better in identifying the non-linearity of viscosity. In order to apply magnetostrictive strips in real circumstances, the performances of  $40\text{ mm} \times 3\text{ mm} \times 30\text{ }\mu\text{m}$  strip sensor are studied under different temperatures and it's found that magnetostrictive strip of this size has good performance in identifying the non-linearity of viscosity within broad temperature range.

#### **References:**

- [1] C.A. Grimes, S.C. Roy, S. Rani, Q. Cai, Theory, Instrumentation and Applications of Magnetoelastic Resonance Sensors: A Review, *Sensors*, 2011, 11, 2809-2844.

- [2] Etienne Du Tremolet De Lachesserie, *Magnetostriction: Theory and Applications of Magnetoelasticity*. CRC Press, Boca Raton, 1993.
- [3] C.A. Grimes, C.S. Mungle, K.F. Zeng, M.K. Jain, W.R. Dreschel, M. Paulose, K.G. Ong, Wireless Magnetoelastic Resonance Sensors: A Critical Review, *Sensors* 2 (2002) 294-313.
- [4] P.G. Stoyanov, C.A. Grimes, A remote query magnetostrictive viscosity sensor, *Sens. Actuat. B Chem.* 2000, 80, 8-14.
- [5] "<http://www.tannasco.com/images/RefOil-CatalystGuide2.pdf>", Tannas Co. 4800 James Savage Rd., Midland, MI 48642.

## CHAPTER 4

# PIEZOELECTRIC CANTILEVER SENSORS TO IDENTIFY THE NONLINEARITY OF VISCOSITY

### 4.1 Introduction

Magnetostrictive strip sensors discussed above can be acted as useful alternatives to traditional viscometers. However, this device works at comparatively high-shear rates (vibration frequency) and with small vibration amplitudes. And for non-Newtonian liquids, the results are not directly comparable to those obtained from conventional viscometers which work at rather low shear rates. So cantilever sensors are designed here, in which vibration has usually lower resonance frequencies and higher vibration amplitudes, making them more suitable for non-Newtonian liquids.

According to actuating and sensing technologies and operating principles, cantilevers can be classified into three different modes: static, heat, and dynamic modes [1-3]. In static deflection mode, unbalanced surface stress is caused by the different mechanic loads on the upper and lower surfaces of a cantilever leading to a perceptible deflection up or down as in Figure 4.1(a) [4, 5]. In heat (bimetallic) mode, a thin metal layer is coated on the cantilever surface. The temperature change of the cantilever will bend the cantilever due to the difference between thermal expansion coefficients of these two layers (coat and substrate) as presented in Figure 4.1(b). Several nanometers deflection of the cantilever can be measured with only  $10^{-5}$ K temperature changes [1, 3]. Compared to the above two modes, the dynamic mode cantilever can be more easily applied in viscosity determination because whether in

static or heat mode, we need to know the deflection or bend curvature of the cantilever in liquid to determine the viscosity property. And most liquids are opaque or not clear enough to check the cantilever deflection. In dynamic mode, the cantilever acts as an oscillator in Figure 4.1(c) and vibrates among the surrounding medium. The damping force which reflects the viscosity property of medium is acting on the cantilever. And with the medium changing, the damping force also changes. The damping force increases and thus lowers the resonance frequency, just like QCM. In this research, we use piezoelectric cantilevers which are actuated by an external electric field, and the vibration of cantilevers can be easily monitored by measuring the impedance of piezoelectric cantilevers via impedance analyzer.

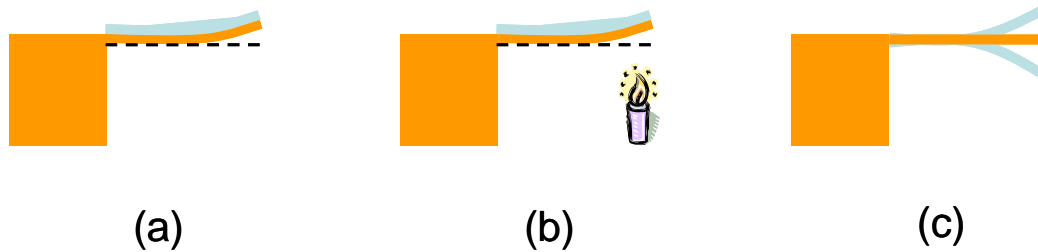


Figure 4.1. Three different operation modes of cantilever sensor: (a) static mode, where unbalance mechanic loads on upper and lower surfaces lead to the bending of cantilever; (b) heat mode sensing temperature changes by static bending caused by different thermal expansion coefficient of two layers (coat and substrate), and (c) dynamic mode sensing the visco-drag force added on the cantilever by resonance frequency change.

Piezoelectricity is the ability of a material to generate an electric potential in response to applied mechanical stress or strain [6]. This effect is formed in crystals that have no center of symmetry, and the piezoelectric effect is reversible. The reverse piezoelectric effect is that a mechanical deformation is generated as the response to an external electric field.

## 4.2 Configuration of piezoelectric cantilever sensor

Cantilevers made of different materials have been developed as transducers used in sensors. A typical cantilever usually has a long and thin beam fixed at one end with support.



And a resonator such as cantilever that has a lower resonance frequency and higher shear vibration amplitude is comparable with conventional viscosity measurement. Cantilevers generate shear waves in viscous liquids during mechanical vibration. The resonance frequency and cantilever damping are affected by the viscosity of the liquid, which can be used for viscosity sensing. Acting as viscosity sensor platform, cantilevers' resonance frequencies change with different damping forces on the beam [7-10]. The cantilever oscillation will be damped and its resonance frequency also decreases when it is surrounded by a highly viscous medium. Cantilevers can therefore be applied as viscometers.

It is known that the  $n^{\text{th}}$ -mode flexural resonance frequency of an undamped cantilever with one end firmly clamped can be expressed as [11]:

$$f_n = \frac{\lambda_n^2}{2\pi\sqrt{12}} \frac{d}{L^2} \sqrt{\frac{E}{\rho(1-\nu^2)}} \quad (n = 0, 1, 2, \dots) \quad (4-1)$$

where the  $\lambda_n^2$  ( $\lambda_0=1.875$ ) is the dimensionless  $n^{\text{th}}$ -mode eigenvalue,  $d$  and  $L$  are the thickness and length of the cantilever, while  $E$ ,  $\rho$ , and  $\nu$  are the effective Young's modulus, density, and the Poisson's ratio of the beam material.

When cantilever is put into visco-liquid, the damping force will act on the sensor surface and change the characteristic frequency; also with the conditions of the visco-liquid change, the damping force changes. By monitoring the frequency shift of the sensor due to the damping force caused by the circumstance change, we can have a perspective view of the visco-liquid. Here the fundamental resonance frequency  $f_0$  ( $n = 1$ ) is selected due to the strong signal level.

Piezoelectric cantilever sensors have rather lower resonance frequencies and higher vibration amplitudes compared to magnetostrictive strip sensors with similar size. The

piezoelectric cantilevers used in this research are unimorph type, which consists of two layers: an active layer and an inactive layer. The configuration of a piezoelectric cantilever is shown in Figure 4.2. The active layer used here is a piezoelectric ceramics PZT (CUI Inc, Tualatin, OR); the inactive layer is brass thick film.

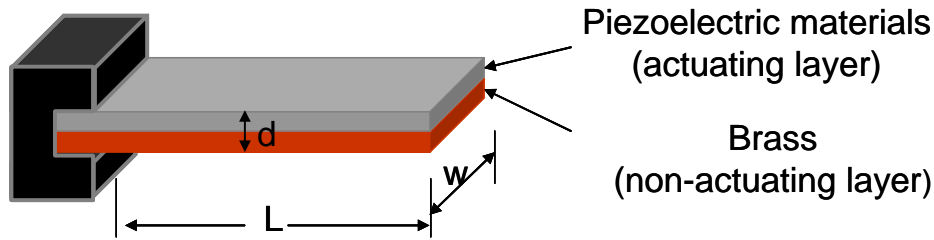


Figure 4.2. The schematic of piezoelectric cantilever sensor for visco-liquids.

In Table 4.1, the properties of cantilever beam such as density, Young's modulus, Poisson's ratio were given. The thickness is 0.25mm and 0.25mm for the actuating layer and non-actuating layer, respectively. The volumes of these two layers are only thickness dependent because the two layers have the same length and width. And the average density calculated from PZT ceramics and brass can be regarded as the density of piezoelectric cantilever.

Materials	Density (g/cm <sup>3</sup> )	Young's modulus (GPa)	Thickness (mm)	Poisson's ratio
PZT piezoelectric ceramics	7.5 [12]	63 [12]	25	0.3 [13]
brass	8.34	110 [14]	25	0.3
PZT/brass bilayers	7.92	86.5	50	0.3

Table 4.1. The effective material properties of PZT piezoelectric ceramics layer, brass layer and cantilever beam.

The principle of piezoelectric cantilever unimorph as visco-sensor platform is presented in Figure 4.3. The unimorph device oscillates under alternative electric field due to the active layer and inactive layer being bonded together. Characteristic resonance frequencies will

decrease when the medium changes to highly viscous liquid due to visco-drag acting on the unimorph. Different resonance frequency shifts can express the properties (such as viscosity) of the surrounding liquid medium. And the non-linearity of liquid viscosity can be obtained by analyzing the characteristic resonance frequencies shift.

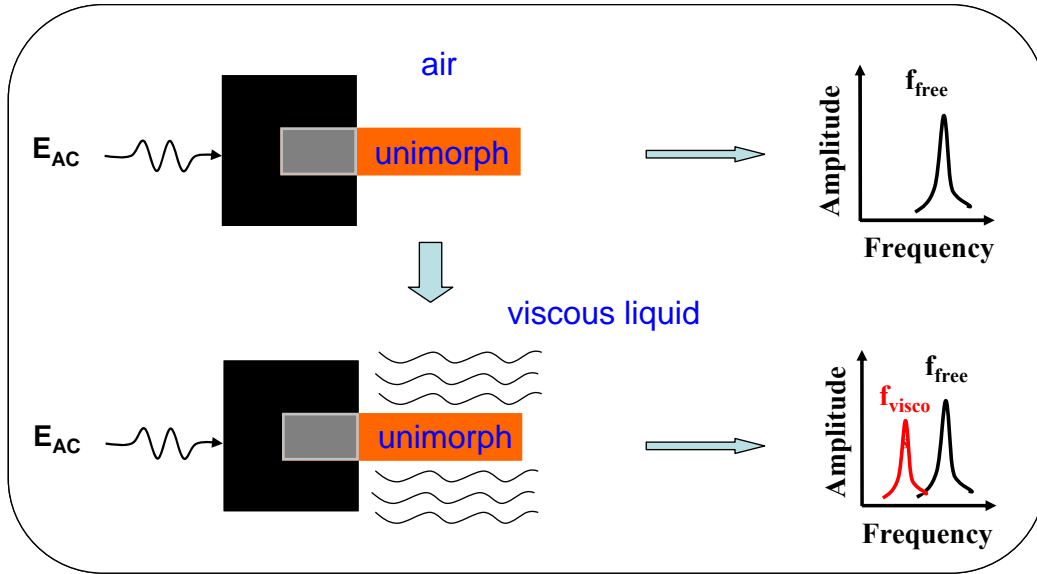


Figure 4.3. The schematic of principle of piezoelectric cantilever unimorph as visco-sensor platform.

### 4.3 Theory

The wave function of the bending vibration mode of a regular cantilever beam (dimension: length  $L$ , width  $W$  and thickness  $d$ ) can be presented as [11]:

$$\frac{\partial^2 y}{\partial t^2} + \frac{\bar{E}I}{\rho A} \frac{\partial^4 y}{\partial x^2} = 0 \quad (4-2)$$

where  $y$  is the bending deformation of the beam at the point  $x$  as shown in Figure 4.4,  $\bar{E}$  and  $\rho$  are the effective Young's modulus and effective mass density of the beam materials;  $I$  is moment of inertia for a rectangular beam, and  $A$  is the cross section area of the cantilever beam.

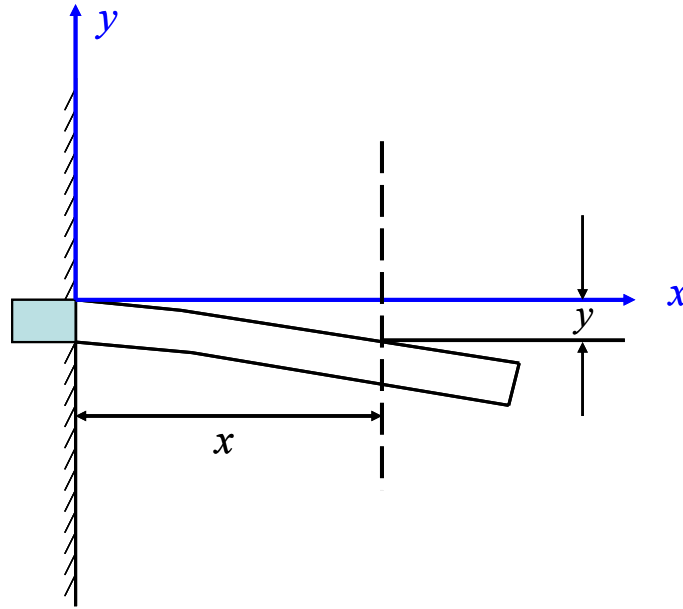


Figure 4.4. The schematic of rectangular cantilever, rigidly clamped at one end and free at the other.

For a rectangular beam with width  $W$  and thickness  $d$ ,  $A$  and  $I$  are given by [11]:

$$A = Wd \quad (4-3)$$

$$I = \frac{1}{12}Wd^3 \quad (4-4)$$

With the assumption of a cantilever beam structure with  $W \gg d$ , the effective Young's modulus is expressed by:

$$\bar{E} = \frac{E}{1 - \sigma^2} \quad (4-5)$$

where  $\sigma$  is the Poisson's ratio and  $E$  is the Young's modulus of cantilever material.

For harmonic oscillations  $y = y' e^{j\omega t}$  ( $\omega$  is the resonance frequency), we can combine with Equation (4-2) and get:

$$\frac{\bar{E}I}{\rho A} \frac{\partial^4 y'}{\partial x^4} - \omega^2 y' = 0 \quad (4-6)$$

which can be written as

$$\frac{\partial^4 y'}{\partial x^4} = \left(\frac{\lambda}{L}\right)^4 y' \quad (4-7)$$

$$\text{where } \left(\frac{\lambda}{L}\right)^4 = \frac{\rho A \omega^2}{EI} \quad (4-8)$$

The general solution of the wave function equation above is:

$$y'(x) = c_1 \cos\left(\frac{\lambda}{L}x\right) + c_2 \sin\left(\frac{\lambda}{L}x\right) + c_3 \cosh\left(\frac{\lambda}{L}x\right) + c_4 \sinh\left(\frac{\lambda}{L}x\right) = 0 \quad (4-9)$$

where,  $c_1$ ,  $c_2$ ,  $c_3$  and  $c_4$  are the constants, and  $\lambda$  is the non-dimensional parameter.

The boundary conditions of the cantilever beam rigidly fixed at one end and free at the other end are [11]:

$$y'(0) = 0, \quad \left. \frac{dy'(x)}{dx} \right|_{x=0} = 0, \quad \left. \frac{d^2 y'(x)}{dx^2} \right|_{x=L} = 0, \quad \text{and} \quad \left. \frac{d^3 y'(x)}{dx^3} \right|_{x=L} = 0 \quad (4-10)$$

The first two boundary conditions are from the fact that one end of the cantilever is rigidly clamped. The third and fourth boundary conditions are from the facts that there is no shear force acting at the free end of the beam (at  $x=L$ ) and no bending moment. Since the flexural vibration of the cantilever is at resonance frequencies, the characteristic equations are given by the general solution (4-9) and the boundary conditions [11]:

$$\coth \frac{\lambda}{2} = \tan \frac{\lambda}{2} \quad (4-11)$$

$$\coth \frac{\lambda}{2} = -\tan \frac{\lambda}{2} \quad (4-12)$$

The characteristic eigenvalues of resonance vibration can be deduced from equations (4-11) and (4-12). And the resonance frequencies of normal vibration are obtained by inserting eigenvalues into equation (4-8):

$$\omega_n = 2\pi f_n = \frac{\lambda_n^2}{L^2} \sqrt{\frac{EI}{\rho A}} \quad (4-13)$$

The  $n^{\text{th}}$ -mode flexural resonance frequency of an undamped cantilever with one end firmly clamped can be expressed as [11] in equation (4-1).

#### 4.4 Experimental and measurement setup

To prepare the cantilever, buzzers were chosen (model: CEB-35D26, thickness: 0.5mm from Digi-Key Corporation) and diced to different size strips for cantilever preparing, and cantilevers were prepared with aluminum holders, as shown in Figure 4.5.

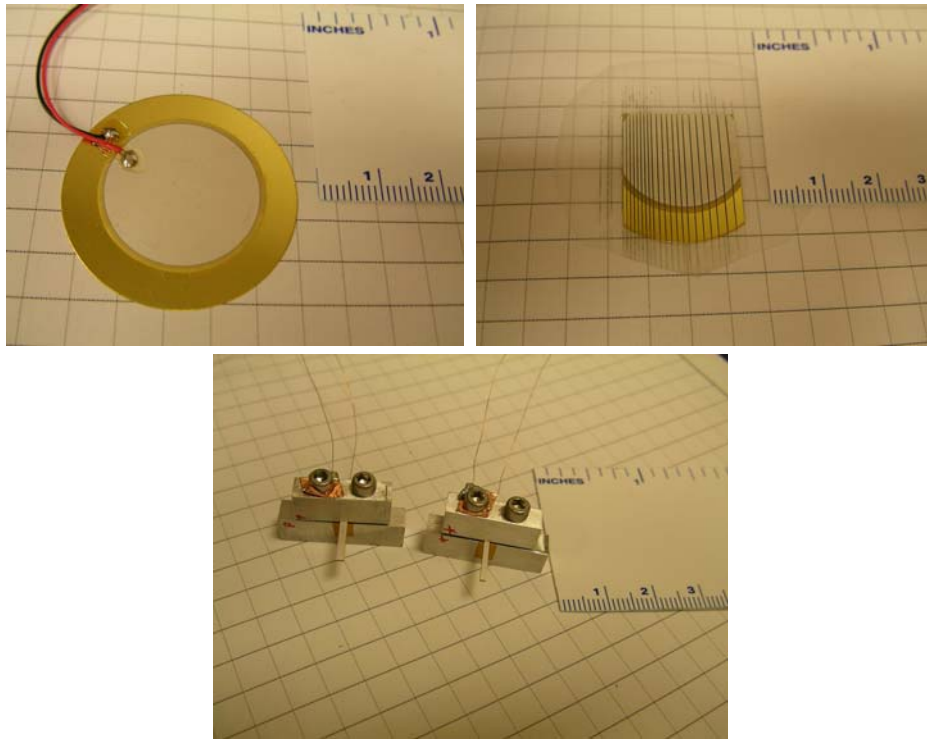


Figure 4.5. The process of prepare the piezoelectric cantilever sensor for visco-liquids.

The performance of the visco-liquid sensor system, piezoelectric cantilever, was evaluated by completely immersing the sensor in the liquid as shown in Figure 4.6. And the signal was measured by Agilent 4294A precision impedance analyzer which treats piezoelectric cantilever as a capacitor when it vibrates. With cantilever immersing into a changing medium, the signals also change, as the Figure 4.7 shown.

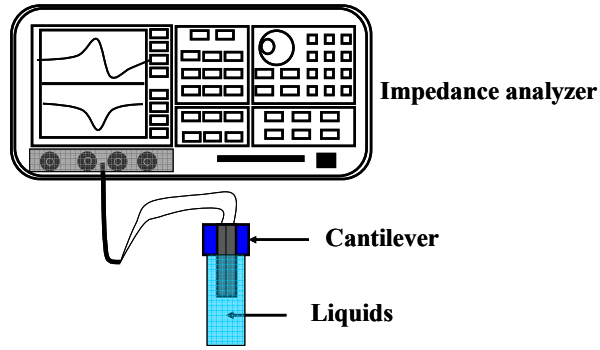


Figure 4.6. Set-up of impedance analyzer measurement of piezoelectric cantilever.

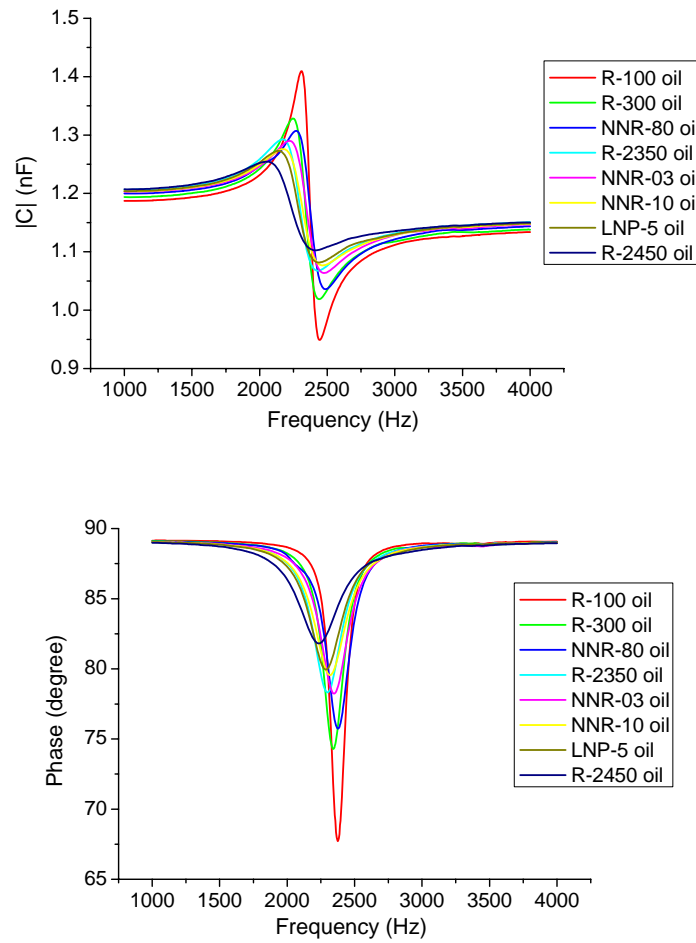


Figure 4.7. The capacitance and phase vs. frequency of  $9 \text{ mm} \times 0.7 \text{ mm} \times 0.5 \text{ mm}$  piezoelectric cantilever sensor in different oils.

PZT cantilever (9 mm × 0.7 mm × 0.5 mm) at 0.5V Osc level				
Media	$f_r$ (Hz)	$f_0$ (Hz)	$f_r'$ (Hz)	$\eta$ (mPa·s)
R-100	2308.75	2376.25	2443.75	19.88
R-300	2248.75	2342.5	2440	61.94
<b>NNR-80</b>	2271.25	2376.25	2485	78.29
R-2350	2170	2297.5	2428.75	152.5
<b>NNR-03</b>	2222.5	2346.25	2477.5	173.2
<b>NNR-10</b>	2173.75	2316.25	2466.25	214.3
LNP-5	2140	2286.25	2440	215.4
R-2450	2053.75	2233.75	2413.75	372.7

Table 4.2. Resonance frequencies of 9 mm × 0.7 mm × 0.5 mm PZT cantilever sensor in oils.

And by the same method mentioned in last chapter, the properly chosen function of characteristic frequencies vs. one of the three characteristic frequencies of cantilever in different oils are given below in Figure 4.8. From the figure, a gap can be found between Newtonian and non-Newtonian oils curves. The difference of Y-axis function between magnetostrictive strip and piezoelectric cantilever is due to unlike vibration mechanisms of these two AW devices. And for each AW device, it should have a unique properly chosen function of characteristic frequencies as Y-axis.

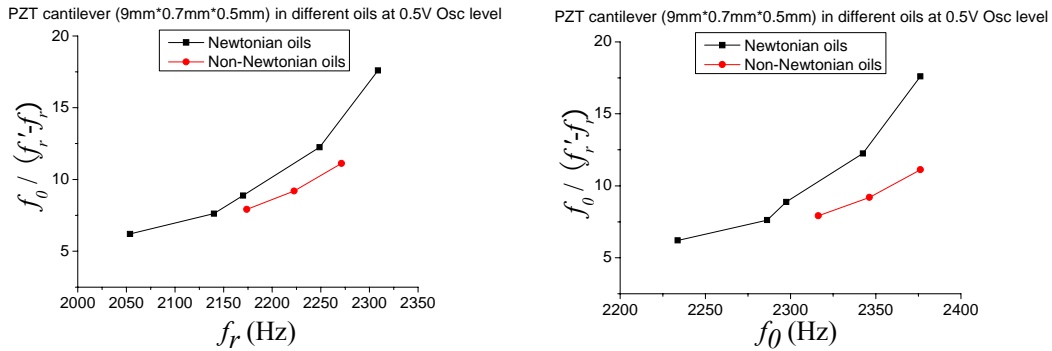


Figure 4.8. Properly chosen function of characteristic frequencies vs. one of the three characteristic frequencies of 9 mm × 0.7 mm × 0.5 mm PZT cantilever in oils.



#### 4.5 The performance comparison of PZT cantilevers with same length and thickness but different width and performance comparison of PZT cantilevers with different length but same width and thickness

The viscous drags which act on the main surface and the edge are very different even for the same cantilever as shown in Figure 4.9. And this will affect the performance of the cantilever. And the optimized results can be achieved by studying the performances of different length-width ratio piezoelectric cantilevers.

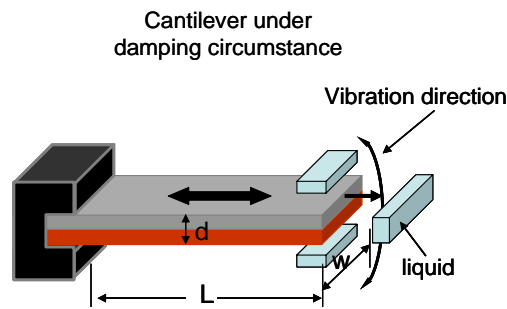


Figure 4.9. The schematic of piezoelectric cantilever sensor oscillation in visco-liquids.

From the Equation (4-1), we can find the flexural resonance frequencies of cantilever with one end firmly clamped are independent of the width of cantilever beam  $W$ . However due to different visco drags acting on the main surface and edges of the cantilever, the beams with the same length and thickness but different width will have different characteristic resonance frequencies. And PZT cantilevers with 6.8mm length and thickness 0.5mm but different width (0.3mm, 0.7mm and 1.0mm) were studied in different reference oils as shown below:

(1) 6.8 mm × 0.3 mm × 0.5 mm PZT cantilever;

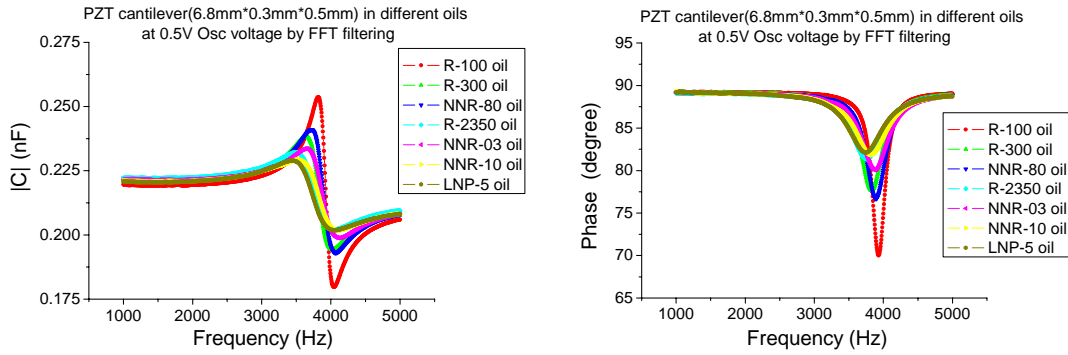
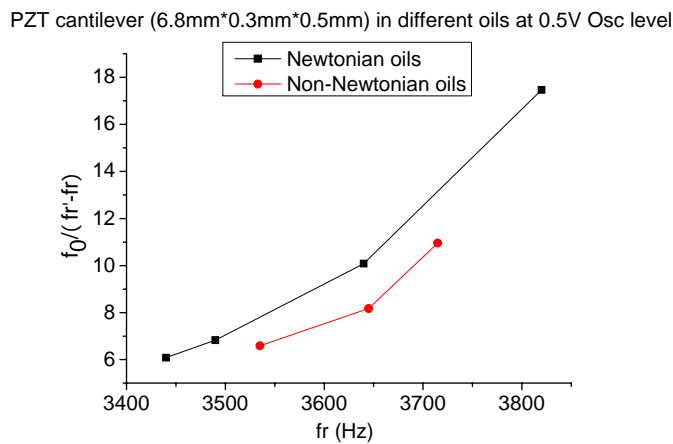


Figure 4.10. Resonance behaviors of 6.8 mm × 0.3 mm × 0.5 mm PZT cantilever sensor in oils.

PZT cantilever (6.8 mm × 0.3 mm × 0.5 mm) at 0.5V Osc level				
Media	$f_r$ (Hz)	$f_0$ (Hz)	$f_r'$ (Hz)	$\eta$ (mPa·s)
R-100	3820	3930	4045	19.88
R-300	3640	3830	4020	61.94
<b>NNR-80</b>	3715	3890	4070	78.29
R-2350	3490	3755	4040	152.5
<b>NNR-03</b>	3645	3880	4120	173.2
<b>NNR-10</b>	3535	3820	4115	214.3
LNP-5	3440	3740	4055	215.4

Table 4.3. Resonance frequencies of 6.8 mm × 0.3 mm × 0.5 mm PZT cantilever sensor in oils.



PZT cantilever (6.8mm\*0.3mm\*0.5mm) in different oils at 0.5V Osc level

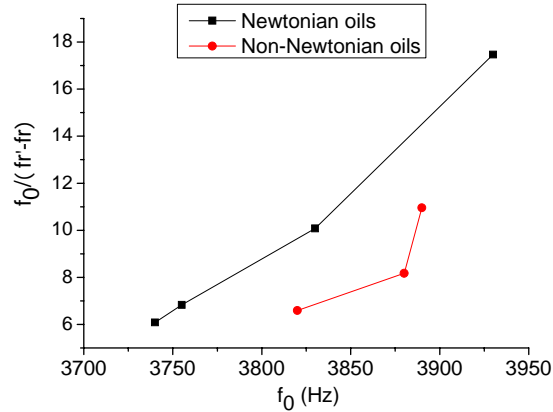


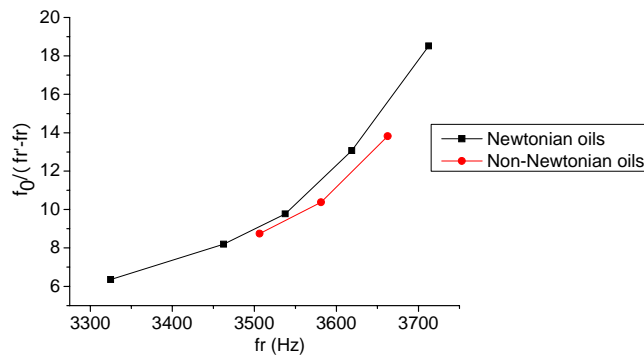
Figure 4.11. Properly chosen function of characteristic frequencies vs. one of the three characteristic frequencies of 6.8 mm × 0.3 mm × 0.5 mm PZT cantilever in oils.

(2) 6.8 mm × 0.7 mm × 0.5 mm PZT cantilever;

PZT cantilever (6.8 mm × 0.7 mm × 0.5 mm) at 0.5V Osc level				
Media	$f_r$ (Hz)	$f_0$ (Hz)	$f_r'$ (Hz)	$\eta$ (mPa·s)
R-100	3712.5	3818.75	3918.75	19.88
R-300	3618.75	3756.25	3906.25	61.94
<b>NR-80</b>	3662.5	3800	3937.5	78.29
R-2350	3537.5	3725	3918.75	152.5
<b>NR-03</b>	3581.25	3762.5	3943.75	173.2
<b>NR-10</b>	3506.25	3718.75	3931.25	214.3
LNP-5	3462.5	3687.5	3912.5	215.4
R-2450	3325	3612.5	3893.75	372.7

Table 4.4. Resonance frequencies of 6.8 mm × 0.7 mm × 0.5 mm PZT cantilever sensor in oils.

PZT cantilever (6.8mm\*0.7mm\*0.5mm) in different oils at 0.5V Osc level



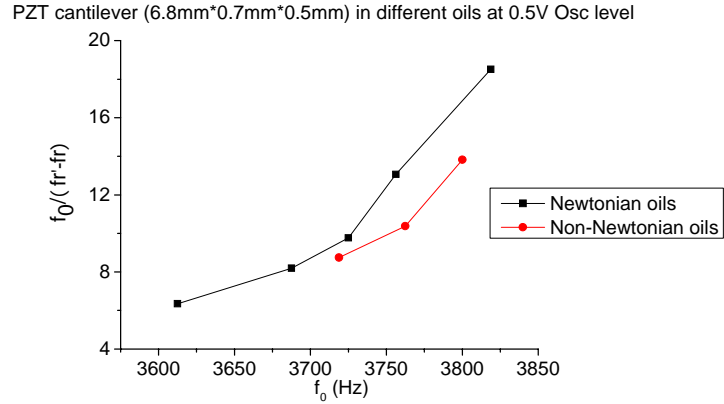
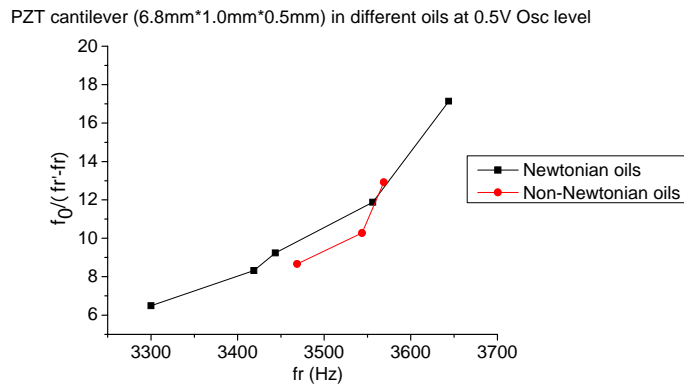


Figure 4.12. Properly chosen function of characteristic frequencies vs. one of the three characteristic frequencies of 6.8 mm × 0.7 mm × 0.5 mm PZT cantilever in oils.

(3) 6.8 mm × 1.0 mm × 0.5 mm PZT cantilever;

PZT cantilever (6.8 mm × 1.0 mm × 0.5 mm) at 0.5V Osc level				
Media	$f_r$ (Hz)	$f_0$ (Hz)	$f_r'$ (Hz)	$\eta$ (mPa·s)
R-100	3643.75	3750	3862.5	19.88
R-300	3556.25	3712.5	3868.75	61.94
<b>NNR-80</b>	3568.75	3712.5	3856.25	78.29
R-2350	3443.75	3637.5	3837.5	152.5
<b>NNR-03</b>	3543.75	3725	3906.25	173.2
<b>NNR-10</b>	3468.75	3681.25	3893.75	214.3
LNP-5	3418.75	3637.5	3856.25	215.4
R-2450	3300	3568.75	3850	372.7

Table 4.5. Resonance frequencies of 6.8 mm × 1.0 mm × 0.5 mm PZT cantilever sensor in oils.



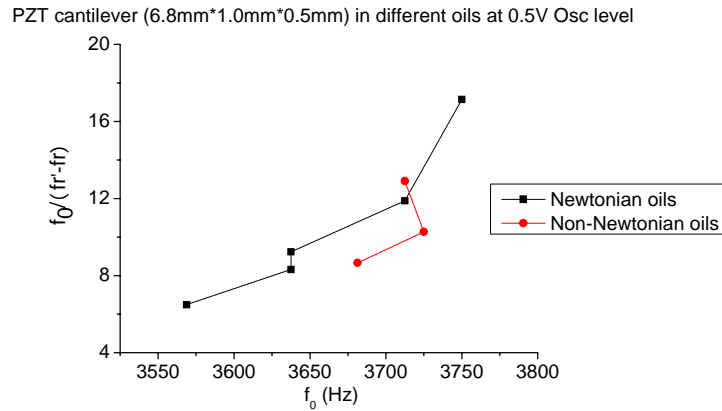


Figure 4.13. Properly chosen function of characteristic frequencies vs. one of the three characteristic frequencies of 6.8 mm × 1.0 mm × 0.5 mm PZT cantilever in oils.

By selecting the same function of characteristic frequencies ( $\frac{f_0}{f_r - f_r}$ ) as the Y-axis and one of the three characteristic frequencies ( $f_r$  or  $f_0$ ) as the X-axis, we have Figure 4.11, 4.12 and 4.13, in which we find the gap between Newtonian and non-Newtonian oils becomes wider with length-width ratio increases. It can be explained by the role of viscous drags which act on the cantilever edge becoming more and more important with the length-width ratio increasing. And by using a large length-width ratio cantilever sensor, tiny changes of viscous drags from some polymer coils which are thought of as the genesis of non-linearity can be detected. The conclusion is that a cantilever sensor of same length and thickness with smaller width has better performance in this study. By comparing Figure 4.8 and Figure 4.12 which are the performances of 9 mm × 0.7 mm × 0.5 mm and 6.8 mm × 0.7 mm × 0.5 mm PZT cantilevers in oils, difference between Newtonian and non-Newtonian oils becomes more obvious with an increase in cantilever length. And also by using a longer cantilever, the vibration signal could be stronger. The conclusion is that a longer cantilever with same width and thickness has better performance in this study.

## 4.6 Conclusions

Properly chosen function of characteristic frequencies vs. one of the three characteristic frequencies ( $f_r$  or  $f_0$ ) as the X-axis method is developed to identify the non-linearity of viscosity and also differentiate Newtonian oils and non-Newtonian oils. The resonance behaviors of cantilever sensors with different length in different oils are studied, and the performances of the same length cantilever sensors with different length-width ratios are also investigated. The results show that a longer cantilever with the same width and thickness has better performance in identifying non-linearity of viscosity, and a cantilever sensor of same length & thickness with a smaller width has better performance in differentiating Newtonian oils and non-Newtonian oils.

### References:

- [1] R. Berger, Ch. Gerber, H.P. Lang, J.K. Gimzewski, *Micromechanics: A toolbox for femtoscale science: "Towards a laboratory on a tip"*, *Microelectronic Engineering* 35 (1-4) (1997) 373-379.
- [2] H.P. Lang, M. Hegner, E. Meyer, Ch. Gerber, *Nanomechanical from atomic resolution to molecular recognition based on atomic force microscopy technology*, *Nanotechnology* 13(5) (2002) 29-36.
- [3] R. Berger, H.P. Lang, Ch. Gerber, J.K. Gimzewski, J.H. Fabian, L. Scandella, E. Meyer, H.-J. Güntherodt, *Micromechanical thermogravimetry*, *Chemical Physics Letters* 294(4-5) (1998) 363-369.
- [4] R. Berger, E. Delamarche, H.P. Lang, C. Gerber, J.K. Gimzewski, E. Meyer, H.-J. Güntherodt, *Surface stress in the self-assembly of alkanethiols on gold*, *Science* 276 (5321) (1997) 2021-2024.
- [5] J. Fritz, M.K. Baller, H.P. Lang, T. Strunz, E. Meyer, H.-J. Güntherodt, E. Delamarche, Ch. Gerber, J.K. Gimzewski, *Stress at the solid-liquid interface of self-assembled monolayers on gold investigated with a nanomechanical sensor*, *Langmuir* 16(25) (2000) 9694-9696.

- [6] B. Jaffe, W. R. Cook Jr., and H. Jaffe, *Piezoelectric Ceramics*. Academic Press, New York, 1971.
- [7] H.P. Lang, M. Hegner, C. Gerber, Cantilever Array Sensors, *Materials Today* 8, 30-36 (2005).
- [8] S. K. Vashist, A Review of Microcantilevers for Sensing Applications, *Journal of Nanotechnology* Online, June 2007.
- [9] J. W. Yi, W. Y. Shih, and W. H. Shih, "Effect of length, width, and mode on the mass detection sensitivity of piezoelectric unimorph cantilevers," *Journal of Applied Physics*, vol. 91, pp. 1680-1686, 2002.
- [10] A. Agoston, F. Keplinger, B. Jakoby, "Evaluation of a Vibrating Micromachined Cantilever Sensor for Measuring the Viscosity of Complex Organic Liquids", *Sensors and Actuators A* 123–125, Elsevier, p82–86, 2005.
- [11] Merhaut, J. *Theory of Electroacoustics*; Gerber, R.: New York, McGraw-Hill Inc., 1981.
- [12] <http://www.memsnet.org/material/leadzirconatetitanatepzt/>
- [13] G. A. C. M. Spierings, G. J. M. Dormans, W. G. J. Moors, M. J. E. Ulenaers, P. K. Larsen, "Stresses in Pt/Pb(Zr,Ti)O<sub>3</sub>/Pt thin-film stacks for integrated ferroelectric capacitors", *J. Appl. Phys.* 78 (1995) 1926-1933.
- [14] [http://www.engineeringtoolbox.com/young-modulus-d\\_417.html](http://www.engineeringtoolbox.com/young-modulus-d_417.html)

## CHAPTER 5

### NUMERICAL SIMULATIONS TO IDENTIFY THE NONLINEARITY OF VISCOSITY

#### 5.1 Introduction

Friction plays an important role in different systems and exhibits general aspects that show in all tribological processes. The development of lubricating liquids and low-friction surfaces in technological devices has attracted more and more researchers' interests. The old, simple empirical laws of friction do not always apply to such systems due to surface structure or roughness. There are many surface types which can be smooth or rough, elastic, plastic or viscoelastic, dry or lubricated, and other different types. The pressure between two shearing surfaces can vary from around 1 Pa to several GPa within microseconds. These extreme conditions cannot be simply interpreted by "linear" theories and friction behaviors have not been understood at the fundamental level.

Viscosity is a scale of the resistance of a fluid to the deformation under shear stress or extensional stress. It is commonly regarded as "thickness", or resistance to flow. Viscosity describes a fluid's internal resistance to flow and sometimes can be treated as a measure of fluid friction [1]. All real fluids have some resistance to stress, but a fluid which has no resistance to shear stress is known as an ideal fluid or inviscid fluid. The study of viscosity is known as rheology [2]. Viscosity converts kinetic energy of motion into heat energy, like the friction process between moving solids. And viscosity can be considered as fluid friction. In order to have some understanding of how energy transfer takes place during the friction process and how viscosity acted as fluid friction, it is necessary to have some fundamental knowledge of how solids and liquids act on each other as in a friction process. Compared to



the solid/solid case which has the equation  $F = \mu N$  to describe the friction force, the liquid/solid case is different. Because liquid can flow, the whole common area between solid and liquid has good contact even at low pressures. And friction force has little dependence on pressure over a very wide range.

Isaac Newton was the first one to define the coefficient of viscosity by a quantitative method. In order to simplify the visco drag analysis, he designed an experiment in which the fluid in the study was contained between two large parallel horizontal plates. The bottom plate was firmly fixed, and the upper plate moved at a steady speed  $v_0$ . The visco drag force from the fluid was measured at different speeds  $v_0$  and different plate spacings (Although Newton's experiment did not perform very well, his theoretical reasoning and equations were fine, and the concept was confirmed experimentally by Poiseuille in 1849 using liquid flow in tubes).

Most common liquids of simple structures (water, glycerin, oil, etc) are *Newtonian fluids* whose viscosity is independent of shear rate. However fluids with complicated structures (polymer melts or solutions, suspensions, etc) are generally *non-Newtonian*, whose viscosity changes with shear rate and velocity.

Due to the nonlinearity of non-Newtonian liquids and viscosity dependence on specific parameters (such as shear rate and oscillation frequency), different viscosity measurement methods tend to produce different viscosity values.

The viscous drag acting on an object moving in a fluid can be generally expressed by Equation (5-1) [3, 4].

$$F = \frac{\eta \cdot A \cdot v}{H} \quad (5-1)$$

where  $F$  is viscous drag,  $\eta$  is the viscosity of the fluid,  $A$  is the surface area in contact with the fluid,  $v$  is the relative velocity of the object and  $H$  is the radius of the vessel of the fluid around the object in which the layers of the fluid experience friction.

## 5.2 Theoretical model (in Newtonian & non-Newtonian liquids) and numerical simulation

For magnetostrictive strip sensors immersed in liquid which vibrates with a simple harmonic driving force, the vibration can be defined as a forced-damped vibration. The oscillation equation for an external driving force  $F_{ext} = A \sin \omega t$  and viscous friction is as below [5], and the displacement  $x$  can be obtained from Equation (5-3):

$$F = m\ddot{x} = -kx - b\dot{x} + F_{ext} = -kx - b\dot{x} + A \sin \omega t \quad (5-2)$$

$$\ddot{x} + B\dot{x} + \omega_0^2 x = h \sin \omega t \quad (5-3)$$

$$B = \frac{b}{m}, \quad \omega_0^2 = \frac{k}{m}, \quad h = \frac{A}{m} \quad (5-4)$$

For a Newtonian liquid,  $\eta$  here is independent of shear rate and oscillation frequency, and the analytical solution can be easily obtained; however, for a non-Newtonian liquid,  $\eta = \eta(\dot{\gamma})$  is related to shear rate, which makes Equation (5-3) hard to solve. However, by the experiment results,  $\eta(\dot{\gamma})$  and its nonlinear behaviors can be demonstrated. And by proper numerical simulation, we can compare simulation results with the experiment results and check the validity of the equation.

## 5.3 Model in Newtonian liquids and numerical simulation

For the solution of forced vibrations in *Handbook of Physics* [5]:

It is a particular solution to the inhomogeneous equation.

$$\ddot{x} + B\dot{x} + \omega_0^2 x = h \sin \omega t$$

Particular analytical solution:

$$x^* = \frac{h}{\sqrt{B^2\omega^2 + (\omega_0^2 - \omega^2)^2}} \sin(\omega t + \varphi), \text{ where } \varphi = \arctan \frac{-B\omega}{\omega_0^2 - \omega^2}$$

The extreme value of vibration amplitude appears at  $\frac{\partial x^*}{\partial \omega} = 0$ .

$$\text{That is, } \frac{\partial \left( \frac{h}{\sqrt{B^2\omega^2 + (\omega_0^2 - \omega^2)^2}} \right)}{\partial \omega} = 0.$$

$$\Rightarrow -\frac{1}{2} [B^2\omega^2 + (\omega_0^2 - \omega^2)^2]^{-\frac{3}{2}} [2B^2\omega + 2(\omega_0^2 - \omega^2)(-2\omega)] = 0$$

$$\Rightarrow \omega^2 = \omega_0^2 - \frac{1}{2}B^2 \Rightarrow \omega = \sqrt{\omega_0^2 - \frac{1}{2}B^2}$$

can only acquire one frequency for extreme value of vibration amplitude.

The result matches the figures shown in *Handbook of Physics*, and only one characteristic resonance frequency can be obtained by Equation (5-3) [5].

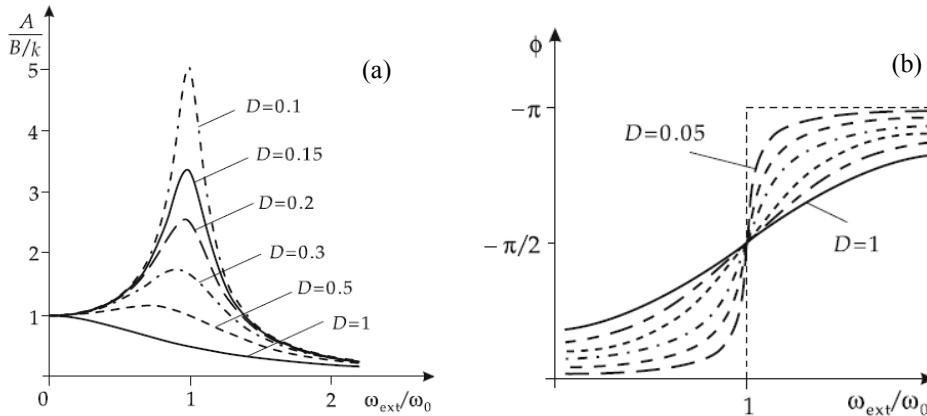


Figure 5.1. (a) Forced damped vibration. Normalized amplitude  $\frac{A}{B/k}$  as a function of  $\omega_{ext}/\omega_0$  for various degrees of damping  $D$ ; (b) Phase shift  $\phi$  as function of  $\omega_{ext}/\omega_0$  for various degrees of damping  $D$  [5].

Only one resonance frequency can be obtained from the analytical solution of the forced-damped vibration equation, which differs from the experimental results. In

experiments, three experimental characteristic frequencies can be easily obtained simultaneously for each liquid by one measurement of the selected AW sensor.

And these three frequencies are used to set up the model. For Newtonian oil, due to the independence of viscosity with shear rate, one experimental parameter, such as  $f_r$ , is enough to describe the liquid viscosity. While in non-Newtonian oil, viscosity changes with shear rate and velocity. Some more parameters are needed to present this nonlinearity, such as  $f_r, f_r'$  and  $f_0$ . As discussed in Chapter 1, normally  $f_r$  is selected at the maximum signal point (maximum vibration amplitude),  $f_r'$  is selected at the minimum signal point and  $f_0$  is picked up somewhere between these two points. These three experimental characteristic frequencies distribute within a rather broad range in which displacement, velocity and shear rate change greatly. The nonlinearity of viscosity is also apparent in this range. So the information of the whole resonance behavior curve should be fully used to illustrate the liquid properties by using three experimental characteristic frequencies  $f_r, f_r'$  and  $f_0$ .

In order to match the experimental results, which obtain three characteristic frequencies, some modifications have to be added into the analytical solution. Due to the relationship of magnetization M and magnetic field H, the solution of Equation (5-3) is modified as below:

Original:

$$\ddot{x} + B\dot{x} + \omega_0^2 x = h \sin \omega t$$

$$x^* = \frac{h}{\sqrt{B^2 \omega^2 + (\omega_0^2 - \omega^2)^2}} \sin(\omega t + \varphi), \text{ where } \varphi = \arctan \frac{-B\omega}{\omega_0^2 - \omega^2}$$

Modified (add a linear part into the solution):

$$x^* = \frac{h}{\sqrt{B^2 \omega^2 + (\omega_0^2 - \omega^2)^2}} e^{i(\omega t + \varphi)} + C_1 H_0 e^{i\omega t}, C_1 \text{ is a constant.} \quad (5-5)$$

Let  $A(\omega_0, \omega) = \frac{h}{\sqrt{B^2 \omega^2 + (\omega_0^2 - \omega^2)^2}}$ ,  $H_0' = C_1 H_0$  and  $H_0 = \frac{h}{\omega_0^2}$  (which is the value of

$A(\omega_0, \omega)$  when  $\omega = 0$  and corresponds the initial vibration amplitude without external driving force)

$$\begin{aligned} \text{Then } x^* &= A(\omega_0, \omega)e^{i(\omega t + \varphi)} + H_0' e^{i\omega t} = A(\omega_0, \omega)(\cos \varphi + i \sin \varphi)e^{i\omega t} + H_0' e^{i\omega t} \\ &= [A(\omega_0, \omega) \cos \varphi + H_0'] \cdot e^{i\omega t} + iA(\omega_0, \omega) \sin \varphi \cdot e^{i\omega t} \end{aligned}$$

Amplitude:

$$|signal| = |x^*| = \sqrt{[A(\omega_0, \omega) \cos \varphi + H_0']^2 + A^2(\omega_0, \omega) \sin^2 \varphi} = \sqrt{A^2 + H_0'^2 + 2AH_0' \cos \varphi}$$

Phase:

$$\varphi' = \arctan \frac{A \sin \varphi}{A \cos \varphi + H_0'}$$

For the amplitude:

$$|signal| = |x^*| = \sqrt{[A(\omega_0, \omega) \cos \varphi + H_0']^2 + A^2(\omega_0, \omega) \sin^2 \varphi} = \sqrt{A^2 + H_0'^2 + 2AH_0' \cos \varphi}$$

$$\text{where } \varphi = \arctan \frac{-B\omega}{\omega_0^2 - \omega^2} = \arctan \frac{B\omega}{\omega^2 - \omega_0^2}.$$

Extreme values of amplitude appear at  $\frac{\partial x^*}{\partial \omega} = 0$

$$\Rightarrow 2A \frac{\partial A}{\partial \omega} + 2H_0' \cos \varphi \frac{\partial A}{\partial \omega} - 2AH_0' \sin \varphi \frac{\partial \varphi}{\partial \omega} = 0$$

$$\Rightarrow (2A + 2H_0' \cos \varphi) \frac{\partial A}{\partial \omega} - 2AH_0' \sin \varphi \frac{\partial \varphi}{\partial \omega} = 0$$

$$\begin{aligned}
&\Rightarrow \left( 2 \frac{h}{\sqrt{4\beta^2 \omega^2 + (\omega_0^2 - \omega^2)^2}} + 2H_0' \cos \varphi \right) \cdot h \cdot \left( -\frac{1}{2} \right) [4\beta^2 \omega^2 + (\omega_0^2 - \omega^2)^2]^{-\frac{3}{2}} \\
&\cdot [8\beta^2 \omega + 2(\omega^2 - \omega_0^2) \cdot 2\omega] - 2 \frac{hH_0'}{\sqrt{4\beta^2 \omega^2 + (\omega_0^2 - \omega^2)^2}} \sin \varphi \\
&\cdot \left\{ \frac{1}{1 + \left( \frac{2\beta\omega}{\omega^2 - \omega_0^2} \right)^2} \cdot \left[ \frac{2\beta}{\omega^2 - \omega_0^2} + 2\beta\omega \cdot (-1)(\omega^2 - \omega_0^2)^{-2} \cdot 2\omega \right] \right\} = 0 \\
&\Rightarrow \left( \frac{h}{\sqrt{4\beta^2 \omega^2 + (\omega_0^2 - \omega^2)^2}} + H_0' \cos \varphi \right) \left( \frac{1}{2} \right) \frac{1}{4\beta^2 \omega^2 + (\omega_0^2 - \omega^2)^2} \cdot [8\beta^2 \omega + 4(\omega^2 - \omega_0^2)\omega] \\
&+ H_0' \sin \varphi \left[ \frac{(\omega^2 - \omega_0^2)^2}{4\beta^2 \omega^2 + (\omega_0^2 - \omega^2)^2} \cdot \frac{-2\beta(\omega^2 + \omega_0^2)}{(\omega^2 - \omega_0^2)^2} \right] = 0 \\
&\Rightarrow \left( \frac{h}{\sqrt{4\beta^2 \omega^2 + (\omega_0^2 - \omega^2)^2}} + H_0' \cos \varphi \right) \frac{2\beta^2 \omega + (\omega^2 - \omega_0^2)\omega}{4\beta^2 \omega^2 + (\omega_0^2 - \omega^2)^2} - H_0' \sin \varphi \frac{\beta(\omega^2 + \omega_0^2)}{4\beta^2 \omega^2 + (\omega_0^2 - \omega^2)^2} = 0 \\
&\Rightarrow \left( \frac{h}{\sqrt{4\beta^2 \omega^2 + (\omega_0^2 - \omega^2)^2}} + H_0' \cos \varphi \right) [2\beta^2 \omega + (\omega^2 - \omega_0^2)\omega] - H_0' \sin \varphi \cdot \beta(\omega^2 + \omega_0^2) = 0 \\
&\Rightarrow \left( \frac{h}{\sqrt{4\beta^2 \omega^2 + (\omega_0^2 - \omega^2)^2}} + H_0' \frac{\omega^2 - \omega_0^2}{4\beta^2 \omega^2 + (\omega_0^2 - \omega^2)^2} \right) [2\beta^2 \omega + (\omega^2 - \omega_0^2)\omega] \\
&- H_0' \frac{2\beta\omega}{4\beta^2 \omega^2 + (\omega_0^2 - \omega^2)^2} \cdot \beta(\omega^2 + \omega_0^2) = 0 \\
&\Rightarrow [h \cdot \sqrt{4\beta^2 \omega^2 + (\omega_0^2 - \omega^2)^2} + H_0'(\omega^2 - \omega_0^2)] \cdot \omega \cdot (2\beta^2 + \omega^2 - \omega_0^2) - H_0' \cdot 2\beta\omega \cdot \beta(\omega^2 + \omega_0^2) = 0 \\
&\Rightarrow [h \cdot \sqrt{4\beta^2 \omega^2 + (\omega_0^2 - \omega^2)^2} + H_0'(\omega^2 - \omega_0^2)](2\beta^2 + \omega^2 - \omega_0^2) - 2H_0'\beta^2(\omega^2 + \omega_0^2) = 0 \\
&\Rightarrow h \cdot \sqrt{4\beta^2 \omega^2 + (\omega_0^2 - \omega^2)^2} (2\beta^2 + \omega^2 - \omega_0^2) + H_0'(\omega^2 - \omega_0^2)^2 - 4H_0'\beta^2 \omega_0^2 = 0
\end{aligned}$$

Let  $\omega^2 = Y$ ,  $Y > 0$

$$\Rightarrow h \cdot \sqrt{4\beta^2 Y + (\omega_0^2 - Y)^2} (2\beta^2 + Y - \omega_0^2) + H_0'(Y - \omega_0^2)^2 - 4H_0'\beta^2 \omega_0^2 = 0$$

for this quadratic equation, two solutions exist which correspond the maximum value and minimum value of the amplitude. And based on similar procedures, the extreme value of phase can be also obtained. These results are in accordance with the experimental results, which usually get three characteristic frequencies.

And from the modified results (adding the linear part), we can get three characteristic resonance frequencies by simulations of the equations solution in Figure 5.2. Matlab 7.0 is used for numerical simulation. In the case below:  $B=100$ ,  $h=1000$ ,  $\omega_0=10^3$ ,  $H'_0 = C_1 H_0 = \frac{1}{2} H_0 = \frac{1}{2} \cdot 0.001 = 0.0005$ .

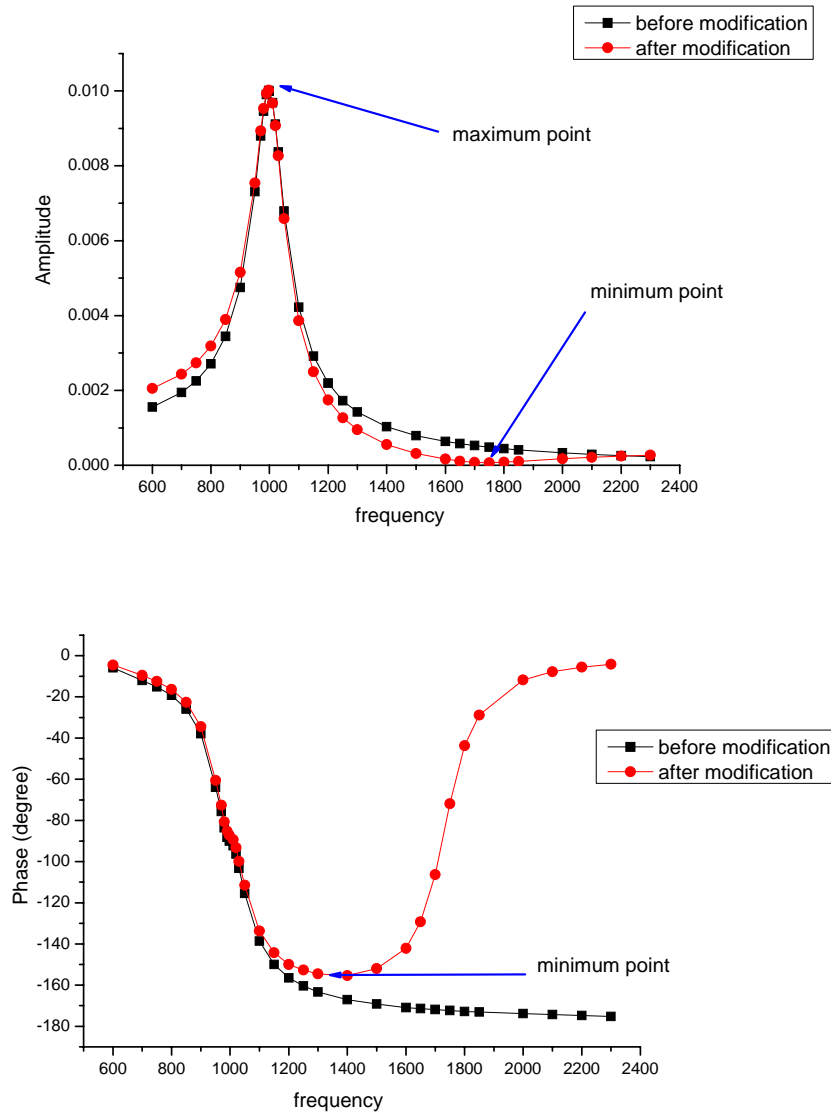


Figure 5.2. Three characteristic resonance frequencies obtained by numerical simulations of the differential Equation (5-3) (before and after modification).

And the analytical expressions of three characteristic frequencies based on the modified

solution can be obtained as below:

$$\ddot{x} + B\dot{x} + \omega_0^2 x = h \sin \omega t$$

$B$  stands for damping factor,  $\omega_0$  is the intrinsic angular frequency of sensor without damping,

$h$  is the amplitude of driving force, and  $\omega$  is the angular frequency of driving force.

The solution is  $x^*(t) = A(\omega_0, \omega)e^{i(\omega t + \varphi)}$ , where  $A(\omega_0, \omega) = \frac{h}{\sqrt{B^2 \omega^2 + (\omega_0^2 - \omega^2)^2}}$ ,

$$\varphi(\omega_0, \omega) = \arctan \frac{-B\omega}{\omega_0^2 - \omega^2}.$$

$$\text{And } \begin{cases} \sin \varphi = \frac{-B\omega}{\sqrt{B^2 \omega^2 + (\omega_0^2 - \omega^2)^2}} \\ \cos \varphi = \frac{\omega_0^2 - \omega^2}{\sqrt{B^2 \omega^2 + (\omega_0^2 - \omega^2)^2}} \end{cases}$$

$$\text{when } \omega = 0, |x^*| = \frac{h}{\omega_0^2}.$$

By adding the linear part  $H_0' e^{i\omega t}$ :

$$\begin{aligned} x^*(t) &= A(\omega_0, \omega)e^{i(\omega t + \varphi)} + H_0' e^{i\omega t} = A(\omega_0, \omega)(\cos \varphi + i \sin \varphi)e^{i\omega t} + H_0' e^{i\omega t} \\ &= [A(\omega_0, \omega) \cos \varphi + H_0'] e^{i\omega t} + iA(\omega_0, \omega) \sin \varphi \cdot e^{i\omega t} \end{aligned}$$

Amplitude:

$$|signal| = |x^*| = \sqrt{[A(\omega_0, \omega) \cos \varphi + H_0']^2 + A^2(\omega_0, \omega) \sin^2 \varphi} = \sqrt{A^2 + H_0'^2 + 2AH_0' \cos \varphi}$$

Phase:

$$\varphi' = \arctan \frac{A \sin \varphi}{A \cos \varphi + H_0'}$$

$$\begin{aligned} |signal| = |x^*| &= \sqrt{A^2 + H_0'^2 + 2AH_0' \cos \varphi} = \left( \frac{h^2}{B^2 \omega^2 + (\omega_0^2 - \omega^2)^2} + H_0'^2 + \frac{2H_0' \cdot h(\omega_0^2 - \omega^2)}{B^2 \omega^2 + (\omega_0^2 - \omega^2)^2} \right)^{\frac{1}{2}} \\ &= \left( \frac{h^2 + 2H_0' h(\omega_0^2 - \omega^2)}{B^2 \omega^2 + (\omega_0^2 - \omega^2)^2} + H_0'^2 \right)^{\frac{1}{2}} \end{aligned}$$



$$\begin{aligned}\varphi' &= \arctan \frac{A \sin \varphi}{A \cos \varphi + H_0'} = \arctan \left( \frac{\frac{h}{\sqrt{B^2 \omega^2 + (\omega_0^2 - \omega^2)^2}} \cdot \frac{-B\omega}{\sqrt{B^2 \omega^2 + (\omega_0^2 - \omega^2)^2}}}{\frac{h}{\sqrt{B^2 \omega^2 + (\omega_0^2 - \omega^2)^2}} \cdot \frac{\omega_0^2 - \omega^2}{\sqrt{B^2 \omega^2 + (\omega_0^2 - \omega^2)^2}} + H_0'} \right) \\ &= \arctan \left( \frac{-Bh\omega}{h(\omega_0^2 - \omega^2) + H_0'[B^2 \omega^2 + (\omega_0^2 - \omega^2)^2]} \right)\end{aligned}$$

1.  $|x^*|$  has extreme values while  $\frac{\partial |x^*|}{\partial \omega} = 0$ , which corresponds  $f_r$  (resonance

frequency) and  $f_r'$  (anti-resonance frequency).

$$\Rightarrow \frac{2H_0' h(-2\omega) \cdot [B^2 \omega^2 + (\omega_0^2 - \omega^2)^2] - [h^2 + 2H_0' h(\omega_0^2 - \omega^2)] \cdot [B^2 \cdot 2\omega + 2(\omega^2 - \omega_0^2) \cdot 2\omega]}{[B^2 \omega^2 + (\omega_0^2 - \omega^2)^2]^2} = 0$$

$$\Rightarrow (-2H_0') \cdot [B^2 \omega^2 + (\omega_0^2 - \omega^2)^2] - [h + 2H_0'(\omega_0^2 - \omega^2)] \cdot [B^2 + 2(\omega^2 - \omega_0^2)] = 0$$

$$\Rightarrow 2H_0'(\omega^2 - \omega_0^2)^2 - 2h(\omega^2 - \omega_0^2) - hB^2 - 2H_0'B^2\omega_0^2 = 0$$

Let  $\omega^2 - \omega_0^2 = y$ ,

$$\text{Then } 2H_0'y^2 - 2hy - hB^2 - 2H_0'B^2\omega_0^2 = 0$$

$$\Rightarrow y = \frac{2h \pm \sqrt{4h^2 - 4 \cdot 2H_0'(-hB^2 - 2H_0'B^2\omega_0^2)}}{2 \cdot 2H_0'} = \frac{h \pm \sqrt{h^2 + 2H_0'hB^2 + 4H_0'^2B^2\omega_0^2}}{2H_0'}$$

$$\Rightarrow \omega^2 = \omega_0^2 + \frac{h \pm \sqrt{h^2 + 2H_0'hB^2 + 4H_0'^2B^2\omega_0^2}}{2H_0'}$$

we can get  $|x^*|$  has extreme values when

$$\omega = \sqrt{\omega_0^2 + \frac{1}{2} \left( \frac{h}{H_0'} \pm \sqrt{\left( \frac{h}{H_0'} \right)^2 + 2 \left( \frac{h}{H_0'} \right) B^2 + 4B^2 \omega_0^2} \right)},$$

corresponding to  $\omega_- \rightarrow 2\pi f_r$  (resonance frequency) and  $\omega_+ \rightarrow 2\pi f_r'$  (anti-resonance

frequency).

$$\begin{cases} \omega_+^2 = \omega_0^2 + \frac{h + \sqrt{h^2 + 2H_0'hB^2 + 4H_0'^2B^2\omega_0^2}}{2H_0'} \\ \omega_-^2 = \omega_0^2 + \frac{h - \sqrt{h^2 + 2H_0'hB^2 + 4H_0'^2B^2\omega_0^2}}{2H_0'} \end{cases}$$

2.  $\varphi$  has extreme value while  $\frac{\partial \varphi}{\partial \omega} = 0$ , which corresponds  $f_0$  (experimental-resonance frequency)

$$\Rightarrow \frac{\partial \left( \frac{-Bh\omega}{h(\omega_0^2 - \omega^2) + H_0' [B^2 \omega^2 + (\omega_0^2 - \omega^2)^2]} \right)}{\partial \omega} = 0$$

$$\Rightarrow h(\omega_0^2 - \omega^2) + H_0' [B^2 \omega^2 + (\omega_0^2 - \omega^2)^2] - \omega \cdot \{-2h\omega + H_0' [2B^2 \omega + 2(\omega^2 - \omega_0^2) \cdot 2\omega]\} = 0$$

$$\Rightarrow h\omega_0^2 + h\omega^2 - H_0' B^2 \omega^2 + H_0' (\omega_0^2 - \omega^2)^2 - 4H_0' (\omega^2 - \omega_0^2) \omega^2 = 0$$

$$\text{Let } \omega^2 - \omega_0^2 = y \Rightarrow \omega^2 = y + \omega_0^2,$$

$$\text{Then } h\omega_0^2 + h(y + \omega_0^2) - H_0' B^2 (y + \omega_0^2) + H_0' y^2 - 4H_0' y(y + \omega_0^2) = 0$$

$$-3H_0' y^2 + y(h - H_0' B^2 - 4H_0' \omega_0^2) + (2h\omega_0^2 - H_0' B^2 \omega_0^2) = 0$$

$$3y^2 + y \left( \frac{-h}{H_0'} + B^2 + 4\omega_0^2 \right) + (B^2 \omega_0^2 - 2 \frac{h}{H_0'} \omega_0^2) = 0$$

$$\Rightarrow \omega^2 - \omega_0^2 = y = \frac{\frac{h}{H_0'} - B^2 - 4\omega_0^2 \pm \sqrt{\left(\frac{h}{H_0'} - B^2 - 4\omega_0^2\right)^2 - 12\left(B^2 \omega_0^2 - 2 \frac{h}{H_0'} \omega_0^2\right)}}{6}$$

$$\Rightarrow \omega^2 - \omega_0^2 = y = \frac{\frac{h}{H_0'} - B^2 - 4\omega_0^2 \pm \sqrt{\left(\frac{h}{H_0'} - B^2 - 4\omega_0^2\right)^2 - 12\left(B^2 \omega_0^2 - 2 \frac{h}{H_0'} \omega_0^2\right)}}{6}$$

(choose "+", because  $y$  should be positive.)

$$\Rightarrow \omega = \sqrt{\frac{2\omega_0^2 + \frac{h}{H_0'} - B^2 + \sqrt{\left(2\omega_0^2 + \frac{h}{H_0'} - B^2\right)^2 + 12\left(\frac{h}{H_0'} \omega_0^2 + \omega_0^4\right)}}{6}},$$

corresponding to  $2\pi f_0$  (experimental-resonance frequency).

From these analytical expressions, we can check whether the three characteristic frequencies change with  $h$  value or not in Newtonian liquids. In the linear part  $H_0' e^{i\omega t}$  and

$H_0' = C_1 H_0$ ,  $C_1$  is a constant and  $H_0 = \frac{h}{\omega_0^2}$ . Then give a certain value  $\frac{1}{2}$  to constant  $C_1$ , and

get  $H'_0 = \frac{h}{2\omega_0^2}$  to verify the results.

Get:

$\omega = \sqrt{2\omega_0^2 \pm \sqrt{\omega_0^4 + 2B^2\omega_0^2}}$  , corresponding to  $\omega_- \rightarrow 2\pi f_r$  (resonance frequency) and  $\omega_+ \rightarrow 2\pi f'_r$  (anti-resonance frequency).

$\omega = \sqrt{\frac{4\omega_0^2 - B^2 + \sqrt{(4\omega_0^2 - B^2)^2 + 36\omega_0^4}}{6}}$  , corresponding to  $2\pi f_0$  (experimental-resonance frequency).

By the above derivation, we can find that the three characteristic frequencies do not change with  $h$  value in Newtonian liquids and only relates to  $B$  (amplitude of damping factor, which in this case stands for visco drag) and  $\omega_0$  (intrinsic angular frequency of sensor without damping, which is determined by sensor materials and sensor size), which are in accordance with the experiments.

Then the numerical simulations are used to solve the differential equation (5-3). Matlab 7.0 is used for numerical simulation. Below are the numerical simulation results:

$$\ddot{x} + B\dot{x} + \omega_0^2 x = h \sin \omega t$$

( $\omega_0=1.6 \times 10^4$ , B changes from 1500 to 9000)

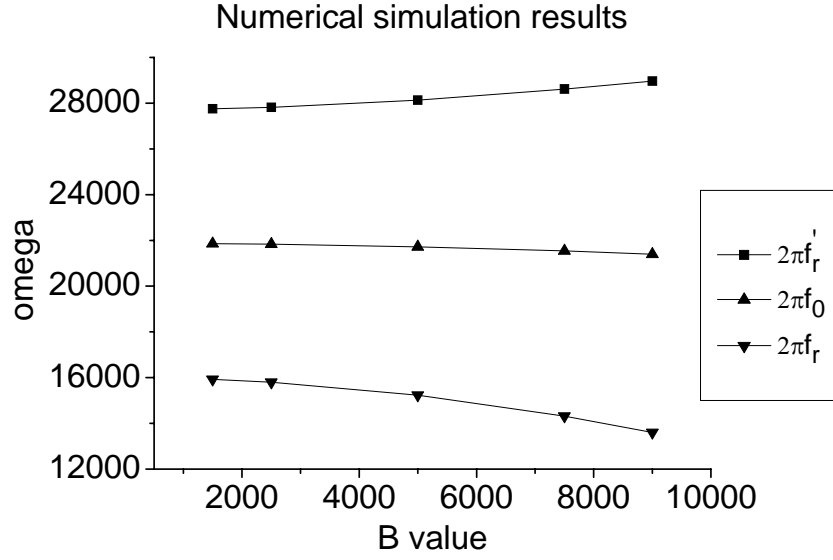


Figure 5.3. Numerical simulation solutions of the differential Equation (5-3).

From Figure 5.3, we can find the trends of characteristic frequencies  $f_r$  and  $f_0$  with damping factor are in accordance with the experiment results, and  $f_r'$  seems to increase with damping factor increasing, while in experiments  $f_r'$  decreases very slowly with damping factor increasing.

### 5.3.1 The study of relationship of three characteristic frequencies with $B$ value

$B$  is the damping drag added on the sensor. Normally it depends on the circumstance, surface roughness of sensor, and so forth.

**For  $f_r$  and  $f_r'$ :**

$$\omega^2 = \omega_0^2 + \frac{1}{2} \left( \frac{h}{H_0} \pm \sqrt{\left( \frac{h}{H_0} \right)^2 + 2 \left( \frac{h}{H_0} \right) B^2 + 4B^2 \omega_0^2} \right),$$

corresponding to  $\omega_- \rightarrow 2\pi f_r$  (resonance frequency) and  $\omega_+ \rightarrow 2\pi f_r'$  (anti-resonance frequency).

For  $f_r$  and  $f_r'$ , to find the trend with  $B$ , we only need to check whether  $\frac{\partial \omega^2}{\partial B}$  is positive or

not.

$$\frac{\partial \omega^2}{\partial B} = 2\omega \frac{\partial \omega}{\partial B} \Rightarrow \text{only need to check the symbol of } \pm [4(\frac{h}{H_0})B + 8B\omega_0^2].$$

For  $f_r'$ , choose "+"  $\Rightarrow \frac{\partial \omega}{\partial B} > 0$ , means  $f_r'$  increases with  $B$  increasing.

For  $f_r$ , choose "-"  $\Rightarrow \frac{\partial \omega}{\partial B} < 0$ , means  $f_r$  decreases with  $B$  increasing.

**For  $f_0$ :**

$$\omega^2 = \omega_0^2 + \frac{\frac{h}{H_0} - B^2 - 4\omega_0^2 + \sqrt{(\frac{h}{H_0} - B^2 - 4\omega_0^2)^2 - 12(B^2\omega_0^2 - 2\frac{h}{H_0}\omega_0^2)}}{6}$$

Check  $\frac{\partial \omega^2}{\partial B}$ , and found  $\frac{\partial \omega}{\partial B} < 0$ , means  $f_0$  decreases with  $B$  increasing.

The trends of all these three characteristic frequencies change with  $B$  are in accordance with Figure 5.3.

**For  $f_r$  and  $f_r'$ :**

$$\omega^2 = \omega_0^2 + \frac{1}{2}(\frac{h}{H_0} \pm \sqrt{(\frac{h}{H_0})^2 + 2(\frac{h}{H_0})B^2 + 4B^2\omega_0^2}),$$

corresponding to  $\omega_- \rightarrow 2\pi f_r$  (resonance frequency) and  $\omega_+ \rightarrow 2\pi f_r'$  (anti-resonance frequency).

$$\frac{\omega^2}{\omega_0^2} = 1 + \frac{1}{2}(\frac{h}{H_0\omega_0^2} \pm \sqrt{(\frac{h}{H_0\omega_0^2})^2 + 2(\frac{h}{H_0})\frac{B^2}{\omega_0^4} + 4\frac{B^2}{\omega_0^2}}),$$

$$\omega_+^2 - \omega_-^2 = \sqrt{(\frac{h}{H_0})^2 + 2(\frac{h}{H_0})B^2 + 4B^2\omega_0^2}$$

$$\omega_+^2 + \omega_-^2 = 2\omega_0^2 + \frac{h}{H_0}$$

Because  $\frac{h}{H_0}$  is related to the driving force of sensor and relays on the system, let  $\frac{h}{H_0} = 2\omega_0^2$

to simplify the result, then

$$\omega_+^2 - \omega_-^2 = \sqrt{\left(\frac{h}{H_0}\right)^2 + 2\left(\frac{h}{H_0}\right)B^2 + 4B^2\omega_0^2} = 2\sqrt{\omega_0^4 + 2B^2\omega_0^2}$$

$$\omega_+^2 + \omega_-^2 = 2\omega_0^2 + \frac{h}{H_0} = 4\omega_0^2$$

That means  $\omega_+^2 + \omega_-^2$  does not change with an increase in  $B$  (visco-drag).

And

$$\begin{aligned} \omega^2 &= \omega_0^2 + \frac{1}{2}\left(\frac{h}{H_0} \pm \sqrt{\left(\frac{h}{H_0}\right)^2 + 2\left(\frac{h}{H_0}\right)B^2 + 4B^2\omega_0^2}\right), \\ &= \omega_0^2 + \frac{1}{2}(2\omega_0^2 \pm \sqrt{4\omega_0^4 + 8B^2\omega_0^2}) = \omega_0^2 + (\omega_0^2 \pm \sqrt{\omega_0^4 + 2B^2\omega_0^2}) = \omega_0^2 + (\omega_0^2 \pm \omega_0^2 \sqrt{1 + 2\frac{B^2}{\omega_0^2}}) \\ &\approx \omega_0^2 + [\omega_0^2 \pm \omega_0^2(1 + \frac{B^2}{\omega_0^2})] \quad (\text{because } \frac{B^2}{\omega_0^2} \ll 1, \text{ some approximations are made}) \end{aligned}$$

$$\begin{aligned} &= \omega_0^2 + [\omega_0^2 \pm (\omega_0^2 + B^2)] \\ \Rightarrow \begin{cases} \omega_-^2 = \omega_0^2 - B^2 \\ \omega_+^2 = 3\omega_0^2 + B^2 \end{cases} &\Rightarrow \begin{cases} \omega_- = \sqrt{\omega_0^2 - B^2} = 2\pi f_r \\ \omega_+ = \sqrt{3\omega_0^2 + B^2} = 2\pi f_r' \end{cases} \end{aligned}$$

**For  $f_0$ :**

$$\omega^2 = \omega_0^2 + \frac{\frac{h}{H_0} - B^2 - 4\omega_0^2 \pm \sqrt{\left(\frac{h}{H_0} - B^2 - 4\omega_0^2\right)^2 - 12(B^2\omega_0^2 - 2\frac{h}{H_0}\omega_0^2)}}{6}$$

$$\omega^2 = \frac{4\omega_0^2 - B^2 + \sqrt{(4\omega_0^2 - B^2)^2 + 36\omega_0^4}}{6}$$

(because  $\frac{B^2}{\omega_0^2} \ll 1$ , some approximations are made)

$$\omega^2 = \frac{4\omega_0^2 - B^2 + \sqrt{52\omega_0^4} \cdot (1 - \frac{B^2}{13\omega_0^2})}{6} = \frac{4\omega_0^2 - B^2 + \sqrt{52} \cdot (\omega_0^2 - \frac{B^2}{13})}{6} \approx 1.87\omega_0^2 - 0.26B^2$$

$$\Rightarrow 2\pi f_0 = \sqrt{1.87\omega_0^2 - 0.26B^2}$$

$$\Rightarrow \begin{cases} 2\pi f_r = \sqrt{\omega_0^2 - B^2} \\ 2\pi f_0 = \sqrt{1.87\omega_0^2 - 0.26B^2} \\ 2\pi f_r' = \sqrt{3\omega_0^2 + B^2} \end{cases}$$

Compare the decreasing rate of  $f_r$  and  $f_0$  with the B (visco-drag) increasing:

**For  $f_r$  and  $f_r'$ :**

$$\omega^2 = \omega_0^2 + \frac{1}{2} \left( \frac{h}{H_0} \pm \sqrt{\left(\frac{h}{H_0}\right)^2 + 2\left(\frac{h}{H_0}\right)B^2 + 4B^2\omega_0^2} \right),$$

$$\frac{\partial \omega^2}{\partial B} = \pm \frac{\frac{h}{H_0} B + 2B\omega_0^2}{\sqrt{\left(\frac{h}{H_0}\right)^2 + 2\left(\frac{h}{H_0}\right)B^2 + 4B^2\omega_0^2}}$$

$$\left(\frac{\partial \omega^2}{\partial B}\right)_{f_r} = - \frac{\frac{h}{H_0} B + 2B\omega_0^2}{\sqrt{\left(\frac{h}{H_0}\right)^2 + 2\left(\frac{h}{H_0}\right)B^2 + 4B^2\omega_0^2}}$$

**For  $f_0$ :**

$$\omega^2 = \omega_0^2 + \frac{\frac{h}{H_0} - B^2 - 4\omega_0^2 + \sqrt{\left(\frac{h}{H_0} - B^2 - 4\omega_0^2\right)^2 - 12\left(B^2\omega_0^2 - 2\frac{h}{H_0}\omega_0^2\right)}}{6}$$

$$\left(\frac{\partial \omega^2}{\partial B}\right)_{f_0} = \frac{1}{6} \left\{ -2B + \frac{1}{2} \cdot \frac{1}{\sqrt{\left(\frac{h}{H_0} - B^2 - 4\omega_0^2\right)^2 - 12\left(B^2\omega_0^2 - 2\frac{h}{H_0}\omega_0^2\right)}} \right.$$

$$\cdot \left[ 2\left(\frac{h}{H_0} - B^2 - 4\omega_0^2\right) \cdot (-2B) - 24B\omega_0^2 \right] \}$$

$$= \frac{1}{6} \left( -2B + \frac{2B^3 - 4B\omega_0^2 - 2\frac{h}{H_0}B}{\sqrt{\left(\frac{h}{H_0} - B^2 - 4\omega_0^2\right)^2 - 12\left(B^2\omega_0^2 - 2\frac{h}{H_0}\omega_0^2\right)}} \right)$$

$$= -\frac{1}{3}B + \frac{B^3 - 2B\omega_0^2 - \frac{h}{H_0}B}{3\sqrt{\left(\frac{h}{H_0} - B^2 - 4\omega_0^2\right)^2 - 12\left(B^2\omega_0^2 - 2\frac{h}{H_0}\omega_0^2\right)}}$$

Compare  $f_0$  with  $f_r$ , compare  $\left(\frac{\partial\omega^2}{\partial B}\right)_{f_r}$  with  $\left(\frac{\partial\omega^2}{\partial B}\right)_{f_0}$ :

$$\left(\frac{\partial\omega^2}{\partial B}\right)_{f_0} - \left(\frac{\partial\omega^2}{\partial B}\right)_{f_r} = -\frac{1}{3}B + \frac{B^3 - 2B\omega_0^2 - \frac{h}{H_0}B}{3\sqrt{\left(\frac{h}{H_0} - B^2 - 4\omega_0^2\right)^2 - 12\left(B^2\omega_0^2 - 2\frac{h}{H_0}\omega_0^2\right)}} + \frac{\frac{h}{H_0}B + 2B\omega_0^2}{\sqrt{\left(\frac{h}{H_0}\right)^2 + 2\left(\frac{h}{H_0}\right)B^2 + 4B^2\omega_0^2}}$$

(because  $\frac{B^2}{\omega_0^2} \ll 1$ , some approximations are made, such as  $\sqrt{1 + \frac{2B^2}{\omega_0^2}} \approx 1 + \frac{B^2}{\omega_0^2}$ )

$$\Rightarrow \left(\frac{\partial\omega^2}{\partial B}\right)_{f_0} - \left(\frac{\partial\omega^2}{\partial B}\right)_{f_r} > 0$$

That means for  $f_0$ , its decreasing rate with an increase in B (visco-drag) is slower than that of  $f_r$ , which coincides with the trends in Figure 5.3.

#### 5.4 Model in non-Newtonian liquids and numerical simulation

For non-Newtonian liquids, the form of the differential Equation (5-3) needs to be changed due to viscosity changing with the shear rate. The viscosity change is described by the Carreau model:  $\eta(\dot{\gamma}) = \eta_\infty + \frac{\eta_0 - \eta_\infty}{[1 + (\lambda\dot{\gamma})^2]^p}$  and power law model which is the simplification of Carreau model. And the differential Equation (5-3) changes into:

$$\ddot{x} + B\dot{x}^n + \omega_0^2x = h \sin \omega t \quad (5-6)$$

where  $n$  is the viscosity index (power law index). And this kind of differential equation has no analytical solution when  $n$  is not equal to 1. So the numerical simulations are used to solve the differential Equation (5-6). Matlab 7.0 is used for numerical simulation.

$$\ddot{x} + B\dot{x} + \omega_0^2x = h \sin \omega t \quad (5-3)$$

$B = C_0\eta$ , where  $\eta$  changes with shear rate based on Carreau model:



$$\eta(\dot{\gamma}) = \eta_{\infty} + \frac{\eta_0 - \eta_{\infty}}{[1 + (\lambda\dot{\gamma})^2]^p}$$

Let  $\eta_{\infty}=0.001\text{Pa}\cdot\text{s}=1\text{cP}=1\text{mPa}\cdot\text{s}$ ,  $\eta_0=0.1\text{Pa}\cdot\text{s}=100\text{cP}=100\text{mPa}\cdot\text{s}$ ,  $\lambda=0.1$ ,  $p=0.2$ ,  $C_0=15000$ , different  $h$ ,  $\omega_0=1.6\times 10^4$ .

Checking and simulating the maximum shear rate with different  $h$  values (means different driving force) results in Table 5.1 below:

$h$	velocity (m/s)	shear rate ( $\text{s}^{-1}$ )
0.1	$7.025\times 10^{-5}$	0.82
0.5	$3.376\times 10^{-4}$	3.95
1	$7.075\times 10^{-4}$	8.28
3	$2.912\times 10^{-3}$	34.1
5	$6.45\times 10^{-3}$	75.5
10	0.01975	$2.31\times 10^2$
50	0.2635	$3.08\times 10^3$
500	8.35	$9.77\times 10^4$
10000	392	$4.59\times 10^6$

Table 5.1. Maximum shear rate with different  $h$  value.

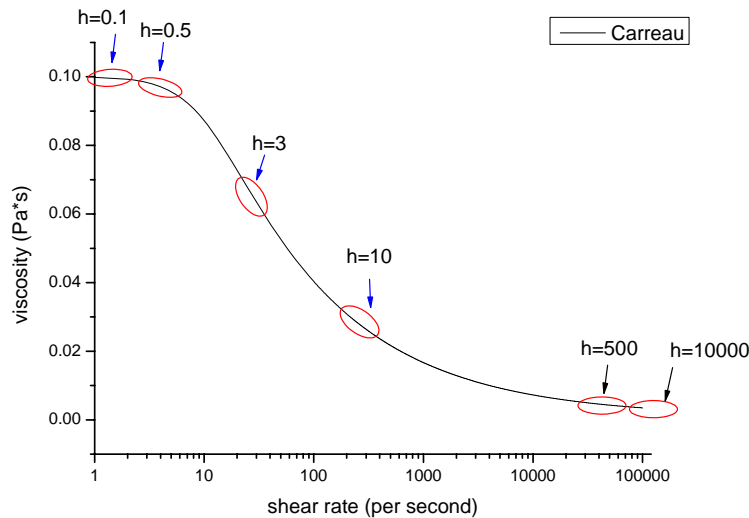


Figure 5.4. The relationship of typical Carreau model viscosity and shear rate with different driving force amplitude.

From Figure 5.4, we find that non-Newtonian liquids behave like Newtonian liquids at

rather low shear rates and high shear rates, in which ranges viscosity does not change with shear rate. So based on this conclusion, we should get similar results by the method we proposed before, which can distinguish these two types of liquids. Figure 5.5 following shows the simulation results. We can find the two curves approach to each other at high shear rate and meet at low shear rate, which matches with the experiment results and Figure 5.4, and is also in accord with the facts that the Carreau-type non-Newtonian liquids behaves as Newtonian liquids at low shear rates and high shear rates. And this also approves the validity of the method proposed in this study.

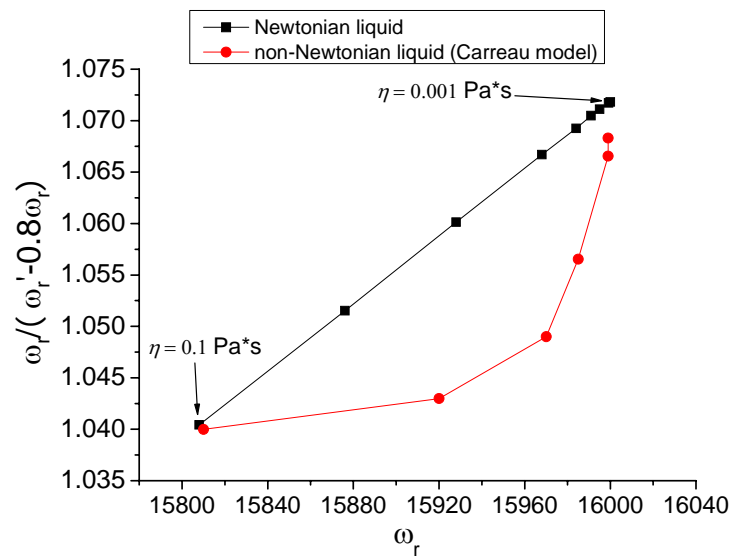


Figure 5.5. Different  $h$  (non-Newtonian liquids with different viscosity) compared with different Newtonian liquids at same range of resonance frequency.

**References:**

[1] Symon, Keith, *Mechanics* (Third ed.). Addison-Wesley. 1971.  
 [2] L. D. Landau and E. M. Lifshitz, *Fluid Mechanics*, Pergamon, London, 1959,  
 [3] James A. Fay, *Introduction to Fluid Mechanics*, MIT press, 1994.

[4] J. Watkins, An introduction to biomechanics of sport and exercise. New York: Churchill Livingstone Elsevier, 2007, pp 196.

[5] John Harris, Walter Benenson and Horst Stöcker, *Handbook of physics*, Springer , 2002, pp 275-276.

## CHAPTER 6

### CONCLUSIONS AND PERSPECTIVES

As a fluid sensor platform, magnetostrictive strip and cantilever have some unique advantages over others, such as wireless and good performances in liquids by choosing magnetostrictive strip, and a large vibration displacement by selecting cantilever. To fully exploit these advantages, resonance behaviors of the magnetostrictive strip and the PZT cantilever are systemically studied to improve the sensor applications. Different factors which may have effects on resonance behaviors of magnetostrictive strip are studied intensively, such as DC bias field influence and locations effect. And the point of view that AC-driving field could influence resonance frequencies of sensor was proposed. Proofs from three independent methods (lock-in amplifier, impedance analyzer and network analyzer) were given to support this view that resonance frequencies decrease with increases in the AC-driving field. By recognizing this effect, the intrinsic resonance frequencies could be found. The measurement results of lock-in amplifier and impedance analyzer are compared to study the principle difference between these two methods. And also by using different coils in the impedance analyzer method, the view that the impedance analyzer measures the signal from sensor and equivalent circuits is proved. Combined with former results from the AC-driving field, it is found that coils with a small diameter and long length are good for resonance behaviors measurement. The location effects study shows the center of the pick-up coil is the best position to measure the vibration signals of the magnetostrictive strip sensor.

A new method by using properly chosen function of characteristic frequencies versus one of three frequencies is developed to identify the non-linearity of viscosity and also differentiate Newtonian oils and non-Newtonian oils. With the studies of the resonance

behaviors of magnetostrictive strips with different lengths in different oils, and the performances of same length magnetostrictive strips with different length-width ratios, it is found that the geometry of AW sensor is important. Longer length is better and also larger length-width ratio is better in identifying the non-linearity of viscosity. And a magnetostrictive strip of  $40 \text{ mm} \times 3 \text{ mm} \times 30 \text{ }\mu\text{m}$  has good performance in identifying the non-linearity of viscosity within broad temperature range.

The studies of resonance behaviors of cantilever sensors with different lengths in different oils and the performances of same length cantilever sensors with different length-width ratios illustrates that a longer cantilever with same width and thickness has a better performance in identifying non-linearity of viscosity, and cantilever sensor of the same length and thickness with a smaller width has better performance in differentiating Newtonian oils and non-Newtonian oils.

And numerical simulation of the vibration of the strip sensor shows non-Newtonian liquids behave like Newtonian liquids at rather low shear rates and high shear rates, in which ranges viscosity does not change with shear rate and act totally different with Newtonian liquids at intermediate shear rates. So based on this conclusion, similar results can be obtained by the method proposed here, which can distinguish these two types of liquids. And this also proves the validity of the method proposed in this study.

A solid background for further improvement of fluid sensor platform was set up by the results reported in this study.

- 1) From a fundamental view, important information for the understanding of the resonance behaviors of magnetostrictive strip was given by the experimental results reported in

Chapter 2. Not only DC bias field but also AC-driving field could influence resonance frequencies of a magnetostrictive strip sensor. During the sensors application, different persons choose different device and may use different AC-driving fields, which could affect the resonance frequencies of the magnetostrictive strip. Further research is needed to study the magnetostrictive strip resonator from both physics and materials science to establish the correct equation to get the intrinsic resonance frequency in different circumstances. And based on other comparisons of different measurement methods, this research will provide instruction on improving the magnetostrictive strip resonator system design.

- 2) The viscous drags which act on main surface and edge are very different even for the same magnetostrictive strip, and this will affect the performance of magnetostrictive strip. Edge effect of magnetostrictive strip needs to be studied by changing the edge shape of strip sensor to improve the design of magnetostrictive strip resonator system.
- 3) A new method by using the properly chosen function of characteristic frequencies versus one of three frequencies is developed to identify the non-linearity of viscosity and also differentiate Newtonian oils and non-Newtonian oils in Chapter 3 and 4. All studies show that a magnetostrictive strip with longer length and larger length-width ratio has better performance in identifying non-linearity of viscosity. Further research on this topic would be interesting. A balance between performance and portability of the sensor system needs to be found because we cannot use a magnetostrictive strip as large as we want. In addition, a portable device can be designed for the cantilever resonator for further application.

4) As shown in Chapter 5, the non-linearity of viscosity is critical in differentiating Newtonian fluids and non-Newtonian fluids. However, due to the non-linearity of the differential equation, only numerical simulation solutions can be obtained in the studies of non-Newtonian fluids. And a time-consuming issue also needs to be solved for high resonance frequencies vibration simulations due to a large coefficient of the differential equation. Although the tendency of the simulation to vary is the same as experiment results, some improvements still need to be added in the simulation to be closer to the real cases for instruction of future sensor system design.